An *in vitro* biomolecular breadboard for prototyping synthetic biological circuits

Thesis by
Zachary Zhipeng Sun

In Partial Fulfillment of the Requirements for the
Degree of
Doctor of Philosophy

CALIFORNIA INSTITUTE OF TECHNOLOGY
Pasadena, California
2016
Defended June 22, 2015

This manuscript is dedicated to

My grandmother, 梁兰真
(January 1, 1928 – April 1, 2011)

and

My mother and father

Acknowledgements

The period of June 2011 – April 2012 was a tumultuous one for me; at that time I questioned if scientific research was truly my passion, and the transition from medical school to graduate school had been rough. Integral to helping me decide to conduct this PhD was the help and support of my MD/PhD directors, **Kelsey Martin** and **Stephen Smale**, and my rotation advisor **Bruce Hay** – they gave me time to reflect and to make an informed decision about what I wanted to explore. I especially thank Steve for his support and his mentorship during the period and his advice on labs to seek and career paths to pursue. Most importantly, **Richard Murray** gave me the chance to give synthetic biology research another go, and truly let me explore whether continuing down the basic science research track was appropriate. I am grateful for the opportunity, and looking back I am confident I made the correct one.

I was privileged to enter graduate school with the tools necessary to conduct meaningful research. I thank **George Church**, **Farren Isaacs**, **Alain Viel**, and **David Jeruzalmi**, four of my mentors from my undergraduate years, for introducing me to synthetic biology and for patiently staying with me as I learned the ropes – even if it meant months and months of failed cloning attempts. They are truly inspiring people, showing me not only the meaning of hard work but also the importance of balance. My mentors gave me the independence to pose questions and to explore at my own pace, and to accept failure and to dream big.

While in the Murray lab, I have been surrounded by inquisitive minds and by a caring community of supportive graduate students and postdocs. I would like to thank the lab members and my collaborators and friends **Enoch Yeung**, **Jongmin Kim**, **Yutaka Hori**, **Anu Thubagere**, **Marcella Gomez**, **Vipul Singhal**, and **Clare Hayes**. Special thanks to Enoch, with whom I have enjoyed countless intellectual conversations about all realms of science, and who inspires me to

work to my fullest; and to Jongmin, who has been a wonderful mentor and friend. I would also like to thank **Adam Abate**, **Jong Seto**, and **Chris Ochs** at UCSF for a great summer of research experience and camaraderie, and **Henrike Niederholtmeyer** at EPFL for being a most thoughtful collaborator.

During my time at Caltech I have also been lucky to be surrounded with supportive friends and loved ones who have been my true support network. I thank **Roland** and **Michelle Palvolgyi**, **Paul Nguyenfa**, **Angelico Razon**, **Allen Kwong**, **Wesley Gaschler**, **Arnav Methta**, **Benji Uy**, and **Angela Du**. Special thanks for my roommate of 2 ½ years and great friend from medical school, Roland, for being there for me the whole time. Also, special thanks to Angela, my girlfriend who I met during PhD training. You've seen the good and the bad, and stuck with me through it all; I couldn't ask for a more dedicated friend and partner.

My thesis committee has given me great advice, both during and outside of committee meetings. I would like to thank **David Baltimore**, for being a wonderful and inspiring role model and for providing thoughtful career advice. I would also like to thank **Michael Elowitz** – thank you for the opportunity to rotate and learn about your research, and for all of your insightful comments on my work, especially on our repressilator-inspired paper. Finally, **Vincent Noireaux** has been a wonderful mentor – I've enjoyed the opportunity to work closely on cell-free lysates and to coauthor papers with you, and am humbled by your technical depth and breadth.

To **Richard Murray**: you have been truly an inspiring and amazing mentor and friend. I have learned so much while working with you, and not just about science, but in how to treat people well, how to be a true leader, and how to inspire others. It is clear that you deeply care about your students' well-being and success from a very personal level above all else. I

appreciate the freedom you have given me to explore during the PhD, and I could not have asked for a better mentor.

Finally, to my family, **Mingui Sun**, **Yingze Zhang**, and **Liann Sun**: there is no way I would be here now without your unfaltering support and dedication. Thank you for pushing me to achieve and for supporting me along the way, and for helping me find what I truly enjoy doing. I am extremely thankful our family is in good health, and I'm excited to see what is in store for us in the future.

Abstract

Biomolecular circuit engineering is critical for implementing complex functions *in vivo*, and is a baseline method in the synthetic biology space. However, current methods for conducting biomolecular circuit engineering are time-consuming and tedious. A complete design-build-test cycle typically takes weeks' to months' time due to the lack of an intermediary between design *ex vivo* and testing *in vivo*. In this work, we explore the development and application of a "biomolecular breadboard" composed of an *in-vitro* transcription-translation (TX-TL) lysate to rapidly speed up the engineering design-build-test cycle. We first developed protocols for creating and using lysates for conducting biological circuit design. By doing so we simplified the existing technology to an affordable ($0.03/uL) and easy to use three-tube reagent system. We then developed tools to accelerate circuit design by allowing for linear DNA use in lieu of plasmid DNA, and by utilizing principles of modular assembly. This allowed the design-build-test cycle to be reduced to under a business day. We then characterized protein degradation dynamics in the breadboard to aid to implementing complex circuits. Finally, we demonstrated that the breadboard could be applied to engineer complex synthetic circuits *in vitro* and *in vivo*. Specifically, we utilized our understanding of linear DNA prototyping, modular assembly, and protein degradation dynamics to characterize the repressilator oscillator and to prototype novel three- and five-node negative feedback oscillators both *in vitro* and *in vivo*. We therefore believe the biomolecular breadboard has wide application for acting as an intermediary for biological circuit engineering.

Table of Contents

Chapter 1: Introduction to biomolecular circuit engineering and to cell-free systems

Overview of thesis

This thesis explores the development and application of an intermediary for engineering biomolecular circuits. Biomolecular circuit engineering typically involves designing a circuit and immediately implementing the circuit *in vivo* to test its functionality, with minor (if any) simulation and testing outside the end chassis. This differs from other engineering-oriented disciplines. For example, architecture utilizes software (AutoCAD) and simulations to characterize a structure, while aeronautics uses "wind tunnels" to test prototypes of planes. In this thesis, we seek to bridge this gap by using transcription-translation (TX-TL) cell-free lysates as an intermediary for going from design to completion for biomolecular circuit engineering. We term this intermediary a "biomolecular breadboard" to emphasize its ability to conduct prototyping.

Chapter 1 presents an introduction to synthetic biology and biomolecular circuit engineering, framing the problem in the context of the field. We also delve into the rich history of the base technology, cell-free lysates, to understand previous work conducted in the field and the current cutting-edge.

In Chapter 2 we outline our protocol for creating and using TX-TL. This protocol allows for accessibility of TX-TL to labs with basic biological infrastructure, and drastically simplifies the execution of a TX-TL reaction from the previous standard. We find that TX-TL creation costs $0.03/uL, with a typical reaction size of 10 uL.

Chapter 3 seeks to further accelerate the design-build-test cycle by removing the limitation to use plasmid DNA. Plasmid DNA requires cloning to be created in high yields and generally requires a cellular host to replicate. In contrast, linear DNA can be created from purely *in vitro* methods and can reduce design-build-test cycles to under a day. However, exonucleases present in TX-TL readily digest linear DNA, and it is unclear if circuits made of linear DNA look like those of plasmid DNA. We protect linear DNA using gamS, a lambda phase protein, and characterize its activity. We then create a modular and rapid assembly system to build DNA *ex vivo* rapidly.

Chapter 4 characterizes an important cellular process, protein degradation dynamics, in the breadboard. *In vivo*, synthetic circuit dynamics are maintained by cellular division and protein degradation. This allows circuit components to reach steady state. However, in a batch mode TX-TL reaction there is no cellular dilution and minimal protein degradation from existing AAA+ proteases. We show that ClpXP AAA protease can be supplemented in the breadboard to selectively degrade proteins. This is done without significant resource utilization. While it does not compensate for cellular dilution, protein degradation can aid in implementing circuit dynamics.

Chapter 5 applies the breadboard to build novel synthetic circuits going from design to completion *in vitro* and *in vivo*, utilizing the technology developed in Chapters 2-4. A critical unresolved question is the ability to transition *in vitro* circuit prototyping to the *in vivo* environment. We partially address this question in Chapter 5 by demonstrating the prototyping of synthetic 3-node and 5-node negative feedback oscillators *in vitro* and implementing the designs successfully *in vivo*. We compare our results *in vitro* and *in vivo* and find that many circuit characteristics, such as the dependence of oscillation period on dilution time, circuit architecture,

and protein degradation, are conserved in both systems. We end up with a framework to use for prototyping.

We conclude in Chapter 6 with a discussion of the biomolecular breadboard findings. We also discuss other work that has demonstrated the utility of the biomolecular breadboard, and future planned work. In particular, we focus on the necessity to completely characterize the *in vitro* to *in vivo* transition, introduce work on a high-throughput method associating *in vitro* and *in vivo* metrics, and evaluate the breadboard for commercialization potential.

Overview of synthetic biology and biomolecular circuit engineering

While no consensus exists on what synthetic biology "is," there is general acceptance that it relies heavily on engineering complexity (Heinemann & Panke 2006; Endy 2005). Engineering can be conducted towards understanding natural phenomena like cell signaling (Sprinzak et al. 2010), or to build completely novel functions such as artificial logic gates (Moon et al. 2012) or pathogen sensors (Saeidi et al. 2011; Kotula et al. 2014). To facilitate engineering, the field has developed a myriad of tools, from rapid methods of conducting genomic engineering (Wang et al. 2009; Le Cong et al. 2013) to databases of standardized parts (Y.-J. Chen et al. 2013; Stanton et al. 2014; Mutalik et al. 2013) to cheap DNA synthesis and sequencing (Kosuri et al. 2010; Eid et al. 2009). At its extreme, there are automated "foundries" to merge all of these technologies into a parallelized synthetic circuit build-and-test platform (Smanski et al. 2014; Temme et al. 2012).

To conduct engineering, all of these tools accept in one way or another a fundamental restriction – the need for conducting final testing in a cell. This brings many limitations. The time spent exponentially increases with circuit size (Moon et al. 2012) or with organism complexity (C.-H. Chen et al. 2007). While there are some attempts to get around final testing in a cell with predictive modeling (Ellis et al. 2009), these methods are not in wide use likely due to the inability of models to capture cellular complexity. It is enlightening to go over the current cloning and testing process to see what parts are most time-consuming and demanding.

The current cloning and testing process

The main restriction of the cloning and testing process is the need to have all plasmids in a compatible expression mode with the cell. For prokaryotes, this involves ensuring that origins of replications responsible for replicating the plasmids are compatible among general families

(Couturier et al. 1988). To do so, larger circuits need to have multiple pieces built on one plasmid, which requires utilizing methods of DNA assembly.

For example, assume three coding sequences A, B, and C compose a circuit to be expressed in *E. coli*. The initial step requires assembling each coding sequence into an expressible unit composed of a promoter and/or regulatory region, terminator, and a compatible vector. Many methods can be used to assemble the DNA, including BioBricks Assembly (Lee et al. 2011), Golden Gate Assembly (Engler et al. 2009; Sarrion-Perdigones et al. 2011), Ligation-based methods (de Kok et al. 2014), and Isothermal Assembly (Gibson et al. 2009). While the assembly is typically 1-3 hours, assembly is not 100% efficient and can have multiple error modes, from non-ideal assembly conditions (salt, non-pure DNA) to excessive secondary structure (Casini et al. 2014). Many of these conditions are not predictable until after the multiple-day to a week process of transformation, screening, and sequencing. In addition, if the coding sequences are toxic or over-expressed, the host cell may either mutate the plasmid or carry a load precluding its growth (Miroux & J. E. Walker 1996; Baneyx 1999). Therefore, each cycle may require multiple iterations of testing and debugging to be successful, which can take significant time.

Assuming the initial cloning is successful, each of the expression cassettes for A, B, and C must then be cloned into one plasmid using the same procedure as before. Larger segments typically lead to less efficient ligation reactions (Gibson et al. 2009). Additionally, repeat regions introduced from redundant vectors can lead to deletions and plasmid instability (Lilley 1981). Finally, plasmids may hit a size barrier for replication, which can further decrease efficiency and require alternative cloning strategies (Cheah et al. 1987).

After cloning is complete, the circuit is ready for testing in the final chassis, the cell. This involves a final transformation of the circuit plasmids into the host. For well-characterized bacteria such as *E. coli* this process is relatively straightforward. However, other bacteria may be resistant to transformation, resulting in additional time of diagnosis and testing. A classic example is *Wolbachia*, a bacteria that is clinically important for reducing malaria load (T. Walker et al. 2011) but only transformable by selected bacteriophage (Fujii et al. 2004). Finally, with successful transformation the circuit may introduce too high of a metabolic load to be characterized (Ceroni et al. 2015). However, assuming everything goes correctly the circuit may simply not work for many heterologous reasons, from design constraints to strain dependence (Kelly et al. 2009). Failure modes require additional design build test cycles, which add to engineering time. Given these limitations, it is not surprising that one of the success stories of synthetic biology – the engineering of artemisinin production by *E. coli* and by yeast – required an estimated 150 person-years of labor to complete (Keasling 2014).

To elucidate the gains of a possible *in vitro* intermediate, we will review a core application area in synthetic biology, that of metabolic engineering, and note the requirements in the metabolic engineering process.

Core application area: Metabolic engineering

Metabolic engineering is the process of optimizing production of a metabolite within a cellular environment by manipulation of the genetic pathways needed to create the metabolite. The metabolic engineering market size is large for synthetic biology, with an estimate of $50 billion (2011) for all bio-catalyzed processes (Murphy 2011). In addition, metabolic engineering typically requires large-scale engineering of large pathways, and epitomizes the need for a faster *in vitro* intermediate.

A primary success story in synthetic biology has been the production of artemisinin from microbial sources to treat malaria. Artemisinin is a potent anti-malarial naturally formed in the *Artemisia annua* plant. Isolation from plant sources yields 5 kg of drug per 1000 kg of plants, requiring 2.5 acres to grow and costing $900-1600/kg (Hale et al. 2007). To increase yields and reduce costs, attempts to produce artemisinin in *E. coli* begun in 2003 (Martin et al. 2003), culminating in optimization in 2006 (Ro et al. 2006) and 2009 (Tsuruta et al. 2009) and production in yeast in 2013 (Paddon et al. 2013) at 5 kg/200 L of culture, replacing the previous 2.5 acre requirement.

The final pathway used to create artemisinic acid, a precursor to artemisinin, is shown in Figure 1 (Paddon et al. 2013). This pathway contains at least 16 enzymes up-regulated to convert acetyl-CoA into artemisinic acid. The complexity of the pathway can be seen in the branch-off from FPP to amorphadiene; in order to maximize amorphadiene yield, it is necessary to repress ergosterol-related production to shift metabolic flux to amorphadiene. While this pathway is very complex for implementation in *E. coli*, previous work was conducted strictly in *E. coli* using enzymes from yeast (Martin et al. 2003). Many basic pathway properties, such as enzyme conversion efficiencies and binding affinities, were addressed by utilizing protein variants *in vivo*. With 16 enzymes or more, however, the optimization space is vast; modifying individual components *in vivo* requires extensive cloning and characterization work. An *in vitro* system can speed up the optimization cycle by allowing for high-throughput and modular testing.

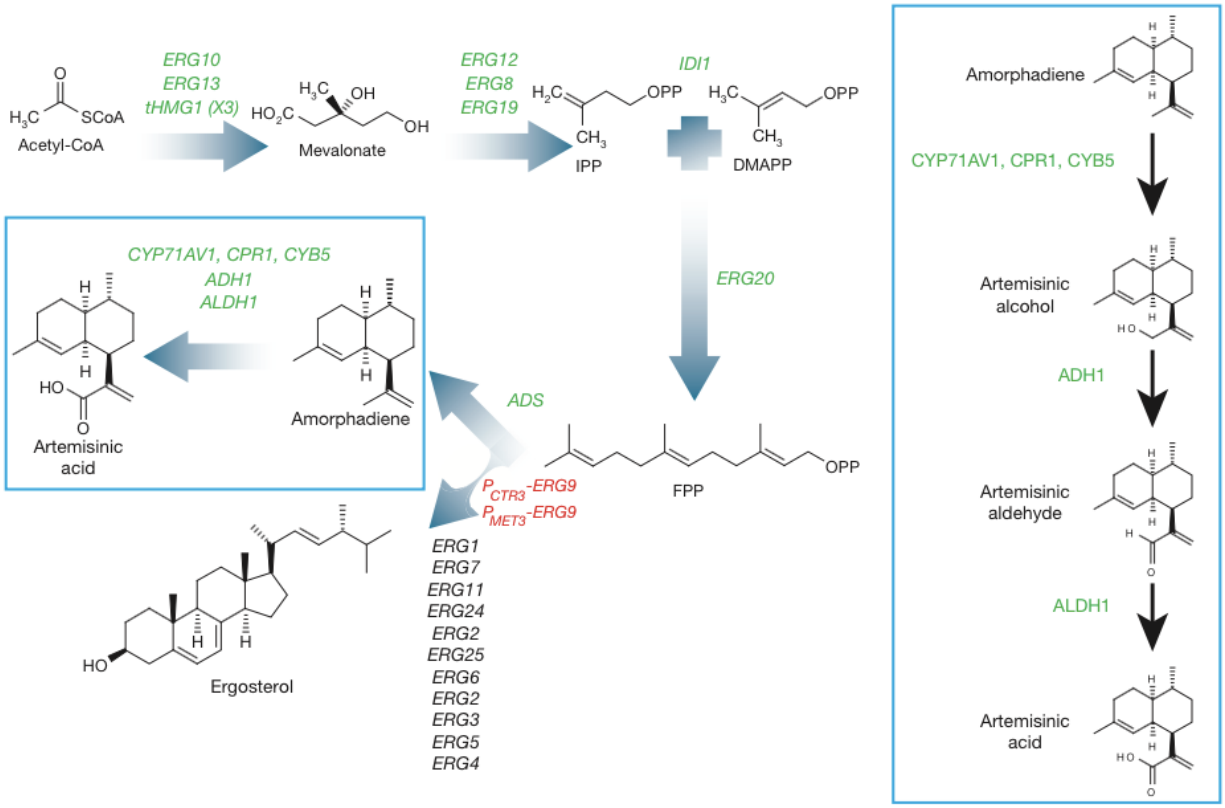

Figure 1. Artemisinic acid production in yeast. Production of artemisinin in yeast, showing pathway going from acetyl-CoA to artemisinic acid. In blue boxes is a zoom-in of amorphadiene conversation to artemisinic acid. Figure courtesy {Paddon:2013ik}.

Another example of metabolic engineering of large pathways involves the production of useful commodity chemicals. These can include 1,3-Propanediol (Nakamura & Whited 2003), 1-Butanol (Atsumi et al. 2008), and 1-Propanol (Shen & Liao 2008), among others whose processes are commercially proprietary. We focus on 1,4-Butanedol (BDO), a commodity chemical for producing plastics (Yim et al. 2011). This pathway to produce 1,4-BDO in *E. coli* from succinate or alpha-ketoglutarate consists of seven enzymes, of which two are naturally expressed in *E. coli* and five are heterologous. These enzymes are expressed from genomic integrations or from compatible plasmids, and are optimized for 1,4-BDO production. Unlike the artemisinin pathway, the 1,4-BDO pathway also heavily relies on metabolic flux analysis to

determine limiting steps and to provide insights on optimizing endpoint production (Wiechert 2001).

Since implementing the pathway *in vivo*, new work has commenced to try to collect data *in vitro*, both to determine stoichiometry of enzymes necessary for optimal production and to conduct purely experimental flux analyses (Wu et al. 2015). *In vitro*, it was found that the enzyme pathway can also express 1,4-BDO in a batch mode reaction Additionally, the conversion of 4-Hydroxybutyrate to downstream metabolites was found as a limiting step. These results lend promise to using an *in vitro* system as an intermediate to learn more about the pathway to be engineered and to limit *in vivo* manipulations.

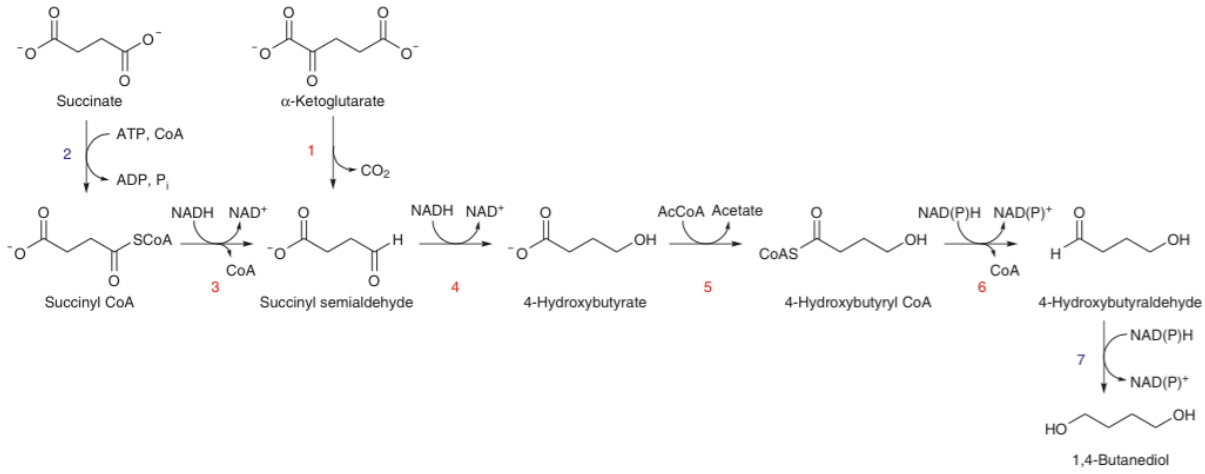

Figure 2. 1,4-Butanediol(BDO) production in E. coli. Production of 1,4 BDO in E. coli. Numbered in black are steps catalyzed with naturally occurring enzymes, and in red are steps with heterologous genes. Figure courtesy {Yim:2011ee}.

Overview of cell-free systems

In this thesis we propose utilizing a cell-free transcription and translation system as the basis for the biomolecular breadboard intermediary from design to implementation *in vivo*. Cell-free systems have a rich history as one of the original platforms in which biological experiments were conducted. In this section, we explore the history of cell-free systems as well as the latest work in utilizing cell-free systems for circuit prototyping.

Historical use and development of cell-free systems

Cell-free systems have been in use since the 1950's to explore basic biological phenomena (Hoagland et al. 1958; Wood & Berg 1962). This was partially out of necessity, as *E. coli* was not transformable before 1970 (Mandel & Higa 1970) and there were no tools for conducting DNA manipulation (and little understanding of DNA, as the double helix structure had just been identified in 1953 (Watson & Crick 1953)). Research into enabling longevity of cell-free systems (J Heinrich Matthaei 1961) revealed as well the basis for discovering the amino acid code (Nirenberg & Matthaei 1961), which ultimately won the Nobel Prize in Medicine in 1968.

Zubay's 1973 review of cell-free systems (Zubay 1973), itself a modification of Nirenberg's protocols, is widely cited as the source of the original cell-free "S30" protocol in use today. As summarized in (Holland & Bundy 2012), extract preparation can be divided up into discrete segments: growth, lysis, clarification, "run-off" reaction (temperature incubation for set periods of time), dialysis, and final clarification. Zubay's 1973 protocol relies on clarification spins at 30,000 x g, resulting in the "S30" moniker. This protocol was generally used as-is until the 1990's, and significant work was done in utilizing the protocol for characterizing DNA

replication (Diaz et al. 1981), enterotoxins (Lathe et al. 1980), and high-yield protein synthesis using continuous flow (Spirin et al. 1988).

Improvements have been made on the original cell-free protocol, namely in process optimization, lysis methods, and energy systems. In the former area, specific modifications of interest include the exclusion of a dialysis step (T. W. Kim et al. 2006), optimization of runoff time (Kwon & Jewett 2015), and reduction of spin speeds to 12,000 x g (T.-W. Kim et al. 2008). A variety of lysis methods have also been employed, from the original French press method (Zubay 1973) to sonication (Kwon & Jewett 2015; Holland & Bundy 2012), to homogenization (Liu et al. 2005; Yang et al. 2012) and physical lysis (bead-beating) (Kigawa et al. 2004; Shin & Noireaux 2010a). Finally, a variety of energy sources exist to power cell-free systems, such as pyruvate (Jewett & Swartz 2004), phosphoenolpyruvate (D.-M. Kim & Swartz 2001), 3-phosphoglyceric acid (Shin & Noireaux 2012), glucose (T.-W. Kim et al. 2007), and maltose (Caschera & Noireaux 2013). All of these improvements generally seek to improve overall yield from cell-free reactions, as the field shifted to emphasizing yields from pure *in vitro* expression of specialized proteins. While these improvements allowed for increased protein production, the utility of cell-free systems shifted away from being used as a tool for understanding natural phenomena and more towards pure protein production.

Cell-free systems for circuit prototyping

In parallel with S30 extract development, work was conducted on a novel cell-free system from individual components (Shimizu et al. 2001). Marketed as PURExpress©, this system has been useful in conducting controlled cell-free reactions, as the environment does not have degradation of mRNA and DNA. This property allowed for PURExpress to be used in specialized protein production applications (Sawasaki et al. 2002) despite its low yield compared

to traditional S30 systems. In addition, it found a niche use as an environment for building biochemical circuits. Examples of circuits built include switches (J. Kim et al. 2006) and oscillators (J. Kim & Winfree 2011).

The first real foray into building circuits in lysates, however, was done in 2003 when wheat germ extract was supplemented with components to demonstrate activation and repression cascades (Noireaux et al. 2003). This effort was expanded to *E. coli* in 2005 (Noireaux et al. 2005) and further in 2010, when native non-T7 regulatory systems were utilized to express genes (Shin & Noireaux 2010a; Shin & Noireaux 2010b) and later switches, cascades, and logic gates (Shin & Noireaux 2012). The latter implementation, which is the application of the TX-TL protocol developed in Chapter 2, was unique, as it used regulatory regions that were from native *E. coli* versus those from T7 phage. The most complex circuit example to date was then implemented in TX-TL with an assembly of active, virulent T7 bacteriophage from 40 kbp and 60 genes (Shin et al. 2012). These experiments indicated that complexity could be prototyped *in vitro*. Recent work has also demonstrated circuits with real-world applicability, namely using RNA aptamers to build Ebola sensors on lyophilized TX-TL on paper (Pardee et al. 2014) and *in vitro* oscillators in cell-like microfluidic arrays (Karzbrun et al. 2014).

Before the work done in this thesis, it was unclear if cell-free systems could not only prototype circuits *in vitro* but also act as an intermediate between the *in vitro* and the *in vivo* environment. For this to be true, there must be a predictive capacity of *in vitro* systems for the *in vivo* environment. Only the combination of S30-based lysates and native-regulation circuits can produce this trait. During the duration of thesis work, initial work was conducted characterizing *in vitro* to *in vivo* predictive capability for basic transcriptional and translational units (Chappell et al. 2013), as well as implementation of RNA-based cascades *in vitro* and *in vivo* (Takahashi et

al. 2014). We hope that the work presented in Chapters 2-5 and planned future work demonstrates predictability between the *in vitro* and *in vivo* environment and establishes that cell-free systems can be used as a "biomolecular breadboard" to enable rapid biological systems engineering.

References

Atsumi, S. et al., 2008. Metabolic engineering of Escherichia coli for 1-butanol production. *Metab Eng*, 10(6), pp.305–311.

Baneyx, F., 1999. Recombinant protein expression in Escherichia coli. *Curr Opin Biotechnol*, 10(5), pp.411–421.

Caschera, F. & Noireaux, V., 2013. Synthesis of 2.3 mg/ml of protein with an all Escherichia coli cell-free transcription-translation system. *Biochimie*, pp.1–7.

Casini, A. et al., 2014. R2oDNA Designer: Computational Design of Biologically Neutral Synthetic DNA Sequences. *ACS Synth Biol*, 3(8), pp.525–528.

Ceroni, F. et al., 2015. Quantifying cellular capacity identifies gene expression designs with reduced burden. *Nat Methods*.

Chappell, J., Jensen, K. & Freemont, P.S., 2013. Validation of an entirely in vitro approach for rapid prototyping of DNA regulatory elements for synthetic biology. *Nucleic Acids Res*, 41(5), pp.3471–3481.

Cheah, U.E., Weigand, W.A. & Stark, B.C., 1987. Effects of recombinant plasmid size on cellular processes in Escherichia coli. *Plasmid*, 18(2), pp.127–134.

Chen, C.-H. et al., 2007. A Synthetic Maternal-Effect Selfish Genetic Element Drives Population Replacement in Drosophila. *Science*, 316(5824), pp.597–600.

Chen, Y.-J. et al., 2013. Characterization of 582 natural and synthetic terminators and quantification of their design constraints. *Nat Methods*, 10(7), pp.659–664.

Couturier, M. et al., 1988. Identification and classification of bacterial plasmids. *Microbiological Reviews*, 52(3), pp.375–330.

de Kok, S. et al., 2014. Rapid and Reliable DNA Assembly via Ligase Cycling Reaction. *ACS synthetic ...*, 3(2), pp.97–106.

de los Santos, E., Meyerowitz, J.T. & Mayo, S.L., 2015. Engineering Transcriptional Regulator Effector Specificity using Computational Design and In Vitro Rapid Prototyping: Developing a Vanillin Sensor. *bioRxiv*.

Diaz, R., Nordström, K. & Staudenbauer, W.L., 1981. Plasmid R1 DNA replication dependent on protein synthesis in cell-free extracts of E. coli. *, Published online: 22 January 1981; | doi:10.1038/289326a0*, 289(5795), pp.326–328.

Eid, J. et al., 2009. Real-Time DNA Sequencing from Single Polymerase Molecules. *Science*, 323(5910), pp.133–138.

Ellis, T., Wang, X. & Collins, J.J., 2009. Diversity-based, model-guided construction of synthetic gene networks with predicted functions. *Nature Biotechnology*, 27(5), pp.465–471.

Endy, D., 2005. Foundations for engineering biology. *Nature*, 438(7067), pp.449–453.

Engler, C. et al., 2009. Golden Gate Shuffling: A One-Pot DNA Shuffling Method Based on Type IIs Restriction Enzymes J. Peccoud, ed. *PLoS One*, 4(5), p.e5553.

Fujii, Y. et al., 2004. Isolation and characterization of the bacteriophage WO from Wolbachia, an arthropod endosymbiont. *Biochemical and Biophysical Research Communications*, 317(4), pp.1183–1188.

Gibson, D.G. et al., 2009. Enzymatic assembly of DNA molecules up to several hundred kilobases. *Nat Methods*, 6(5), pp.343–345.

Hale, V. et al., 2007. Microbially Derived Artemisinin: A Biotechnology Solution to the Global Problem of Access to Affordable Antimalarial Drugs. *The American Journal of Tropical Medicine and Hygiene*, 77(6 Suppl), pp.198–202.

Heinemann, M. & Panke, S., 2006. Synthetic biology--putting engineering into biology. *Bioinformatics*, 22(22), pp.2790–2799.

Hoagland, M.B. et al., 1958. A soluble ribonucleic acid intermediate in protein synthesis. *J Biol …*.

Holland, T.M. & Bundy, B.C., 2012. Streamlined extract preparation for Escherichia coli-based cell-free protein synthesis by sonication or bead vortex mixing. *Biotechniques*.

J Heinrich Matthaei, M.W.N., 1961. CHARACTERISTICS AND STABILIZATION OF DNAASE-SENSITIVE PROTEIN SYNTHESIS IN E. COLI EXTRACTS. *Proc Natl Acad Sci U S A*, 47(10), p.1580.

Jewett, M.C. & Swartz, J.R., 2004. Substrate replenishment extends protein synthesis with an in vitro translation system designed to mimic the cytoplasm. *Biotechnol Bioeng*, 87(4), pp.465–471.

Karzbrun, E. et al., 2014. Synthetic biology. Programmable on-chip DNA compartments as artificial cells. *Science*, 345(6198), pp.829–832.

Keasling, J.D., 2014. *TestimonyBefore theSubcommittee on Research and Technology Committee on Science, Space, and Technology United States House of Representatives*,

Kelly, J.R. et al., 2009. Measuring the activity of BioBrick promoters using an in vivo reference standard. *J Biol Eng*, 3, p.4.

Kigawa, T. et al., 2004. Preparation of Escherichia coli cell extract for highly productive cell-free protein expression. *J Struct Funct Genomics*, 5(1-2), pp.63–68.

Kim, D.-M. & Swartz, J.R., 2001. Regeneration of adenosine triphosphate from glycolytic intermediates for cell-free protein synthesis. *Biotechnol Bioeng*, 74(4), pp.309–316.

Kim, J. & Winfree, E., 2011. Synthetic in vitro transcriptional oscillators. *Mol Syst Biol*, 7, p.465.

Kim, J. et al., 2014. Synthetic logic circuits using RNA aptamer against T7 RNA polymerase. *bioRxiv*.

Kim, J., White, K.S. & Winfree, E., 2006. Construction of an in vitro bistable circuit from synthetic transcriptional switches. *Mol Syst Biol*, 2, p.68.

Kim, T.-W. et al., 2008. A highly efficient and economical cell-free protein synthesis system using the S12 extract of Escherichia coli. *Biotechnology and Bioprocess Engineering*, 13(4), pp.464–469.

Kim, T.-W. et al., 2007. Prolonged cell-free protein synthesis using dual energy sources: Combined use of creatine phosphate and glucose for the efficient supply of ATP and retarded accumulation of phosphate. *Biotechnol Bioeng*, 97(6), pp.1510–1515.

Kim, T.W. et al., 2006. Simple procedures for the construction of a robust and cost-effective cell-free protein synthesis system. *J Biotechnol*, 126(4), pp.554–561.

Kosuri, S. et al., 2010. A Scalable Gene Synthesis Platform Using High-Fidelity DNA Microchips. *Nature Biotechnology*, 28(12), p.1295.

Kotula, J.W. et al., 2014. Programmable bacteria detect and record an environmental signal in the mammalian gut. *Proceedings of the National Academy of Sciences of the United States of America*, 111(13), pp.4838–4843.

Kwon, Y.-C. & Jewett, M.C., 2015. High-throughput preparation methods of crude extract for robust cell-free protein synthesis. *Scientific reports*, 5, p.8663.

Lathe, R. et al., 1980. Cell-free synthesis of enterotoxin of E. coli from a cloned gene. *, Published online: 03 April 1980; | doi:10.1038/284473a0*, 284(5755), pp.473–474.

Le Cong et al., 2013. Multiplex Genome Engineering Using CRISPR/Cas Systems. *Science*, 339(6121), pp.819–823.

Lee, T.S. et al., 2011. BglBrick vectors and datasheets: A synthetic biology platform for gene expression. *J Biol Eng*, 5(1), pp.1–14.

Lilley, D.M.J., 1981. In vivo consequences of plasmid topology. *, Published online: 23 July 1981; | doi:10.1038/292380a0*, 292(5821), pp.380–382.

Liu, D.V., Zawada, J.F. & Swartz, J.R., 2005. Streamlining Escherichia Coli S30 Extract Preparation for Economical Cell-Free Protein Synthesis. *Biotechnol Prog*, 21(2), pp.460–

465.

Mandel, M. & Higa, A., 1970. Calcium-dependent bacteriophage DNA infection. *J Mol Biol*, 53(1), pp.159–162.

Martin, V.J.J. et al., 2003. Engineering a mevalonate pathway in Escherichia coli for production of terpenoids. *Nature Biotechnology*, 21(7), pp.796–802.

Miroux, B. & Walker, J.E., 1996. Over-production of Proteins inEscherichia coli: Mutant Hosts that Allow Synthesis of some Membrane Proteins and Globular Proteins at High Levels. *J Mol Biol*, 260(3), pp.289–298.

Moon, T.S. et al., 2012. Genetic programs constructed from layered logic gates in single cells. *Nature*, 491(7423), pp.249–253.

Murphy, A.C., 2011. Metabolic engineering is key to a sustainable chemical industry. *Nat. Prod. Rep.*, 28(8), pp.1406–1425.

Mutalik, V.K. et al., 2013. Precise and reliable gene expression via standard transcription and translation initiation elements. *Nat Methods*, pp.1–15.

Nakamura, C.E. & Whited, G.M., 2003. Metabolic engineering for the microbial production of 1,3-propanediol. *Curr Opin Biotechnol*, 14(5), pp.454–459.

Niederholtmeyer, H. et al., 2015. *A cell-free framework for biological systems engineering*,

Nirenberg, M.W. & Matthaei, J.H., 1961. The dependence of cell-free protein synthesis in E. coli upon naturally occurring or synthetic polyribonucleotides. *Proceedings of the National Academy of Sciences of the United States of America*, 47(10), pp.1588–1602.

Noireaux, V. et al., 2005. Toward an artificial cell based on gene expression in vesicles. *Physical Biology*, 2(3), pp.P1–P8.

Noireaux, V., Bar-Ziv, R. & Libchaber, A., 2003. Principles of cell-free genetic circuit assembly. *Proceedings of the National Academy of Sciences of the United States of America*, 100(22), pp.12672–12677.

Ochs, C.J. & Abate, A.R., 2015. Rapid modulation of droplet composition with pincer microvalves. *Lab Chip*, 15(1), pp.52–56.

Paddon, C.J. et al., 2013. High-level semi-synthetic production of the potent antimalarial artemisinin. *Nature*, 496(7446), pp.528–532.

Pardee, K. et al., 2014. Paper-Based Synthetic Gene Networks. *Cell*, 159(4), pp.940–954.

Ro, D.K. et al., 2006. Production of the antimalarial drug precursor artemisinic acid in engineered yeast. *Nature*, 440(7086), pp.940–943.

Saeidi, N. et al., 2011. Engineering microbes to sense and eradicate Pseudomonas aeruginosa, a human pathogen. *Mol Syst Biol*, 7, p.521.

Sarrion-Perdigones, A. et al., 2011. GoldenBraid: An Iterative Cloning System for Standardized Assembly of Reusable Genetic Modules J. Peccoud, ed. *PLoS One*, 6(7), p.e21622.

Satija, R. et al., 2015. Design of a Toolbox of RNA Thermometers. *bioRxiv*.

Sawasaki, T. et al., 2002. A cell-free protein synthesis system for high-throughput proteomics. *Proceedings of the National Academy of Sciences of the United States of America*, 99(23), pp.14652–14657.

Sen, S., Kim, J. & Murray, R.M., 2013. Designing Robustness to Temperature in a Feedforward Loop Circuit. *bioRxiv*.

Shen, C.R. & Liao, J.C., 2008. Metabolic engineering of Escherichia coli for 1-butanol and 1-propanol production via the keto-acid pathways. *Metab Eng*, 10(6), pp.312–320.

Shimizu, Y. et al., 2001. Cell-free translation reconstituted with purified components. *Nature Biotechnology*, 19(8), pp.751–755.

Shin, J. & Noireaux, V., 2012. An E. coliCell-Free Expression Toolbox: Application to Synthetic Gene Circuits and Artificial Cells. *ACS Synth Biol*, 1(1), pp.29–41.

Shin, J. & Noireaux, V., 2010a. Efficient cell-free expression with the endogenous E. Coli RNA polymerase and sigma factor 70. *J Biol Eng*, 4(1), pp.8–9.

Shin, J. & Noireaux, V., 2010b. Study of messenger RNA inactivation and protein degradation in an Escherichia coli cell-free expression system. *J Biol Eng*, 4(1), pp.9–9.

Shin, J., Jardine, P. & Noireaux, V., 2012. Genome Replication, Synthesis, and Assembly of the Bacteriophage T7 in a Single Cell-Free Reaction. *ACS Synth Biol*, 1(9), pp.408–413.

Siegal-Gaskins, D. et al., 2014. Gene circuit performance characterization and resource usage in a cell-free "breadboard." *ACS Synth Biol*, 3(6), pp.416–425.

Siegal-Gaskins, D., Noireaux, V. & Murray, R.M., 2013. Biomolecular resource utilization in elementary cell-free gene circuits. *2013 American Control Conference (ACC)*, pp.1531–1536.

Smanski, M.J. et al., 2014. Functional optimization of gene clusters by combinatorial design and assembly. *Nature Biotechnology*, 32(12), pp.1241–U104.

Spirin, A.S. et al., 1988. A continuous cell-free translation system capable of producing polypeptides in high yield. *Science*, 242(4882), pp.1162–1164.

Sprinzak, D. et al., 2010. Cis-interactions between Notch and Delta generate mutually exclusive signalling states. *Nature*, 465(7294), pp.86–90.

Stanton, B.C. et al., 2014. Genomic mining of prokaryotic repressors for orthogonal logic gates. *Nat Chem Biol*, 10(2), pp.99–105.

Sun, Z.Z. et al., 2014. Linear DNA for Rapid Prototyping of Synthetic Biological Circuits in an Escherichia coliBased TX-TL Cell-Free System. *ACS Synth Biol*, 3(6), pp.387–397.

Takahashi, M.K. et al., 2015. Characterizing and prototyping genetic networks with cell-free transcription–translation reactions. *Methods*.

Takahashi, M.K. et al., 2014. Rapidly Characterizing the Fast Dynamics of RNA Genetic Circuitry with Cell-Free Transcription-Translation (TX-TL) Systems. *ACS Synth Biol*.

Temme, K., Zhao, D. & Voigt, C.A., 2012. Refactoring the nitrogen fixation gene cluster from Klebsiella oxytoca. *Proceedings of the National Academy of Sciences of the United States of America*, 109(18), pp.7085–7090.

Tsuruta, H. et al., 2009. High-Level Production of Amorpha-4,11-Diene, a Precursor of the Antimalarial Agent Artemisinin, in Escherichia coli A. Gregson, ed. *PLoS One*, 4(2), pp.e4489–12.

Walker, T. et al., 2011. The wMel Wolbachia strain blocks dengue and invades caged Aedes aegypti populations. *Nature*, 476(7361), pp.450–453.

Wang, H.H. et al., 2009. Programming cells by multiplex genome engineering and accelerated evolution. *Nature*, 460(7257), pp.894–898.

Watson, J.D. & Crick, F., 1953. Molecular structure of nucleic acids. *Nature*.

Wiechert, W., 2001. 13C Metabolic Flux Analysis. *Metab Eng*, 3(3), pp.195–206.

Wood, W.B. & Berg, P., 1962. Effect of Enzymatically Synthesized Ribonucleic Acid on Amino Acid Incorporation by a Soluble Protein-Ribosome System from Escherichia Coli. *Proceedings of the National Academy of Sciences of the United States of America*, 48(1), pp.94–&.

Wu, Y.Y. et al., 2015. *Prototyping 1,4-butanediol (BDO) biosynthesis pathway in a cell-free transcription-translation (TX-TL) system*,

Yang, W.C. et al., 2012. Simplifying and streamlining Escherichia coli-based cell-free protein synthesis. *Biotechnol Prog*, 28(2), pp.413–420.

Yeung, E. et al., 2014. Modeling the effects of compositional context on promoter activity in an E. coli extract based transcription-translation system. *53rd IEEE Conference on ….*

Yim, H. et al., 2011. Metabolic engineering of Escherichia coli for direct production of 1,4-butanediol. *Nat Chem Biol*, 7(7), pp.445–452.

Zubay, G., 1973. In-Vitro Synthesis of Protein in Microbial Systems. *Annual Review of Genetics*,

7, pp.267–287.

Chapter 2: Making the breadboard accessible

Published as:

Sun ZZ*, Hayes CA*, Shin J, Caschera F, Murray RM, Noireaux V. Protocols for implementing an Escherichia coli based TX-TL cell-free expression system for synthetic biology. *J. Vis. Exp.* (79), e50762, doi:10.3791/50762 (2013)

* Equal contribution

Short Abstract

This five-day protocol outlines all steps, equipment, and supplemental software necessary for creating and running an efficient endogenous *Escherichia coli* based TX-TL cell-free expression system from scratch. With reagents, the protocol takes 8 hours or less to setup a reaction and collect and process data.

Long Abstract

Ideal cell-free expression systems can theoretically emulate an *in vivo* cellular environment in a controlled *in vitro* platform.[1] This is useful for expressing proteins and genetic circuits in a controlled manner as well as for providing a prototyping environment for synthetic biology.[2,3] To achieve the latter goal, cell-free expression systems that preserve endogenous *Escherichia coli* transcription-translation mechanisms are able to more accurately reflect *in vivo* cellular dynamics than those based on T7 RNA polymerase transcription. We describe the preparation and execution of an efficient endogenous *E. coli* based transcription-translation (TX-TL) cell-free expression system that can produce equivalent amounts of protein as T7-based systems at a 98% cost reduction to similar commercial systems.[4,5] The preparation of buffers and crude cell extract are described, as well as the execution of a three tube TX-TL reaction. The entire protocol takes five days to prepare and yields enough material for up to 3000 single reactions in one preparation. Once prepared, each reaction takes under 8 hours from setup to data collection and analysis. Mechanisms of regulation and transcription exogenous to *E. coli*, such as *lac/tet* repressors and T7 RNA polymerase, can be supplemented.[6] Endogenous properties, such as mRNA and DNA degradation rates, can also be adjusted.[7] The TX-TL cell-free expression system has been demonstrated for large-scale circuit assembly, exploring biological phenomena, and expression of proteins under both T7- and endogenous promoters.[6,8] Accompanying mathematical models are available.[9,10] The resulting system has unique applications in synthetic biology as a prototyping environment, or "TX-TL biomolecular breadboard."

Introduction

Cell-free expression technology began in the 1950's as purely translational, advancing years later to encompass coupled transcription-translation mechanisms using T7 bacteriophage DNA.[11,12] Since then, numerous efforts have been made to optimize the creation of crude cell extract (or *E. coli* S30 extract).[13,14] These optimizations include prolonging cell-free protein synthesis through ATP regeneration or strain modifications, and reducing protocol time and cost.[15-17] Alternative cell-free expression systems exist that use reconstituted components in lieu of crude cell extract for expression.[5] Both crude cell extract and reconstitution methods have been developed for commercial use.

With the advent of synthetic biology, there is an increased need for a well-characterized platform to test and express engineered biological modules and circuits.[18,19] This platform must be versatile, well-characterized, simple to manipulate, and focused on user-supplied components. Despite being developed half a century earlier, cell-free systems based on *E. coli* intrinsically share these requirements, as they are a simplified *in vitro* representation of cellular processes without the complexity of growth and metabolism. Additionally, all of the foundational knowledge from *in vivo* work on *E. coli* applies readily to *E. coli* cell-free systems.

Although cell-free expression systems can have applications in synthetic biology, to date the goal of most cell-free expression systems has been the maximization of protein and metabolite yield. This is accomplished by using T7 bacteriophage transcription of sequences driven by T7 promoters.[20] Although expression is efficient and robust, these systems serve a highly specialized purpose. Cell regulation methods are limited, target DNA templates must be reengineered to include T7 promoters, and certain sequences such as ribosomal complexes cannot be transcribed and assembled.[21,22] Existing cell-free expression systems are unable to

maintain high yields while preserving endogenous regulatory mechanisms, a versatility necessary for synthetic biology.

We have developed an endogenous *E. coli* cell-free expression system that preserves the efficiency of protein expression demonstrated by previous systems but adds additional versatility by allowing expression and regulation based on both endogenous and exogenous (T7 or other) mechanisms. The protocol described here is originally based on Kigawa et al. (2004) and Liu et al. (2005), but has significant modifications. It utilizes Mg- and K- glutamate over Mg- and K-acetate for increased efficiency, removes 2-mercaptoethanol, and lyses cells using a bead-beater.[17,23,24] Bead-beating is chosen over homogenization, pressure-based methods, or sonication due to its lower cost and comparable yields to competing systems.[23] 3-phosphoglyceric acid (3-PGA) is used as the energy source, as it was found to give superior protein yields when compared to creatine phosphate and phosphoenolpyruvate.[4,25] Our system can produce up to 0.75 mg/mL of reporter protein using either a sigma70-based promoter with lambda-phage operators or a T7-driven promoter, similar to yields from other commercial systems.[4,6] Five days are required to produce all necessary reagents (**Figure 1**). Furthermore, it provides a 98% cost reduction compared to comparable commercial cell-free systems – material costs are $0.11 per 10 μL reaction, which rises to $0.26 with labor included (**Figure 2**).

Procedure

Crude Extract Cell Preparation

Preparing crude cell extract over three days **requires two people** to conduct efficiently. The protocol functionally consists of three parts: culture growth (step 1.1 to step 1.11), cell lysis (step 1.12 to step 1.37), and extract clarification (step 1.38 to step 1.52). It is presented divided into days for convenience. Ideal extract can produce 0.75 mg/mL of deGFP from plasmid pBEST-OR2-OR1-Pr-UTR1-deGFP-T500 (addgene #40019), and has a crude cell extract concentration between 27-30 mg/mL of protein.[4] However, extract characteristics vary from batch to batch. The following recipe supplies enough for approximately 3000 single reactions (6 mL crude cell extract). If scaling down, it is recommended to use no less than 1/6 of values given here. Due to time constraints, scaling up is not recommended.

Day 1:

1.1) Prepare bacterial culture media, culture plate, and media supplements as described in **Table 1**. See **Supplemental Material 1** for recipes.

1.2) Streak BL21-Rosetta2 strain from -80°C onto a 2xYT+P+Cm agar plate and incubate for at least 15 hours at 37°C or until colonies are readily visible. *Note: Chloramphenicol (Cm) is used to select for a plasmid encoding rare tRNAs in the BL21-Rosetta2 strain.*

Day 2:

1.3) Prepare buffers and supplements as described in **Table 2**. See **Supplemental Material 1**

for recipes.

1.4) Prepare and sterilize materials required for day 3, including: 6 x 4 L Erlenmeyer flasks with aluminum foil cover (autoclaved), 4 x 1 L sterile centrifuge bottles, funnel (autoclaved), 100 g of 0.1 mm glass beads (autoclaved), 2 stir-bars (autoclaved), 1 L and 500 mL graduated cylinder (autoclaved), 2 x 1 L beakers (autoclaved), 3 mL syringe with 18-gauge needles (sterile), 2-3 float buoys, 2-3 10k MWCO dialysis cassettes (sterile), cuvettes.

1.5) Prepare mini-culture 1. Add 4 mL of 2xYT+P media and 4 µL of Cm to a 12 mL sterile culture tube and pre-warm to 37°C for 30 minutes.

1.6) Inoculate mini-culture 1 with a colony from the 2xYT+P+Cm agar plate. Incubate at 220 rpm, 37°C for 8 hours.

1.7) 7 hours and 30 minutes later, prepare mini-culture 2. Add 50 mL of 2xYT+P media and 50 µL of Cm to a sterile 250 mL Erlenmeyer flask and pre-warm to 37°C for 30 minutes.

1.8) Inoculate mini-culture 2 with 100 µL of mini-culture 1 and incubate at 220 rpm, 37°C for 8 hours.

Day 3:

1.9) Weigh four empty sterile 50 mL Falcon tubes and record mass in **Table 3**. Chill Falcon tubes on ice; these will be subsequently used in step 1.18.

1.10) 7 hours and 30 minutes after step 1.8, prepare final bacterial culture media. Using a sterile 1 L graduated cylinder, transfer 660 mL of 2xYT+P media into each of six 4 L Erlenmeyer flasks and pre-warm to 37°C for 30 minutes. *Note: 4 L or larger Erlenmeyer flasks are recommended for proper aeration.*

1.11) Add 6.6 mL of mini-culture 2 into each 4 L Erlenmeyer flask. Incubate at 220 rpm, 37°C until the culture reaches an OD of 1.5-2.0 at 600 nm (corresponding to mid-log growth phase). Check OD periodically with a 1:10 culture dilution for accuracy. **This step should take no more than 3h – 3h45min; rapid growth and collection during mid-log phase is critical for extract quality.**

1.12) Immediately after growth, transfer all cultures evenly into four 1 L centrifuge bottles and centrifuge at 5000 g for 12 minutes at 4°C to pellet bacterial cells.

1.13) While centrifuging, complete S30A buffer preparation by adding 4 mL of 1 M DTT to 2 L of previously prepared S30A. Mix and maintain buffer on ice.

1.14) When centrifuging is finished, completely remove supernatant from step 1.12 by decanting and blotting the centrifuge bottles on a sterile paper towel.

1.15) Add 200 mL of S30A buffer at 4°C to each of the four centrifuge bottles, and shake the bottles vigorously until **pellet is completely solubilized with no remaining clumps.** Centrifuge the four bottles at 5000 g for 12 minutes at 4°C.

1.16) Completely remove supernatant from previous step by decanting and blotting the centrifuge bottles on a sterile paper towel.

1.17) Repeat steps 1.15 and 1.16.

1.18) Add 40 mL S30A buffer at 4°C to each centrifuge bottle. Transfer each pellet and S30A combination into a chilled Falcon tube from 1.9). *Note: This step is to transfer the pellets into a smaller container.*

1.19) Centrifuge the Falcon tubes at 2000 g for 8 minutes at 4°C. Remove supernatant by decanting.

1.20) Re-centrifuge the Falcon tubes at 2000 g for 2 minutes at 4°C. Completely remove

residual supernatant by pipet. Keep on ice.

1.21) Weigh the four Falcon tubes with pellet and record mass in **Table 3**. Calculate pellet mass, S30A buffer volume needed, and mass of beads needed based on the specific formulas in **Table 3**.

1.22) **Correct loading and bead beating of the pellet is critical to making quality extract, and is the most challenging step. It is recommended to review the video before attempting. Failure to avoid air bubbles and distribute beads evenly will result in inefficient extract.**

1.23) Add the amount of S30A buffer calculated in **Table 3** to each Falcon tube, vortex until homogenous, and return to ice.

1.24) While keeping the other Falcon tubes on ice, add beads intermittently to a single Falcon tube **in three aliquots, each using 1/3 of the total beads**. After addition of each aliquot of beads, vortex for 30 seconds. Place Falcon tube on ice between vortex steps and after final vortex. After last aliquot is added, **ensure beads are uniformly distributed**. **A thick paste should be formed.**

1.25) Prepare a 5 mL (volume) pipet tip by cutting off the end using a sterile razor blade to create a 3-4 mm opening. Dial pipet to 2 mL. *Note: Different pipet sets and tips provide different amounts of suction that may not be sufficient to pull and release thick bead-cell solution; a 1mL pipet tip with end removed can be used in lieu.*

1.26) Place 20 bead-beating tubes on ice.

1.27) Verify high viscosity of cell-bead solution using modified pipet. It should be viscous to the point of barely exiting the pipet tip during ejection. If too viscous, re-adjust pipet tip according to step 1.25. If not viscous enough, beads can be added in increments of **(pellet**

mass * 0.05), to a maximum mass of **(pellet mass * 5.1)**. After each addition of beads, vortex for 30 seconds and return to ice. See **Figure 3a** for a demonstration of viscosity.

1.28) Remove bead-cell solution from Falcon tube using modified pipet, and transfer into a sterile bead-beating tube, filling it three-quarters full with bead-cell solution. Spin **extremely briefly (1s)** on a counter mini-centrifuge to remove air bubbles without redistributing beads. See **Figure 3b-d** for still images of bead-beating tube loading.

1.29) Finish adding bead-cell solution to form a concave meniscus.

1.30) Add a very small drop of bead-cell solution onto the inside of a bead-beating tube cap, **being careful to not impede the outside lip of the cap; otherwise, the bead-beating tube will not close sufficiently.** Tap the cap on a flat surface and **verify that there are no air bubbles on the bottom of the cap**.

1.31) Cap the bead-beating tube with the bead-beating cap from the previous step. Hand to assistant for bead beating. If done correctly, the **cap should be tightly sealed, no air bubbles should be visible, and little (if any) bead-cell solution should overflow.** Redo the loading process if air bubbles are visible or the cap does not fully close.

1.32) Vortex Falcon tube from step 1.24 with the remaining bead-cell solution to ensure even distribution of beads. Repeat steps 1.28 to 1.31 until Falcon tube is empty; then repeat steps 1.24 to 1.31 for each additional Falcon tube.

1.33) **Conduct steps 1.33 to 1.38 simultaneously.** Have assistant take filled bead-beating tubes from 1.31 and place on ice**.** Once two filled bead-beating tubes have been collected and have been on ice for at least one minute, begin bead beating.

1.34) Beat one tube for 30 seconds at 46 rpm. Place upside down on ice for 30 seconds while beating the other tube.

1.35) Repeat previous step such that each filled bead-beating tube has been beat for 1 minute total.

1.36) Repeat steps 1.33 to 1.35 until 8 filled bead-beating tubes (or the maximum amount the centrifuge can hold) have been processed. Then, construct filter apparatus from 15 mL Falcon (**Figure 3e**). Add a new bead-beating cap, flat-part face up, to the bottom of a 15 mL Falcon. Then, remove cap from processed bead-beating tube and **press micro-chromatography column firmly onto end of processed bead-beating tube until completely sealed**. Snap off elution end of micro-chromatography column, and place micro-chromatography column, elution end down, into empty bead-beading tube. Place this complex into 15 mL Falcon. Repeat for all 8 filled bead-beating tubes; keep on ice when complete.

1.37) Centrifuge 8 filter apparatuses, Falcon tube uncapped, at 6000 g for 5 minutes at 4°C to separate extract and pellet from beads.

1.38) **Verify each bead-beating tube has produced viable extract.** Properly beat extract will not be turbid, and the pellet will have two distinct layers. Discard all turbid tubes, and transfer the supernatant from non-turbid tubes into individual 1.75 mL micro-centrifuge tubes, **taking as little pellet as possible**. Keep on ice until all bead-beating tubes have been processed. See **Figure 3f** comparing a correctly vs. incorrectly processed bead-beating tube.

1.39) Centrifuge micro-centrifuge tubes from previous step at 12000 g for 10 minutes at 4°C.

1.40) Transfer **pellet-free supernatant** into empty bead-beating tubes using a pipet, consolidating 500 µL into a new bead-beating tube.

1.41) Incubate previous step, **with bead-beating caps removed**, at 220 rpm, 37°C for 80

minutes. This step digests remaining nucleic acids using endogenous exonucleases released during the bead-beading process, and can be done by standing the bead-beating tube up in a tissue culture tube.

1.42) Prepare dialysis materials. Complete S30B buffer preparation by adding 2 mL of 1 M DTT to 2 L of previously prepared S30B. Mix and add 900 mL into each of two sterile 1 L beakers. Add sterile magnetic stirrer into each beaker; keep at 4°C.

1.43) After step 1.41, **extract should look turbid**. Consolidate extract into 1.5 mL aliquots in 1.75 mL micro-centrifuge tubes, and centrifuge at 12000 g for 10 minutes at 4°C.

1.44) Using a pipet, consolidate **pellet-free supernatant** into 15 mL Falcon tubes on ice, and mix well by capping the tube and inverting. **Save 10 µL of supernatant on ice for step 1.47.**

1.45) Determine total amount of extract produced, and hydrate the necessary number of 10k MWCO dialysis cassettes by submersing in S30B for 2 minutes, assuming 2.5 mL of extract per cassette.

1.46) Load cassettes with 2.5 mL of extract. Each beaker can take up to 2 cassettes; dialyze, stirring, at 4°C for 3 hours. *Note: partial loading of cassettes is acceptable. Dialyzing increases protein production yield.*

1.47) During the previous step, characterize extract protein concentration with a Bradford assay, using extract saved in step 1.44. See **Supplemental Material 2** for details.

1.48) After dialysis is complete, aliquot extract by 1.5 mL in 1.75 mL micro-centrifuge tubes. Centrifuge at 12000 g for 10 minutes at 4°C. A pellet will form at the bottom of the tube.

1.49) Consolidate clear supernatant from previous step by pipetting into a 15 mL Falcon tube on ice. Homogenize by inverting 5-10 times.

1.50) Based on concentration determined by Bradford in step 1.47, determine amount of extract to aliquot into individual 1.75 mL tubes. **Each individual tube should have a volume with 810-900 mg of total protein. Extract should have a total protein concentration greater than 27 mg/mL. This step requires assistance to conduct expediently.** *Note: Aliquot extract below 30 mg/mL into 30 µL aliquots, and scale if concentration is higher; for example, aliquot extract at 28 mg/mL by 30 µL, and aliquot extract at 32 mg/mL by 28.1 µL.*

1.51) Aliquot extract following step 1.50, taking care to avoid bubbles. Flash-freeze extract in liquid nitrogen. *Note: Aliquots with bubbles can be removed by centrifuging at 10000 g for 30 seconds at 4°C.*

1.52) Remove tubes from liquid nitrogen using a strainer and immediately store at -80°C. **Safety: Wear protective eyewear; the caps of extract tubes may come off due to the temperature difference between liquid nitrogen and room temperature.**

Amino Acid Solution Preparation

Amino Acid Solution should be prepared in bulk. The following recipe utilizes one full kit of RTS Amino Acid Sampler, supplying enough for approximately 11000 single reactions. If scaling down, it is recommended to use no less than half a kit. Each amino acid in the stock is supplied at 1.5 mL, 168 mM, except for leucine at 140 mM. The final composition of Amino Acid Solution is leucine, 5 mM, all other amino acids, 6 mM. This is 4x working concentration.

2.1) Remove all 20 amino acids from -20°C and thaw at room temperature. Once thawed, vortex until amino acids dissolve, incubating at 37°C if necessary. After amino acids are dissolved, put all amino acids on ice **except for Asn, Phe, and Cys, which are kept at room temperature. Cys may not fully dissolve.**

2.2) On ice, add 12 mL of sterile water to a sterile 50mL Falcon tube.

2.3) Add 1.5 mL of each amino acid **in the following order**, taking care to vortex the Falcon tube after each addition and to keep the solution on ice: Ala, Arg, Asn, Asp, Gln, Glu, Gly, His, Ile, Lys, Met, Phe, Pro, Ser, Thr, Val, Trp, Tyr, Leu, Cys. Cys can be added as a suspension. **After addition, vortex until solution is relatively clear, incubating at 37°C if necessary. Cys may not fully dissolve.**

2.4) Aliquot Amino Acid Solution into 50 tubes at 26 µL each on ice. Aliquot the rest at 500 µL per tube on ice. The 26 µL aliquots will be used for calibrating extract, while the 500 µL aliquots will be used for preparing buffer. **While aliquoting, vortex the main stock frequently to avoid unequal distribution of suspension.**

2.5) Flash freeze aliquots in liquid nitrogen and store at -80°C. **Safety: Wear protective**

eyewear; the caps of extract tubes may come off due to the temperature difference between liquid nitrogen and room temperature.

2.6) Optional: Conduct an activity assay of newly-made Amino Acid Solution against previously made Amino Acid Solutions.

Energy Solution Preparation

Energy Solution is used both for calibrating crude cell extract and for creating buffer, and should be prepared in bulk. The following recipe supplies enough for approximately 10000 single reactions. If scaling down, it is recommended to use no less than 1/24 of values given here. As the Energy Solution is a significant monetary cost, first time users may want to prepare at 1/24 scale. The final composition of Energy Solution is HEPES pH 8 700 mM, ATP 21 mM, GTP 21 mM, CTP 12.6 mM, UTP 12.6 mM, tRNA 2.8 mg/mL, CoA 3.64 mM, NAD 4.62 mM, cAMP 10.5 mM, Folinic Acid 0.95 mM, Spermidine 14 mM, and 3-PGA 420 mM. This is 14x working concentration. If desired, each individual item in **Table 4** can be stored at -80°C for later use.

3.1) Remove all chemicals in **Table 4** from -80°C, -20°C, or 4°C to room temperature for 30 minutes.

3.2) Prepare stock solutions as described in **Table 4**. See **Supplemental Material 1** for recipes. Place all solutions on ice after preparation.

3.3) In a 15 mL Falcon tube, add **in the following order,** taking care to vortex the Falcon tube after each addition and to keep the solutions on ice: 3.6 mL 2 M HEPES, 144 µL water, 1.39 mL nucleotide mix, 576 µL 50 mg/mL tRNA, 576 µL 65 mM CoA, 276 µL 175 mM NAD, 170 µL 650 mM cAMP, 288 µL 33.9 mM Folinic acid, 144 µL 1 M spermidine, and 3.09 mL 1.4 M 3-PGA.

3.4) Aliquot Energy Solution into 50 tubes at 7 µL each on ice. Aliquot the rest at 150 µL per tube on ice. The 7 µL aliquots will be used for calibrating extract, while the 150 µL aliquots will be used for preparing buffer. **While aliquoting, vortex the main stock**

frequently.

3.5) Flash freeze aliquots in liquid nitrogen and store at -80°C. **Safety: Wear protective eyewear; the caps of extract tubes may come off due to the temperature difference between liquid nitrogen and room temperature.**

3.6) Optional: Conduct an activity assay of newly made Energy Solution against previously made Energy Solutions.

Buffer Preparation

Buffer Preparation requires the completion of Crude Cell Extract Preparation, Amino Acid Solution Preparation, and Energy Solution Preparation. **Each buffer is unique to a batch of crude cell extract.** Mg-glutamate, K-glutamate, and DTT (in that order) are optimized in this section to produce reactions with maximum levels of expression. The following protocol utilizes a pre-written template, TXTL_e(template)_calibration_JoVE.xlsx (**Supplemental Material 3**), to calibrate pre-prepared crude cell extract and prepare buffer. However, one can also calibrate crude cell extract and prepare buffer without the template by optimizing Mg-glutamate, K-glutamate, and DTT manually and setting up buffer such that along with extract, it is 75% of a total reaction volume. If calibrating manually, final reaction conditions can be found in step 5.

4.1) Complete the "General Data" form.

4.2) Thaw on ice 100 mM Mg-glutamate (4°C), 3 M K-glutamate (4°C), 6 mM Amino Acid Solution (26 µL, -80°C), Energy Solution (7 µL, -80°C), 100 mM DTT (-20°C), positive control DNA (-20°C), 40% PEG-8000 (4°C), crude cell extract (-80°C), and water (4°C). *Note: Use 1 nM working concentration pBEST-OR2-OR1-Pr-UTR1-deGFP-T500 (Addgene plasmid 40019) for the positive control (excitation 485 nm, emission 525 nm), or another reference which produces high signal intensity.*[4]

4.3) Prepare seven 10.5 µL reactions, testing a range of 4-10 mM additional Mg-glutamate, by aliquoting set amounts of stock Mg-glutamate into individual micro-centrifuge tubes. *Note: Although 10.5 µL reactions are initially prepared, the final reaction is 10 µL.*

4.4) Prepare master mix as indicated in the template under "Mg-glutamate calibration,"

adding an extra 80 mM of K-glutamate. Keep on ice and **vortex after the addition of each item**. *Note: The values given here and in the template are in addition to the amounts of Mg-glutamate, K-glutamate, and DTT present in the S30B buffer used to make crude cell extract.*

4.5) Add master mix to samples containing Mg-glutamate and prepare reactions. See steps 5.10 to 5.13 for detailed instructions.

4.6) Run reaction at 29°C, either in an incubator or a plate reader.

4.7) Determine optimum Mg-glutamate concentration by end-expression level and maximal rate of protein expression (**Figure 4a**). *Note: Runtimes vary depending on experiment but typically last under 8 hours*.

4.8) Repeat steps 4.2 to 4.7 for K-glutamate under "K-glutamate calibration," setting Mg-glutamate levels to those found in step 4.7.

4.9) Repeat steps 4.2 to 4.7 for DTT under "DTT calibration," setting Mg-glutamate levels to those found in step 4.7 and K-glutamate levels to those found in step 4.8. *Note: We have found that added DTT does not significantly affect end-expression levels.*

4.10) Use values found in calibration under "Buffer composition" to determine the composition of buffer to be prepared. Based on the amount of crude cell extract produced, a master mix recipe is produced for a set amount of buffers.

4.11) Thaw aliquots as listed in master mix recipe on ice. Once thawed, prepare master mix, keeping on ice and **vortexing after the addition of each item**.

4.12) Aliquot by amount stated under "Buffer composition." Flash-freeze buffer tubes in liquid nitrogen. **While aliquoting, vortex the main stock frequently.**

4.13) Remove tubes from liquid nitrogen using a strainer and immediately store at -80°C.

Safety: Wear protective eyewear; the caps of extract tubes may come off due to the temperature difference between liquid nitrogen and room temperature.

Experimental Execution of a TX-TL Reaction

Final reaction conditions are: 8.9-9.9 mg/mL protein (from crude extract), 4.5 mM-10.5 mM Mg-glutamate, 40-160 mM K-glutamate, 0.33-3.33 mM DTT, 1.5 mM each amino acid except leucine, 1.25 mM leucine, 50 mM HEPES, 1.5 mM ATP and GTP, 0.9 mM CTP and UTP, 0.2 mg/mL tRNA, 0.26 mM CoA, 0.33 mM NAD, 0.75 mM cAMP, 0.068 mM folinic acid, 1 mM spermidine, 30 mM 3-PGA, and 2% PEG-8000. **A basic TX-TL reaction has 3 parts (tubes): crude cell extract, buffer, and DNA.** The ratio is: 75% buffer and extract, 25% DNA. **Reactions can vary in volume**, and we use 10 µL by convention to minimize reaction volume and enable running in a 384-well plate. Larger volumes require agitation for proper oxygenation. The following protocol utilizes a pre-written template, TXTL_JoVE.xlsx (**Supplemental Material 4**), to conduct a 10 µL reaction. **Items in purple indicate user-input values, and items in blue indicate additional reagents to add to the reaction.** However, one can also conduct a reaction without the template by following reaction conditions outlined above.

5.1) Complete the "General Data" form.

5.2) Under "Master Mix Preparation," insert the extract percentage value from step 4.1 into the purple box.

5.3) Design your experiment *in silico* using the "Master Mix Preparation" (rows 10-17) and "DNA Preparation" (rows 19-50) sections. Generally, constants can be put into the "Master Mix Preparation" section, while variables can be put into the "DNA Preparation" section. **Minimize samples per experiment to avoid sample evaporation and experimental start time bias.** See **Figure 6** for a sample setup.

5.4) Under "Master Mix Preparation," add reagents such as inducers or proteins, which will go in all samples at a constant concentration. Starting with row 14, fill out the blue

shaded areas, keeping one reagent to each line. Units are relative ratios.

5.5) Under "DNA Preparation," add DNA which will be sample specific. Sample IDs #1 and #2 correspond to positive and negative controls, respectively. Sample IDs #3 and above are user-modifiable for DNA, stock concentration in ng/μL, length in base pairs, desired final concentration in nM, and repeats (of 10 μL reactions). The amount of stock DNA to reach desired final concentration is automatically calculated. The total across the row sums to 10.5*n, where n is the number of repeats. *Note: Although the final reaction volume is 10 μL, the calculations assume a total volume of 10.5 μL per reaction, to account for volume lost during pipetting.*

5.6) Under "DNA Preparation," add reagents or additional DNA which will be sample specific to blue columns. Stock DNA concentrations in nM can be calculated under "DNA Preparation," while sample specific reagents require manual calculation based on a total reaction volume of 10.5*n. The entered volumes are subtracted out of the water volume of the same row.

5.7) Remove needed number of tubes of buffer, crude cell extract, and positive control under "Tubes to thaw," from -20°C or -80°C and thaw on ice.

5.8) Prepare DNA samples. For each sample ID, aliquot out the indicated DNA, water, and user-supplied items per the "DNA Preparation" section into a micro-centrifuge tube, at room temperature. *Note: to avoid sample loss, recently calibrated pipets and low-stick pipet tips and micro-centrifuge tubes are recommended.*

5.9) When tubes from step 5.7 are thawed, prepare the master mix consisting of buffer, extract, and any global user-supplied items based on the orange-shaded boxes, keeping on ice and **vortexing after the addition of each item**. *Note: Extract is extremely viscous.*

Aliquots with bubbles can be removed by centrifuging at 10000 g for 30 seconds at 4°C.

5.10) Add the amount of master mix indicated in the orange cells under "DNA Preparation" (column O) to each DNA sample, and keep at room temperature. **Treat this as the reaction start time.**

5.11) Vortex each sample, and centrifuge at 10000 g for 30 seconds at room temperature to bring down any residual sample and to reduce bubbles.

5.12) If conducting reaction in micro-centrifuge tubes, incubate directly at 29°C. Otherwise, pipet 10 µL of sample into a 384-well plate. *Note: Reactions in volumes greater than 10 µL may require agitation for oxygenation.*

5.13) Centrifuge plate at 4000 g for 30 seconds at room temperature to bring down any residual sample and to reduce bubbles. Seal plate afterwards to prevent evaporation.

5.14) Run reaction at 29°C. *Note: Runtimes vary depending on experiment but typically last under 8 hours*.

Representative Results

We have presented a five day protocol for the preparation of an endogenous *Escherichia coli* based TX-TL cell-free expression system**.** A sample timeline for creating the reagents – crude cell extract and buffer – can be found in **Figure 1**. Once created, these reagents can be stored at -80°C for up to one year. After reagents are created, experimental setup and execution can be done in less than 8 hours.

We optimized the expression conditions of the TX-TL cell-free expression system. Other user-supplied additions, such as buffers or DNA solutions, should be calibrated for toxicity beforehand. For example, different methods of processing plasmids result in different expression due to salt content. We also tested the effect of Tris-Cl elution buffer on reaction efficiency (**Figure 5**).

An example of crude cell extract calibration, referring step 4.1 to 4.9, is shown in **Figure 4a**. In general, our experiments show that the crude cell extract is most sensitive to Mg-glutamate levels, followed by K-glutamate levels. To demonstrate the cell-free expression system, we constructed and tested a negative feedback loop based on *tet* repression.[26] (**Figure 6)**. In the cell-free expression system, the same circuit run with and without aTc shows a 7-fold end-point expression change of deGFP reporter after eight hours of expression. Although this experiment does not require global inducers or repressors, if necessary they can be added under "Master Mix Preparation."

Discussion

The endogenous *Escherichia coli* based TX-TL cell-free expression system described here is an easy-to-run three tube reaction that can take less than eight hours from set up to data collection. The process of creating all reagents requires five days' time total (with significant labor requirements on only one day), but produces crude extract for 3000 reactions and buffer-making reagents for 10000 reactions (**Figure 1**). Furthermore, crude extract and buffer-making reagents are stable for at least 1 year at -80°C, allowing for multiple uses of one preparation.[4] At \$0.11 per 10 μL reaction (\$0.26 including labor), costs are 98% lower than comparable commercial systems (**Figure 2**).

There are some unresolved limitations, however, to the system. The end efficiency of each crude cell extract preparation can vary based on user proficiency and on environmental conditions, although typical yield variation is between 5-10% (**Figure 4b**). As a result, batch-to-batch variability in both end-point expression and in expression dynamics are to be expected. These variations will likely remain until extract is fully characterized or until extract creation is fully automated. If the cell-free expression system is used to conduct sensitive quantitative experiments, it is advisable to run all experiments with the same batch of crude cell extract. The yield from a single crude cell extract batch, about 3000 reactions, should be sufficient for typical experimental courses. Although we suspect variation can be removed by scaling up and automating the procedure, such attempts would involve a substantial resource investment.

Additionally, although end-point expression levels are reasonably easy to determine, more work needs to be done in understanding dynamics intrinsic to the cell-free system. It is known that both resource competition and resource limitation can affect expression dynamics.

For example, limited endogenous sigma 70 can result in a saturating regime with increased DNA template producing an expression profile analogous to that of nucleotide or amino acid depletion.[9,27] However, dynamics do not have to be fully understood to utilize the system. For pure increases of yield, optimization can be done by machine-learning approaches.[28] Questions of resource competition and limitation can be addressed by mathematical models verified using experimental data.

The protocol presented here is optimized for a BL21-Rosetta2 strain, but is generalizable to other *E. coli* strains. Modifications in BL21-Rosetta2, such as the removal of the gene encoding lon protease and the addition of genes encoding rare tRNAs, allow for maximal protein production. We have attempted the protocol with two other extract strains – BL21 only and a BL21 *trxA* knockout –and found 50% less protein yield. We hypothesize that yields similarly decrease when using other strains. Other changes in parameters, such as switching 2xYT growth medium for LB and other rich broths, have resulted in decreased protein yield.

Cell-free expression systems utilizing both endogenous and exogenous transcription-translation machinery and regulation mechanisms have wide applications in both protein and metabolite expression and in synthetic biology.[3,29] Instead of being limited to T7-regulated circuits, one can envision producing complex biomolecules in a user-controllable setting using a mix of native *E. coli* promoters and exogenously supplied transcription and regulation mechanisms. Without limitations of cell division and metabolism, variability in synthetic circuits such as the repressilator or in metabolic engineered pathways such as those producing artemisinin can be reduced or better understood.[30,31] We have used these advantages to implement genetic switches, as well as to understand sigma factor sequestration.[9,32] Such technology can also form the backbone of "minimal" or "artificial" cells – small, well-

characterized, and self-sufficient embodied units of extract.[33,34]

Ultimately, we anticipate immediate uses of this endogenous cell-free expression system as a prototyping environment for synthetic biology. Nicknamed the "TX-TL biomolecular breadboard," the cell-free expression system provides a controllable environment where synthetic circuits ultimately destined for *in vivo* expression can undergo rounds of prototyping – cycles of testing on basic plasmid, linear, or chemically synthetized DNA, followed by analysis and rapid modification. Prototyping rounds can be aided by predictive mathematical models currently being developed. By removing cloning and *in vivo* manipulation for non-final circuits, we anticipate engineering cycle times to be reduced to 1-3 days instead of the current weeks' standard.

Acknowledgements

We thank Jongmin Kim, Dan Siegal-Gaskins, Anu Thubagere, and Enoch Yeung for assistance streamlining the protocol, and Clare Chen and Barclay Lee for assistance in the early stages of the project. This material is based upon work supported in part by the Defense Advanced Research Projects Agency (DARPA/MTO) Living Foundries program, contract number HR0011-12-C-0065 (DARPA/CMO. Z.Z.S. is also supported by a UCLA/Caltech Medical Scientist Training Program fellowship and by a DoD, Air Force Office of Scientific Research, National Defense Science and Engineering Graduate (NDSEG) Fellowship, 32 CFR 168a. The views and conclusions contained in this document are those of the authors and should not be interpreted as representing officially policies, either expressly or implied, of the Defense Advanced Research Projects Agency or the U.S. Government.

Disclosures

The authors declare that they have no competing financial interests.

Figure 1

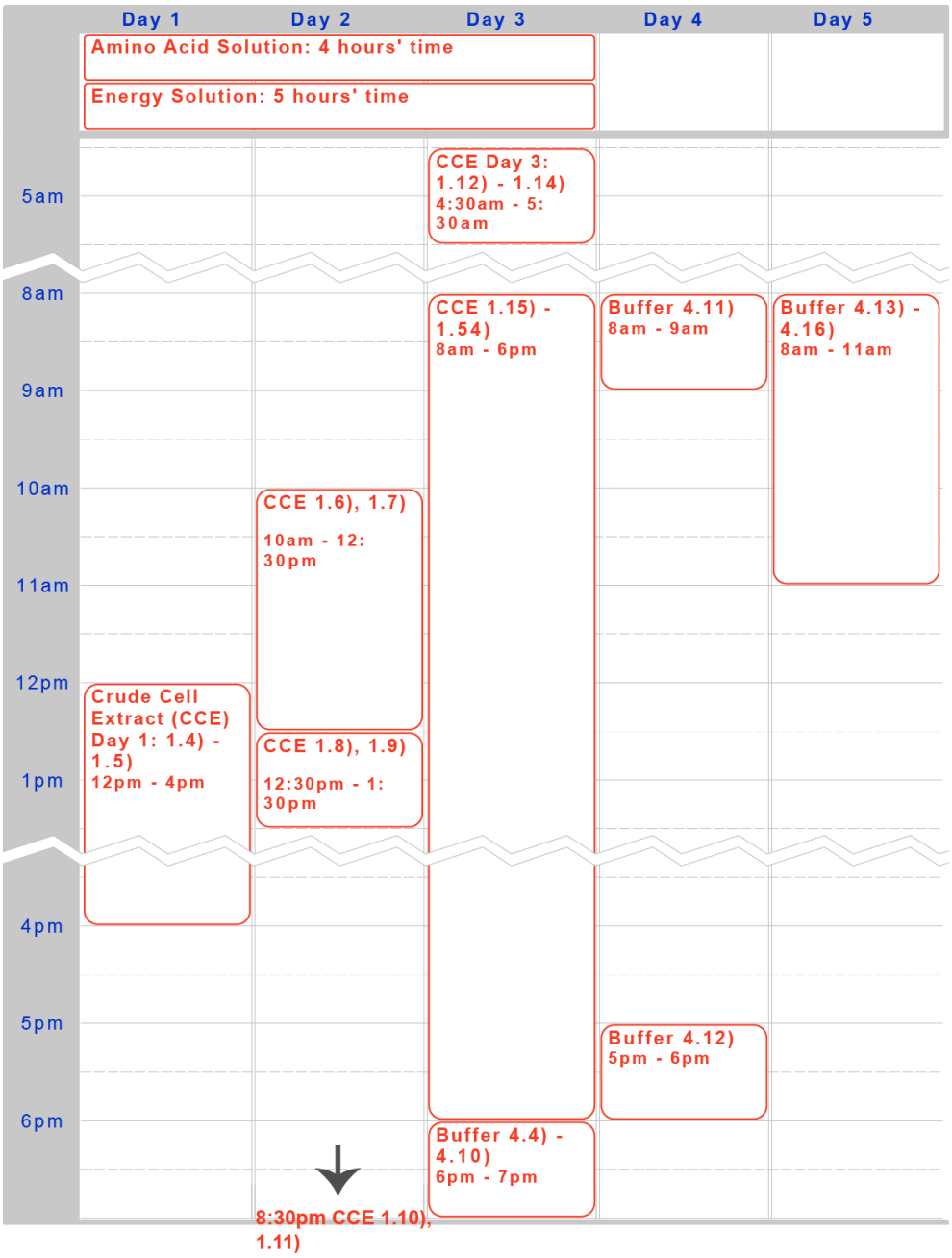

Figure 1. Timeline for crude cell extract, amino acid solution, and energy solution preparation. A five-day timeline for a typical execution of the protocol is given above, optimized for overnight incubations and daytime working steps.

Figure 2

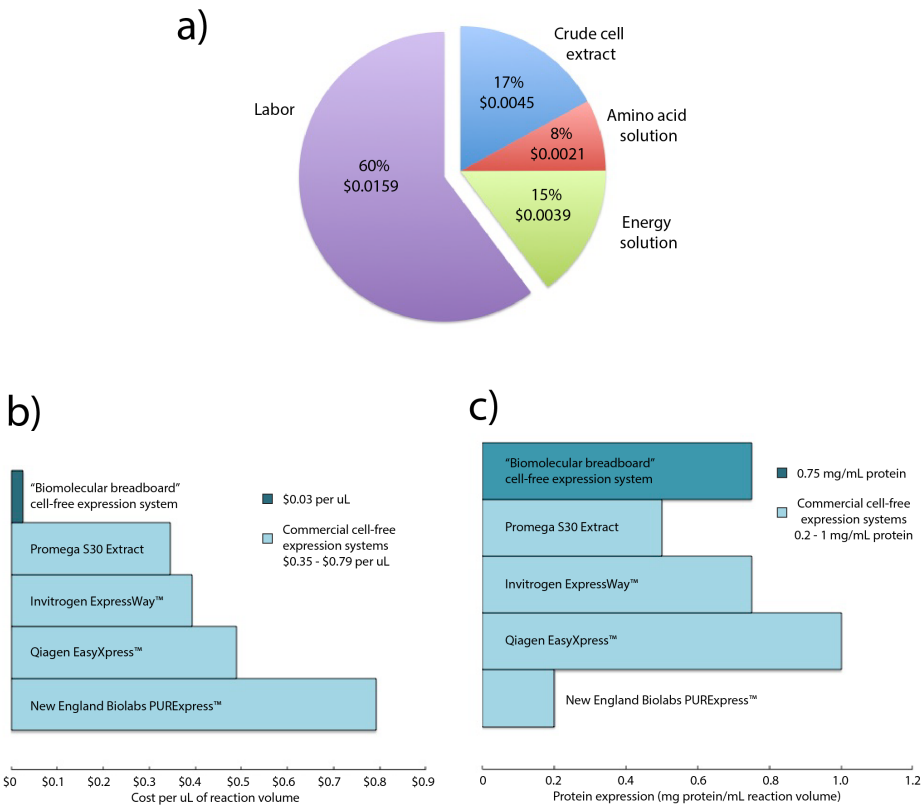

Figure 2. Cost and expression analysis of competing crude cell extracts. a) Breakdown of the costs of labor and materials of the TX-TL cell-free expression system. **Based on costs of reagents as of December 2012, and labor costs of $14 per hour**. b) Comparison of TX-TL cell-free expression system costs vs. other commercial systems. **Costs are broken down per µL, although reaction volumes may vary per kit.** c) Comparison of TX-TL cell-free expression system yield vs. other commercial systems. **Protein expression yield determined by manufacturer standards.**

Figure 3

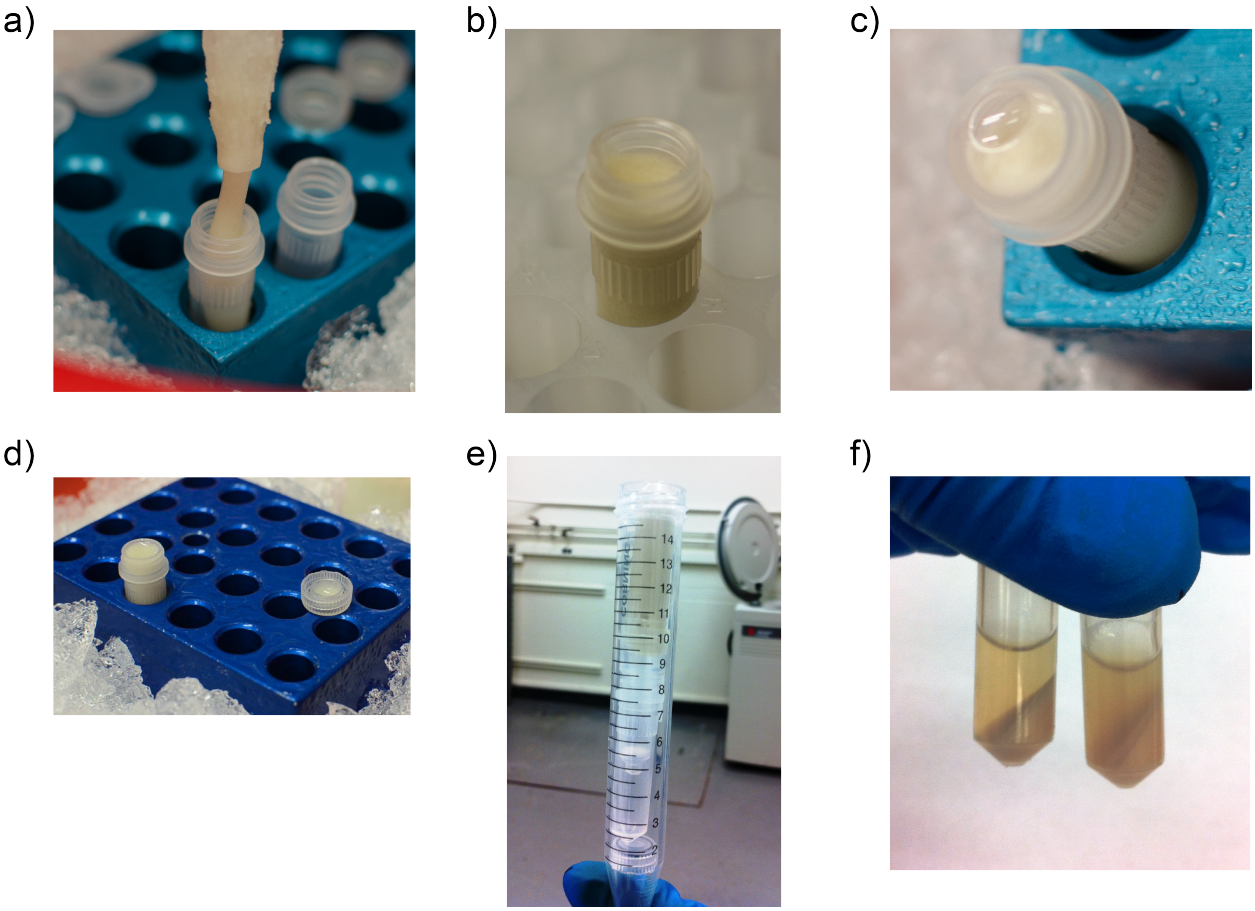

Figure 3. Loading and processing of a bead-beating tube. a) Demonstration of correct viscosity of cell-bead solution. Cell-bead solution will have a viscosity dependent on many factors, including amount of S30A buffer added, amount of beads added, and time spent on ice. **b) Loading of bead-beating tube before quick tabletop centrifugation.** The centrifugation removes bubbles accumulated during loading. **c) Bubbles surfacing after tabletop centrifugation.** The size of the bubbles will vary; they can be popped or removed using a pipet tip. **d) Completely filled bead-beating tube before capping.** A meniscus is formed in the bead-beating tube, and the cap has enough to cover and cause small amounts to overfill. **e) Correctly loaded filter apparatus.** These can be reused. **f) Comparison of correctly vs. incorrectly processed bead-beating tube.** The tube on the left is a well-beat tube – it features a small and well-delineated top layer, and very clear supernatant. The tube on the right is suboptimal, based on the larger, hazy second layer and the hazy supernatant. Tubes that are suboptimal should not undergo additional processing.

Figure 4

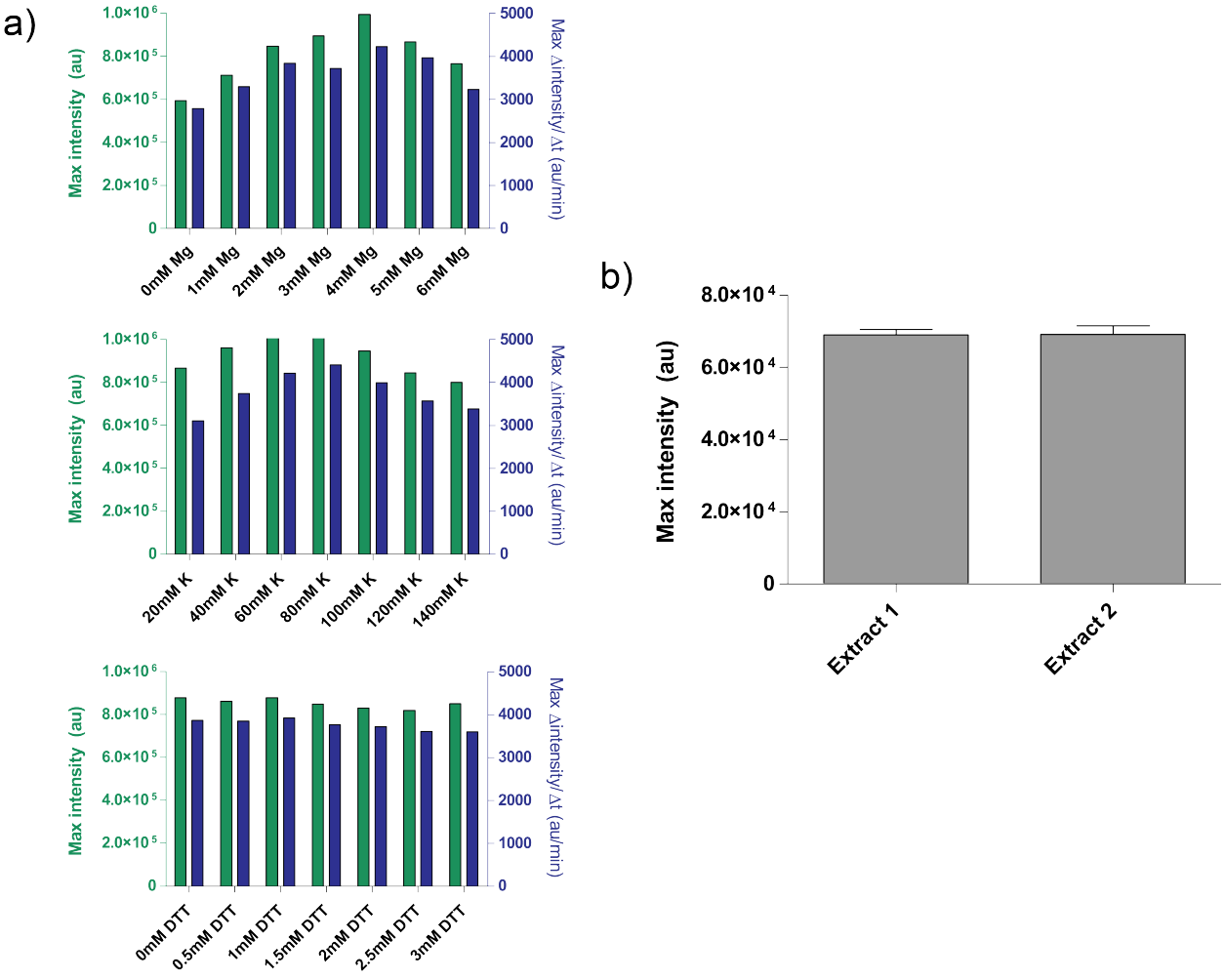

Figure 4. Properties of crude extract preparations. a) Typical calibration plots for crude cell extract. Crude extract is calibrated for additional Mg-glutamate, K-glutamate, and DTT levels, in that order. Shown is endpoint fluorescence after 8 hours, as well as maximal rate of protein production based on a 12-minute moving average. Based on these plots, an acceptable range of additional Mg-glutamate is 4 mM, K-glutamate is 60-80 mM, and DTT is 0-3 mM. Note that every crude extract needs to be calibrated independently for these three variables. **b) Variation from extract preparations.** Endpoint fluorescence of two crude extracts prepared on different dates is shown; error bars are 1 standard deviation from three independent runs on different days.

Figure 5

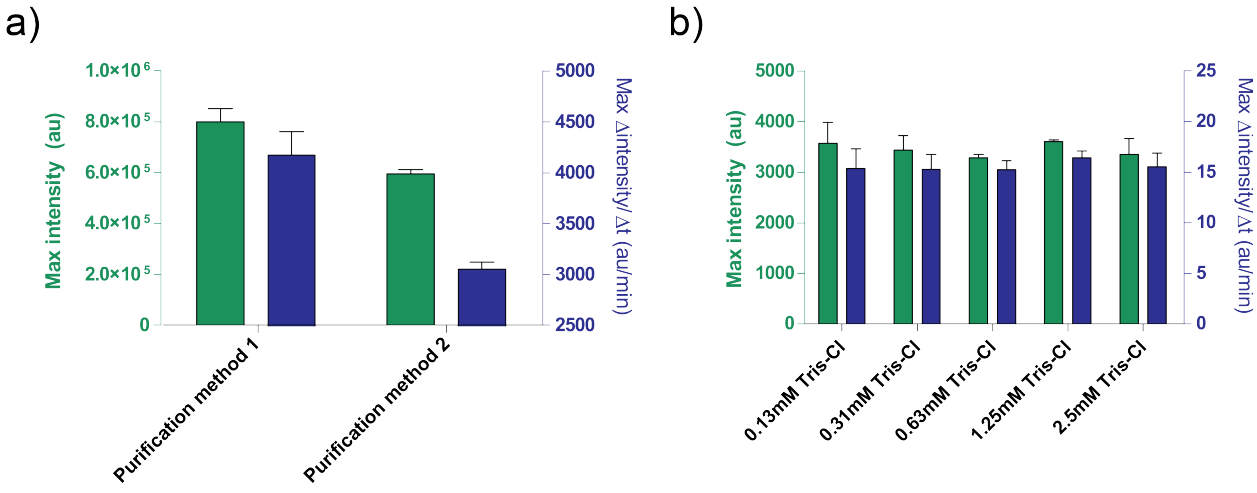

Figure 5. Effects of DNA solution on expression efficiency. a) Comparison of two different purification methods for processing plasmids. 1 nM of pBEST-OR2-OR1-Pr-UTR1-deGFP-T500 is prepared using only a QiaPrep Spin Miniprep Kit (Purification method 1) or post-processed with a QiaQuick PCR purification kit (Purification method 2). Shown is endpoint fluorescence after 8 hours, as well as maximal rate of protein production based on a 12-minute moving average. Error bars are 1 standard deviation from four independent runs on different days. **b) Effect of elution buffer (Tris-Cl).** Different concentrations of Tris-Cl are compared in a cell-free expression reaction based on the expression of 1 nM of pBEST-OR2-OR1-Pr-UTR1-deGFP-T500. Concentrations given are final concentrations of Tris-Cl in the reaction; elution buffer used is 10 mM Tris-Cl. Error bars are 1 standard deviation from three independent runs on different days.

Figure 6

a)

Master Mix Preparation

Ingredient	Stock*	Final*	Master Mix (uL)
B6.X (buffer)	1	0.416666667	35.63
E6 (extract)	1	0.333333333	28.50
()			
()			
()			
()			

*Input as ratio

# Rxns	5

Tubes to Thaw

B6.X (yellow 1.7mL tube)	1
E6 (green and yellow 1.7mL tube)	1
+1 (unlabeled 0.2mL tube)	1

DNA Preparation

ID	Plate Loc.	Name	[Stock] (ng/uL)	Length (bp)	[Stock] (nM)	Repeats	[Final]/rxn (nM)	aTc (uL)	() (uL)	() (uL)	() (uL)	DNA (uL)	Water (uL)	MM to add (uL)	Notes
1		Int. Pos. Control (+1)	19	3202	8.99	1	1					1.17	1.46	7.88	
2		Int. Neg. Control	19	3202	8.99	1	0					0.00	2.62	7.88	
3		aTc only, 5 ug/mL	0	0		1	0	**0.50**	0.00	0.00	0.00			7.88	
4		DNA w/o aTc	233.6	3734	94.79	1	10	0.00	0.00	0.00	0.00	1.11	1.52	7.88	
5		DNA w/ 5 ug/mL aTc	233.6	3734	94.79	1	10	**0.50**	0.00	0.00	0.00	1.11	1.02	7.88	

b)

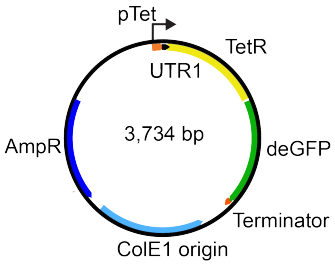

c)

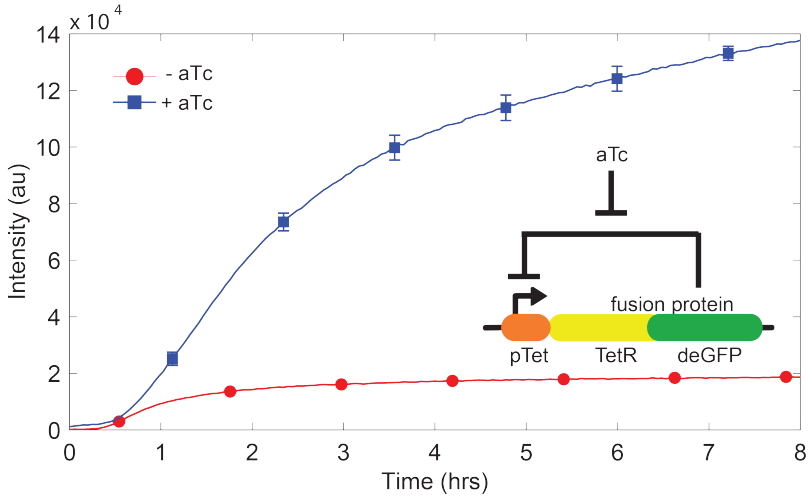

Figure 6. Sample TX-TL run of a negative feedback loop. a) Sample setup of a cell-free execution reaction. Tests "on" vs. "off" state of the negative feedback loop, with positive and negative controls. **b) Plasmid map of negative feedback loop. c) Representative results.** Data reflects experiment in a) and b), with negative control subtracted from signal. Genetic circuit shown in insert. Error bars are 1 standard deviation from three independent runs on different days.

Table 1

Reagents for day 1 of Crude Cell Extract protocol.

Name	Concentration	Amount	Sterilization	Notes
Chloramphenicol (Cm)	34 mg/mL in ethanol	1 mL	Filter sterilize (0.22 μM)	Can be made in larger volumes stored at -20°C for later use.
2xYT+P+Cm agar plate	31 g/L 2xYT, 40 mM potassium phosphate dibasic, 22 mM potassium phosphate monobasic, 34 μg/ml chloramphenicol	1 plate	Autoclave	
2xYT+P media	31 g/L 2xYT, 40 mM potassium phosphate dibasic, 22 mM potassium phosphate monobasic	4 L	Autoclave	

Table 2

Reagents for day 2 of Crude Cell Extract protocol.

Name	Concentration	Amount	Sterilization	Notes
Tris base	2 M	250 mL	Filter sterilize (0.22 μM) or autoclave	Can be stored at room temperature.
DTT	1 M	6 mL	Filter sterilize (0.22 μM)	Can be made in larger volumes and stored at -20°C for later use.
S30A buffer	14 mM Mg-glutamate, 60 mM K-glutamate, 50 mM Tris, pH 7.7	2 L	Autoclave	To reach pH 7.7, titrate with acetic acid. Add DTT to 2 mM final concentration just before use. Store at 4°C.
S30B buffer	14 mM Mg-glutamate, 60 mM K-glutamate, ~5 mM Tris, pH 8.2	2 L	Autoclave	To reach pH 8.2, titrate with 2M Tris. Add DTT to 1 mM final concentration just before use. Store at 4°C.

Table 3

S30A buffer and bead mass calculator, for day 3 of Crude Cell Extract protocol.

	Falcon			
	1	**2**	**3**	**4**
Empty 50 mL Falcon (g)				
50 mL Falcon with pellet (g)				
Pellet mass **(50 mL Falcon with pellet – empty 50 mL Falcon)** (g)				
S30A buffer volume to add **(pellet mass* 0.9)** (mL)				
Total mass of beads to add **(pellet mass * 5.0)** (g)				

Table 4

Reagents to prepare for Energy Solution protocol.

Name	Concentration	Amount	Sterilization	Notes
HEPES	2 M, pH 8	4 mL	None	To reach pH 8, titrate with KOH.
Nucleotide Mix	156 mM ATP and GTP, 94 mM CTP and UTP, pH 7.5	1.5 mL	None	To reach pH 7.5, titrate with KOH.
tRNA	50 mg/mL	600 µL	None	
CoA	65 mM	600 µL	None	
NAD	175 mM, pH 7.5-8	300 µL	None	To reach pH 7.5-8, titrate with Tris at 2 M.
cAMP	650 mM, pH 8	200 µL	None	To reach pH 8, titrate with Tris at 2 M.
Folinic Acid	33.9 mM	300 µL	None	Although only 300 µL is needed, recipe in supplemental is for 1.15 mL.
Spermidine	1 M	150 µL	None	Store at 4°C, heat to 37°C to melt.
3-PGA	1.4 M, pH 7.5	3.2 mL	None	To reach pH 7.5, titrate with Tris at 2 M.

Table 5
Material list.

Name of Reagent/Material	Company	Catalog Number	Comments
2xYT	MP biomedicals	3012-032	
3-PGA	Sigma-Aldrich	P8877	
ATP	Sigma-Aldrich	A8937	
Bacto-agar	BD Diagnostics	214010	
Bead-beating tubes (polypropylene microvials)	BioSpec	522S	
Beads, 0.1 mm dia.	BioSpec	11079101	
BL21 Rosetta 2 *E. coli* strain	Novagen	71402	
Bradford BSA Protein Assay Kit	Bio-rad	500-0201	
cAMP	Sigma-Aldrich	A9501	
Chloramphenicol	Sigma-Aldrich	C1919	
CoA	Sigma-Aldrich	C4282	
CTP	USB	14121	
Cuvettes, 1.5 mL	Fisher	14-955-127	
DTT	Sigma-Aldrich	D0632	
Folinic acid	Sigma-Aldrich	F7878	
GTP	USB	16800	
HEPES	Sigma-Aldrich	H6147	
K-glutamate	Sigma-Aldrich	G1149	
Mg-glutamate	Sigma-Aldrich	49605	
Micro Bio-Spin Chromatography Columns	Bio-Rad	732-6204	

NAD	Sigma-Aldrich	N6522	
Nunc 384-well optical bottom plates	Thermo-Scientific	142761	
Nunc sealing tape	Thermo-Scientific	232701	
PEG-8000	Promega	V3011	
Potassium phosphate dibasic solution	Sigma-Aldrich	P8584	
Potassium phosphate monobasic solution	Sigma-Aldrich	P8709	
RTS Amino Acid Sampler	5 Prime	2401530	
Slide-A-Lyzer Dialysis Cassettes, 10k MWCO (Kit)	Thermo-Scientific	66382	
Spermidine	Sigma-Aldrich	85558	
Tris base	Fischer	BP1521	
tRNA (from *E. coli*)	Roche Applied Science	MRE600	
UTP	USB	23160	
1 L Centrifuge Bottle	Beckman-Coulter	A98813	This is specific for Avanti J-series; obtain equivalent size for centrifuge in use.
4 L Erlenmeyer Flask	Kimble Chase	26500-4000	
Avanti J-26XP Centrifuge	Beckman-Coulter	393127	Or 1L-capable centrifuge equivalent.
Forma 480 Orbital Shaker	Thermo Scientific	480	Or chest-size 6 x 4 L shaker equivalent.

JLA-8.1000 Rotor	Beckman-Coulter	363688	Or 1 L-capable, 5000 g rotor equivalent for centrifuge.
Mini-Beadbeater-1	BioSpec	3110BX	

Supplemental Material 1
Recipes for Items.

Chloramphenicol, 34 mg/mL: Prepare 0.51 g chloramphenicol and add ethanol to 15 mL. Filter sterilize (0.22 μM), aliquot to 1 mL tubes, store at -20°C for later use.

2xYT+P+Cm agar plate: Prepare 1.24 g 2xYT, 1.6mL potassium phosphate dibasic solution @ 1 M, 0.88mL potassium phosphate monobasic solution @ 1 M, 0.6 g agar, and water to 40 mL. Autoclave. Let cool to 50°C and add 40 μL Cm. Aliquot 25 mL into a 100x15 mm petri dish, and let cool for an hour.

2xYT+P media: Prepare 124 g 2xYT, 160 mL potassium phosphate dibasic solution @1 M, 88 mL potassium phosphate monobasic solution @ 1 M, and water to 4 L. Aliquot out into 2x1.88 L and 0.24 L. Autoclave.

Tris base, 2 M: Prepare 60.57 g Tris base and water to 250 mL. Sterilize, store at RT for later use.

DTT, 1 M: Prepare 2.31 g DTT and water to 15 mL. Filter sterilize (0.22 μM), aliquot to 1 mL tubes, store at -20°C for later use.

S30A buffer: Prepare 10.88 g Mg-glutamate and 24.39 g K-glutamate, 50 mL Tris at 2M, acetic acid (to pH 7.7), and water to 2 L. Autoclave, store at 4°C, add 4 mL 1 M DTT before use.

S30B buffer: Prepare 10.88 g Mg-glutamate and 24.39 g K-glutamate, Tris at 2 M (to pH 8.2), and water to 2 L. Autoclave, store at 4°C, add 2 mL 1 M DTT before use.

HEPES: Prepare 1.91 g HEPES (MW 238.21), KOH (to pH 8), and water to 4mL.

tRNA: Prepare 30 mg of tRNA and water to 600 μL.

CoA: Prepare 30 mg of CoA (MW 767.53) and water to 600 µL.

NAD: Add 34.83 mg of NAD (MW 663.43), Tris at 2 M (to pH 7.5-8), and water to 300 µL. (Add 27 µL of Tris at 2 M to bring the solution to pH 7.5-8).

cAMP: Add 42.80 mg of cAMP (MW 329.22), Tris at 2 M (to pH 8), and water to 200 µL. (Add 73 µL of Tris at 2 M to bring the solution to pH 8).

Folinic Acid (33.9 mM): To 20 mg of solid folinic acid calcium salt (MW 511.5), add 1.15 mL water.

Spermidine: Prepare 23.55 µL of spermidine (MW 145.25) and water to 150 µL. Prepare at room temperature after melting briefly at 37°C.

3-PGA: Add 1.03 g of 3-PGA (MW 230.02), Tris at 2 M (to pH 7.5), and water to 3.2 mL. (Add 1.73 mL of Tris at 2 M to bring the solution to pH 7.5).

Nucleotide Mix: Add 145 mg of ATP dipotassium salt dihydrate (MW 619.4), 133 mg of GTP disodium salt (MW 567.14), 79.4 mg of CTP disodium salt dihydrate (MW 563.16), 82.6 mg of UTP trisodium salt dihydrate (MW 586.12), KOH at 15% dilution (to pH 7.5), and water to 1.5 mL. (Add 353 µL of KOH at 15% dilution to bring the solution to pH 7.5).

Supplemental Material 2

Bradford Assay.

6.1) Remove Bradford agent from 4°C and set at room temperature.

6.2) Prepare 50 µL BSA Standard at 1 mg/mL and at 0.1 mg/mL.

6.3) Prepare 40 µL 20x dilution of extract from step 1.47.

6.4) Add 800 µL water to 7 cuvettes.

6.5) Prepare standard cuvettes for 0 mg/mL, 1 mg/mL (10 µL 0.1 mg/mL BSA), 2 mg/mL (20 µL 0.1 mg/mL BSA), 4 mg/mL (4 µL 1 mg/mL BSA), 6 mg/mL (6 µL 1 mg/mL BSA).

6.6) Prepare experimental cuvettes for 2 µL of sample and 4 µL of sample.

6.7) Add 200 µL of Bradford agent to each cuvette and mix well by pipetting. Incubate at room temperature for at least 10 minutes.

6.8) Produce standard curve at OD 595nm using cuvettes from step 6.5. **Reject standard curve if r^2 < 0.95.**

6.9) Determine extract concentration at OD 595nm using cuvettes from step 6.6.

Supplemental Material 3
Buffer calibration spreadsheet.

See TXTL_e(template)_calibration_JoVE.xlsx on www.jove.com

Supplemental Material 4
Cell-free expression run spreadsheet.

See TXTL _JoVE.xlsx on www.jove.com

References

1 Noireaux, V., Bar-Ziv, R. & Libchaber, A. Principles of cell-free genetic circuit assembly. *Proceedings of the National Academy of Sciences of the United States of America* **100**, 12672-12677, doi:DOI 10.1073/pnas.2135496100 (2003).

2 He, M. Y., He, Y. Z., Luo, Q. & Wang, M. R. From DNA to protein: No living cells required. *Process Biochem* **46**, 615-620, doi:DOI 10.1016/j.procbio.2010.11.003 (2011).

3 Forster, A. C. & Church, G. M. Synthetic biology projects in vitro. *Genome Res* **17**, 1-6, doi:Doi 10.1101/Gr.5776007 (2007).

4 Shin, J. & Noireaux, V. Efficient cell-free expression with the endogenous E. Coli RNA polymerase and sigma factor 70. *Journal of biological engineering* **4**, 8, doi:10.1186/1754-1611-4-8 (2010).

5 Shimizu, Y. *et al.* Cell-free translation reconstituted with purified components. *Nat Biotechnol* **19**, 751-755, doi:Doi 10.1038/90802 (2001).

6 Shin, J. & Noireaux, V. An E. coli Cell-Free Expression Toolbox: Application to Synthetic Gene Circuits and Artificial Cells. *Acs Synth Biol* **1**, 29-41, doi:Doi 10.1021/Sb200016s (2012).

7 Shin, J. & Noireaux, V. Study of messenger RNA inactivation and protein degradation in an Escherichia coli cell-free expression system. *Journal of biological engineering* **4**, 9, doi:10.1186/1754-1611-4-9 (2010).

8 Shin, J., Jardine, P. & Noireaux, V. Genome Replication, Synthesis, and Assembly of the Bacteriophage T7 in a Single Cell-Free Reaction. *Acs Synth Biol* **1**, 408-413, doi:Doi 10.1021/Sb300049p (2012).

9 Siegal-Gaskins, D., Noireaux, V. & Murray, R. M. in *American Control Conference* (AACC, Washington, DC, 2013).

10 Karzbrun, E., Shin, J., Bar-Ziv, R. H. & Noireaux, V. Coarse-grained dynamics of protein synthesis in a cell-free system. *Physical review letters* **106**, 048104 (2011).

11 Hoagland, M. B., Stephenson, M. L., Scott, J. F., Hecht, L. I. & Zamecnik, P. C. Soluble Ribonucleic Acid Intermediate in Protein Synthesis. *J Biol Chem* **231**, 241-257 (1958).

12 Wood, W. B. & Berg, P. Effect of Enzymatically Synthesized Ribonucleic Acid on Amino Acid Incorporation by a Soluble Protein-Ribosome System from Escherichia Coli. *Proceedings of the National Academy of Sciences of the United States of America* **48**, 94-&, doi:Doi 10.1073/Pnas.48.1.94 (1962).

13 Zubay, G. In-Vitro Synthesis of Protein in Microbial Systems. *Annu Rev Genet* **7**, 267-287, doi:DOI 10.1146/annurev.ge.07.120173.001411 (1973).

14 Pratt, J. M. in *Transcription and Translation: A Practical Approach* (ed B. D. Hames, Higgins, S. J.) 179-209 (IRL Press, 1984).

15 Kim, H. C. & Kim, D. M. Methods for energizing cell-free protein synthesis. *Journal of bioscience and bioengineering* **108**, 1-4, doi:10.1016/j.jbiosc.2009.02.007 (2009).

16 Michel-Reydellet, N., Calhoun, K. & Swartz, J. Amino acid stabilization for cell-free protein synthesis by modification of the Escherichia coli genome. *Metabolic engineering* **6**, 197-203, doi:10.1016/j.ymben.2004.01.003 (2004).

17 Liu, D. V., Zawada, J. F. & Swartz, J. R. Streamlining Escherichia coli S30 extract preparation for economical cell-free protein synthesis. *Biotechnology progress* **21**, 460-465, doi:10.1021/bp049789y (2005).
18 Andrianantoandro, E., Basu, S., Karig, D. K. & Weiss, R. Synthetic biology: new engineering rules for an emerging discipline. *Molecular systems biology* **2**, 2006 0028, doi:10.1038/msb4100073 (2006).
19 Kwok, R. Five hard truths for synthetic biology. *Nature* **463**, 288-290, doi:10.1038/463288a (2010).
20 Tabor, S. & Richardson, C. C. A bacteriophage T7 RNA polymerase/promoter system for controlled exclusive expression of specific genes. *Proceedings of the National Academy of Sciences of the United States of America* **82**, 1074-1078 (1985).
21 Lewicki, B. T., Margus, T., Remme, J. & Nierhaus, K. H. Coupling of rRNA transcription and ribosomal assembly in vivo. Formation of active ribosomal subunits in Escherichia coli requires transcription of rRNA genes by host RNA polymerase which cannot be replaced by bacteriophage T7 RNA polymerase. *Journal of molecular biology* **231**, 581-593, doi:10.1006/jmbi.1993.1311 (1993).
22 Iskakova, M. B., Szaflarski, W., Dreyfus, M., Remme, J. & Nierhaus, K. H. Troubleshooting coupled in vitro transcription-translation system derived from Escherichia coli cells: synthesis of high-yield fully active proteins. *Nucleic acids research* **34**, e135, doi:10.1093/nar/gkl462 (2006).
23 Kigawa, T. *et al.* Preparation of Escherichia coli cell extract for highly productive cell-free protein expression. *Journal of structural and functional genomics* **5**, 63-68, doi:10.1023/B:JSFG.0000029204.57846.7d (2004).
24 Matsuda, T. *et al.* Improving cell-free protein synthesis for stable-isotope labeling. *Journal of biomolecular NMR* **37**, 225-229, doi:10.1007/s10858-006-9127-5 (2007).
25 Sitaraman, K. *et al.* A novel cell-free protein synthesis system. *Journal of biotechnology* **110**, 257-263, doi:10.1016/j.jbiotec.2004.02.014 (2004).
26 Becskei, A. & Serrano, L. Engineering stability in gene networks by autoregulation. *Nature* **405**, 590-593, doi:10.1038/35014651 (2000).
27 Maeda, H., Fujita, N. & Ishihama, A. Competition among seven Escherichia coli sigma subunits: relative binding affinities to the core RNA polymerase. *Nucleic acids research* **28**, 3497-3503 (2000).
28 Caschera, F. *et al.* Coping with complexity: machine learning optimization of cell-free protein synthesis. *Biotechnology and bioengineering* **108**, 2218-2228, doi:10.1002/bit.23178 (2011).
29 Hodgman, C. E. & Jewett, M. C. Cell-free synthetic biology: thinking outside the cell. *Metabolic engineering* **14**, 261-269, doi:10.1016/j.ymben.2011.09.002 (2012).
30 Elowitz, M. B. & Leibler, S. A synthetic oscillatory network of transcriptional regulators. *Nature* **403**, 335-338, doi:10.1038/35002125 (2000).
31 Tsuruta, H. *et al.* High-level production of amorpha-4,11-diene, a precursor of the antimalarial agent artemisinin, in Escherichia coli. *Plos One* **4**, e4489, doi:10.1371/journal.pone.0004489 (2009).

32 Gardner, T. S., Cantor, C. R. & Collins, J. J. Construction of a genetic toggle switch in Escherichia coli. *Nature* **403**, 339-342, doi:10.1038/35002131 (2000).
33 Jewett, M. C. & Forster, A. C. Update on designing and building minimal cells. *Current opinion in biotechnology* **21**, 697-703, doi:10.1016/j.copbio.2010.06.008 (2010).
34 Noireaux, V. & Libchaber, A. A vesicle bioreactor as a step toward an artificial cell assembly. *Proceedings of the National Academy of Sciences of the United States of America* **101**, 17669-17674, doi:10.1073/pnas.0408236101 (2004).

Chapter 3: Accelerating the breadboard

Published as:
Sun ZZ, Yeung E, Hayes CA, Noireaux V, Murray RM. Linear DNA for rapid prototyping of synthetic biological circuits in an Escherichia coli based TX-TL cell-free system. *ACS Synth. Biol.* (79), 3 (6), pp 387–397, doi:10.1021/sb400131a (2014)

Abstract

Accelerating the pace of synthetic biology experiments requires new approaches for rapid prototyping of circuits from individual DNA regulatory elements. However, current testing standards require days to weeks due to cloning and *in vivo* transformation. In this work, we first characterized methods to protect linear DNA strands from exonuclease degradation in an *Escherichia coli* based transcription-translation cell-free system (TX-TL), as well as mechanisms of degradation. This enabled the use of linear DNA PCR products in TX-TL. We then compared expression levels and binding dynamics of different promoters on linear DNA and plasmid DNA. We also demonstrated assembly technology to rapidly build circuits entirely *in vitro* from separate parts. Using this strategy, we prototyped a four component genetic switch in under 8 hours entirely *in vitro.* Rapid *in vitro* assembly has future applications for prototyping multiple component circuits if combined with predictive computational models.

Introduction

The current mode of building synthetic circuits relies heavily on *in silico* design followed by *in vivo* testing and revision. Complete circuits are cloned into a plasmid for propagation *in vivo*, a labor-intensive and serial process that has a 1-week testing cycle, which scales poorly for complex circuits (Fig. 1a).[1-3] Although large-scale successes have been accomplished by this testing method, there is a significant time cost to this engineering cycle. For example, the industrial production of artemisinin from synthetic circuits in *E. coli and S. cerevisiae* has taken 150 "person-years," of which much time can be attributed to part testing.[4, 5]

This current method ignores a commonly applied process in engineering: testing of circuits in a simplified prototyping environment, such as a breadboard, to decrease complexity and increase iteration speed. Cell-free protein synthesis systems are a simplified alternative to *in vitro* systems that are known for ease-of-use and well-defined features.[6-8] Circuits such as oscillators, switches, and translational regulators[9-11] have been implemented either in reconstituted cell-free systems or in S30 extracts.[12, 13] However, these extracts either lack significant similarity to the *in vivo* environment or are optimized for protein production in lieu of circuit design. The ideal cell-free expression system should act as a "biomolecular breadboard" intermediary between circuit testing and *in vivo* implementation. It should mirror the *E. coli in vivo* state while preserving protein production capability and regulatory mechanisms.[14]

We propose an S30-based transcription-translation system (TX-TL) that we have developed to serve as part of a biomolecular breadboard. This system is currently supported with characterizations of transcriptional and translational processes,

computational models, and protocols for its creation and use.[14-18] We have also demonstrated simple logic gates, cascades, and large-scale assembly of bacteriophage.[14, 19] While most circuits implemented in S30 based extracts utilize plasmid DNA to avoid exonuclease degradation from endogenous RecBCD, linear DNA can be protected from degradation with the RecBCD inhibitor bacteriophage gamS protein both *in vivo* and in other S30 extracts.[20, 21] The ability to run circuits off of linear DNA opens up possibilities for rapid prototyping, as linear DNA can be created in high yields either synthetically or entirely *in vitro* in just a few hours. Linear DNA could also enable applications not possible with plasmid DNA, such as the expression and analysis of toxic proteins by bypassing *in vivo* transformation and selection.

In this paper, we established using linear DNA with the biological breadboard for rapid prototyping (Figure 1b). We first developed protective mechanisms to make linear DNA expression comparable to that of plasmid DNA. We also verified recent findings in other S30 extracts which suggested that transcriptional processes using linear DNA are disparate from those using plasmid DNA.[22] To validate linear DNA as a prototyping medium, we compared expression of linear DNA to plasmid DNA for a family of promoters and demonstrated similar circuit dynamics for a genetic switch. A rapid, entirely *in vitro* assembly technique was then developed to assemble regulatory elements and basic circuits from standard or custom pieces in under 4 hours, with complete testing in under 8 hours. By maintaining an engineering cycle time of 8 hours or less, our technology theoretically enables prototyping of multi-component circuits in a standard business day.

Results and Discussion

Linear DNA can be protected from degradation in TX-TL

We initially sought to characterize the stability of linear DNA in TX-TL. Integral to this is accurate quantification of both linear and plasmid dsDNA concentration, as large errors in quantifying small amounts of dsDNA can introduce significant downstream bias.[23] This is especially true for TX-TL, as some experiments require less than 10 ng/μL of stock dsDNA. Two common methods for dsDNA quantification commonly in use include spectrophotometry and fluorometry. We compared both and established guidelines for measuring linear and plasmid DNA concentrations (Supplemental S1, Figure S1, Table S1).

Unless otherwise stated, all experiments in the paper were done with a single extract batch to avoid extract-to-extract variation[14], and DNA sequences used can be found in Supplemental Information (Supplemental S2).

To determine ideal conditions for expression of a linear DNA template, we compared the production of fluorescent reporter deGFP from plasmid pBEST-OR2-OR1-Pr-UTR1-deGFP-T500 to that of the 810 bp linear DNA product with no steric protection on the 5' or 3' end. This plasmid was previously optimized for high expression in TX-TL.[16] The deGFP synthesis off of linear DNA was less than 2% that of plasmid DNA (Figure 2a). In order to use lower concentrations of DNA templates for prototyping, we expanded upon previous work which added purified lambda gam in an S30 extract to protect DNA from exonuclease degradation.[21] We utilized gamS, a truncated form of lambda gam.[20] We also developed a non-toxic storage buffer for use in TX-TL by conducting a toxicity assay of common protein storage buffer additives in an alternate

extract (Figure S2, Figure S3). Notably, glycerol as a cryoprotectant is highly toxic to TX-TL and required replacement with DMSO. With gamS protein present in the reaction, deGFP synthesis off of the OR2-OR1-Pr-UTR1-deGFP-T500 linear DNA was 37.6% that of plasmid DNA (Figure 2a).

We determined a gamS working concentration of 3.5 μM by comparing the protective ability of dilutions of purified protein on 2 nM of linear DNA without steric protection (Figure 2b). We used this concentration for subsequent experiments. We hypothesize that 3.5 μM is significantly above saturating levels to inactivate RecBCD, as at 3.5 μM and above the incubation of gamS with crude extract did not improve expression, while below 3.5 μM incubation time improved expression (Figure S4). While purified gamS improved linear DNA expression, it showed no toxicity to plasmid DNA expression (Figure 2c).

We also conducted a saturation curve of plasmid and linear DNA by measuring endpoint deGFP concentration as a function of DNA concentration. Using this data, we defined a linear regime and saturation regime (Figure S5). The linear regime is defined as the linear region of DNA concentration and output signal, implying little to no resource limitation. In the saturation regime, increased DNA only marginally increases signal. We defined resource limitation broadly as any aspect limiting an *in vitro* reaction, such as polymerase and ribosome saturation or resource depletion (NTPs, amino acids). We ran circuits in the linear regime of DNA concentration to avoid resource limitation affects. While plasmid DNA entered the saturation regime above 4 nM, linear DNA remained in the linear regime up to 16 nM (Figure 2c). This established a typical working concentration for linear DNA, and suggested the ability to calibrate linear DNA results to

plasmid DNA results by concentration. While much of the discrepancy in saturation can be attributed to promoter strength differences of plasmid versus linear DNA, there may also be contributions from antibiotic resistance cassettes on plasmid DNA diverting resources from the production of deGFP that we did not explore.

With the presence of gamS, we also tested steric protective mechanisms to inhibit degradation by RecBCD and other exonucleases.[21, 24] We first tested two independent non-coding sequences flanking the ends of our linear cassette (Figure 2d). "Sequence 1" was derived from the original plasmid, while "Sequence 2" was from the coding sequences of two long *E. coli* genes, *gltB* and *lhr*, presumed to have no large internal reading frames. Protection was both sequence-specific and length-dependent. 5 bp of protective sequences on each end increased signal 2.4-fold over no protective ends. Protection reached a maximum around 250 bp-500 bp, with 6-fold larger signal over no steric protection. Therefore, unless otherwise specified we used 250 bp of protective sequences for subsequent linear constructs. We also tried protecting linear DNA with 1, 2, or 5 phosphorothioate modifications at the 5' end added by PCR, and found improvement only when 5 bp or less of non-coding DNA protection was present (Figure S6a). Interestingly, 5 phosphorothioates on the 0 bp protection construct significantly changed the dynamics of expression, suggesting a minimum protective length of 15 bp from the -35 promoter region (Figure S6b).

DNA degradation in TX-TL is incomplete from the 5' or 3' end

Little is known about degradation patterns of multiple copies of linear DNA in S30 extract-based systems. Knowing whether each copy is selectively degraded at the 5' end or completely removed from the reaction has ramifications for positioning of circuits

on linear DNA. To directly measure DNA concentration over the linear regime of a TX-TL reaction, we labeled a typical non-saturating amount of linear DNA (2 nM, 25 ng) with a fluorescent probe, AlexaFluor-594, in a complementary spectrum to the deGFP reporter. We first incorporated the probe randomly throughout the linear DNA by PCR using an AlexaFluor-594-5-dUTP, which replaced dTTP (Figure 3a). Despite the labeling, linear DNA retained expression ability as measured by deGFP signal. Negligible DNA was degraded within 1 hour and over 75% remained within 4 hours when templates were protected by gamS, suggesting minimal degradation of template over a typical period of data collection. We also labeled the same template only at the 5' end through PCR by using primers with AlexaFluor-594 covalently bound (Figure 3b). While expression of deGFP was equally conserved, there was significant degradation of AlexaFluor-594 signal as compared to samples labeled throughout the entire linear DNA. We concluded that when gamS and when multiple copies of linear DNA are present, there is incomplete degradation at the 5' end. This is supported by previous data showing only modest expression improvement from increased steric protection lengths (Figure 2d), as well as evidence suggesting the existence of always-active RecBCD complex despite saturating gamS concentration.[25] While RecBCD is the primary dsDNA exonuclease, we cannot discount the action of other dsDNA exonucleases such as ExoVII.[26, 27] To our knowledge, this is the first evidence of an exonuclease degradation mechanism with multiple copies of linear DNA.

We also determined that degradation of linear DNA is a saturated process limited by the amount of exonuclease. We conducted the same degradation assay, but using saturating amounts of DNA (250 ng, 20 nM) and saw no significant degradation at 120

minutes in the presence of gamS (Figure S7). Degradation also seemed invariant to extract preparation conditions. We also made an extract prepared at 29°C, based on previous work where lower preparation temperature decreased exonuclease activity on linear DNA.[28] However, we saw no decreased degradation. Based on these findings, we concluded that linear DNA remained present throughout the TX-TL reaction, and could be significantly protected against exonuclease degradation at high concentrations or with sufficient steric protection.

Linear DNA is an alternative to plasmid DNA for circuit prototyping

Although circuits can be prototyped rapidly using linear DNA, recent studies in other S30 extracts demonstrated a discrepancy between relative expression of linear templates versus plasmid templates.[22] These discrepancies were attributed to structural differences between plasmid and linear DNA, as relative activity was recovered by re-ligation of linear DNA and was independent of translation. We hypothesized that despite structural differences between linear and plasmid DNA, prototyping could still be accomplished by calibrating promoter strength based on DNA concentration between linear and plasmid DNA for constitutive promoters. While a large amount of DNA is needed to obtain signal in other kits, TX-TL allows significant expression for small template concentrations. By working in a linear regime, circuits can be executed such that large amounts of free polymerases and ribosomes exist at all times (Figure S5).

We tested twelve commonly used sigma-70 based promoters and a negative control of random DNA for *in vitro* plasmid strength, *in vitro* linear DNA strength, and *in vivo* strength. Linear DNA was protected with gamS protein and 250 bp of non-coding DNA on either end. Nine promoters are minimal sigma-70 promoters from the Biobrick

parts library (http://parts.igem.org/), while three are inducible and well-characterized.[29, 30] These constructs all identically expressed deGFP downstream of an untranslated region containing a strong RBS "UTR1."[16] When each Biobrick promoter was compared in the linear regime and normalized to J23101, there was no correlation between results *in vivo* and in TX-TL either on plasmid or on linear DNA. (Figure 4a). However, when data was taken at highest concentrations measured there was a correlation, if limited, between results *in vivo* and in TX-TL on plasmid DNA (Figure S8). Figure S8 results are similar to a panel done previously in a separate S30 extract, albeit with a different reporter, weaker RBS, different plasmid, and different temperature.[22] More work needs to be done to reconcile both datasets, although these results suggest that circuits tested in saturated phase on plasmid DNA most accurately represent the *in vivo* environment. In the *in vivo* environment, we speculate high copy plasmids on strong promoters may reach saturated phase expression. Each inducible promoter was also tested constitutively with the repressor inactivated or not present, and limited correlation was found between *in vivo* results and TX-TL results (Figure 4b). Interestingly, inducible promoters seemed to have vastly stronger strength relative to the minimal sigma-70 based promoter panel in TX-TL.

For the Pl-tetO1 and Pl-lacO1 promoters, we also characterized the response in TX-TL of linear and plasmid DNA to varying amounts of inducer in the presence of repressor (Figure 4c). Data was fit to a Hill function with a Hill coefficient of unity (Supplemental S3). Operator binding dynamics were similar, with a Michelis-Menten binding coefficient within two standard deviations for Pl-tetO1 and within one standard deviation for Pl-lacO1. Data for Pl-tetO1 may be biased, however, as TX-TL showed toxicity at values above 10 μM aTc, which seemed to be below saturation phase. We

assumed that for Pl-tetO1 and Pl-lacO1, repression binding and unbinding was similar for linear and plasmid DNA at individual operator site.

To calibrate linear DNA to plasmid DNA for constitutive expression, we tested each promoter at different concentrations. Based on the results of endpoint expression, a saturation curve was produced for both linear and plasmid DNA, where expression was plotted as a function of DNA concentration (Figure 4d). We used a cutoff of $r^2 > 0.975$ to determine a linear regime for each promoter (Figure S9). This data was used to develop a calibration table for linear and plasmid DNA, where the slope of the linear regression line indicated promoter strength in the linear regime (Table 1). A Plasmid:Linear (P:L) ratio was also determined. All promoters were stronger on plasmid DNA than linear DNA, ranging from 1.40-23.74 fold. The carrying capacity of TX-TL was capped at 15 μM. However, independent of promoter strength all constructs approached the saturating regime at 32 nM of linear DNA. This suggested a theoretical limit of DNA carrying capacity independent of absolute signal strength, but we were unable to test concentrations above 32 nM for linear DNA or 16 nM for plasmid DNA.

To demonstrate the ability to prototype circuits using either plasmid or linear DNA, we built a 4-piece genetic switch with two fluorescent outputs, deGFP and deCFP (Figure 5).[31] Linear DNA constructs were derived from plasmid DNA by PCR, and had gamS present as well as 250 bp of steric protection. 2 nM of each reporter and 1 nM of each repressor were used. We then examined the dynamics of the genetic switch by plotting the endpoint expression values at 36 different combinations of IPTG and aTc inducers. When both deGFP and deCFP were scaled for equivalent expression, the genetic switch behaved as expected with deGFP expression at high IPTG and deCFP

expression at high aTc. As predicted, expression from linear DNA at similar concentrations was also lower than for plasmid DNA. Based on this result, we believe linear DNA prototyping is a viable alternative to plasmid DNA prototyping.

Linear DNA can be rapidly assembled for prototyping circuits

After establishing linear DNA circuit prototyping, we sought to create a method for rapid assembly of linear pieces that would enable us to go from assembly to testing in 4-8 hours, and simultaneously allow us to generate plasmid DNA post-transformation (Figure 6a). Unlike other *in vivo* assembly methods, which ultimately require efficiency as well as selectivity, we were primarily concerned with selectivity as our templates would be end amplified by PCR. We also favored rapid cycle times in linear DNA to modularity post-construction, which has been shown to speed up the design cycle *in vivo*.[32] We initially tested three methods of *in vivo* assembly for adoption purely *in vitro*: Isothermal assembly, Chain Reaction Cloning, and Golden Gate assembly.[2, 33, 34] Each method is based on a different mechanism of action – recombination-based cloning, blunt-end cloning, or sticky-end cloning. Of these three, only Isothermal assembly and Golden Gate assembly produced enough yield to obtain constructs.

We first assembled a common network motif, a negatively autoregulated gene[35], from four linear parts using both Isothermal assembly and Golden Gate assembly (Figure S10a). The assembly products were PCR amplified directly afterwards to produce rapid assembly products ready for prototyping in TX-TL. The assembly product was also transformed, cultured, purified, and amplified by PCR to produce a positive control. All constructs were sequenced before testing in TX-TL. When run on an agarose gel, rapid assembly products were of the expected size when compared to a post-transformation

positive control, with higher than 95% purity (Figure S10b). However, while all constructs showed responses to aTc induction some demonstrated significant background activity (Figure S10c). We hypothesized that a non-specific product caused by mis-ligation could significantly bias results. To counteract this, we developed a standard assembly procedure based on Golden Gate assembly. By using a standard assembly, any mis-ligation would be less likely to lead to mis-assembled products capable of expression.

Our standard Golden Gate assembly procedure also allowed us to recycle commonly used parts and to ensure functional activity of the desired product. Our standard consisted of five pieces – a promoter, 5' untranslated region (UTR), coding sequence, terminator, and vector (Figure S11). It was designed to be compatible with previously used non-coding sequences and primers on the pBEST vector backbone. We revised a pre-existing standard for use in TX-TL by creating 4 bp binding overhangs with increased specificity.[36] Using different overhangs with little overlap was necessary, as we found decreased specificity with multiple base pair overlaps. We also designed our PCR primers to overlap at the junction sites of vector and promoter and vector and terminator, respectively, which further minimized non-specific products. This decreased steric protection ends to 31 bp.

Using our standard with pre-made pieces, we rapidly prototyped a Pl-tetO1-deGFP construct and demonstrated functional equivalency in less than 5 hours (Figure 6b-c). A detailed time frame with comparisons to testing using plasmids post-transformation is in Table S2. While the assembly reaction did not produce significant amounts of plasmid, a fragment corresponding to the expected size could be amplified.

Cleaner PCR products of the assembly reaction were produced by minimizing template concentration and by using overlapping PCR primers (Figure S12). Existing non-specific products could also be predicted based on size and gel mobility shifts. We have since tested multiple assemblies using our rapid assembly standard, and found that correct equimolar ratios of starting products are also essential to isolating a clonal product.

For more complex circuits, we verified our rapid assembly procedure by repeating the construction of the genetic switch in Figure 5a, but from rapid assembly products (Figure S13a). Specific bands were formed from PCR off of the rapid assembly product, and TX-TL runs demonstrated similar results for the product and the positive control when responding to IPTG and aTc (Figure S13b-c). This prototyping took under 7 hours of time.

Linear DNA prototyping theoretically allows for large circuits to be tested in a single business day

Our work is primarily focused on the technology development of a rapid prototyping procedure using linear DNA in TX-TL. Therefore, we chose only to demonstrate proof-of-concept assemblies using simple circuits. However, the real return of linear DNA prototyping is in testing large circuits in TX-TL. Unlike traditional testing methods reliant on plasmids, the 4-8 hour benchmark provided by our method is theoretically independent of the number of components tested. For example, to initially test an n-piece circuit *in vivo* would require $\log_3(n)$ rounds of plasmid cloning, assuming assemblies of 5 units at the same time (four regulatory units plus a vector backbone) (Figure 7a-b). This restriction results from the carrying capacity of the cell to maintain a limited number of antibiotic cassettes and origins of replication. However, an initial

testing cycle in TX-TL on linear DNA would require only the theoretical 8 hours, as each construct can be assembled in parallel on linear DNA and immediately tested (Figure 7c). The only restriction would be the resource carrying capacity of the TX-TL reaction. However, large-scale circuit prototyping is limited by the current lack of relatively large synthetic circuits; to our knowledge, the largest currently published circuit is an 11-piece logic gate.[37] Once rapid assembly is established, a larger bottleneck may be the difficulty of formulating and testing novel synthetic circuits with useful function.

To reach the theoretical 8-hour limit for large circuits, the rapid assembly procedure could be automated using robotics with simple pipetting and thermo-cycling capability, as the assemblies rely on standard parts, the final part is PCR amplified, and the resulting part is added to a constant-temperature TX-TL reaction. Unlike traditional methods of testing circuits, there are no cell growth, plasmid miniprep, or centrifugation steps. We have not yet explored automation of the rapid assembly procedure.

Conclusion

In this paper, we described a rapid prototyping procedure for genetic circuits utilizing linear DNA in an *E. coli* TX-TL cell-free system. This was done by characterizing methods of protecting linear DNA, and differences in gene expression between linear and plasmid DNA templates. A rapid assembly procedure entirely *in vitro* was developed, which produced results from standard parts in under 8 hours. For a genetic switch, circuits on linear DNA qualitatively matched circuits on plasmid DNA. Prototyping with linear DNA in TX-TL can decrease cycle times and increase iteration speed.

We demonstrated that linear DNA results could be mapped to plasmid DNA results in the context of individual promoters. However, in the context of circuit design the mapping becomes more complex due to multiple interconnecting relationships. While we saw expected relative circuit behavior for a genetic switch on both linear DNA and plasmid DNA, we did not attempt to map results from one mode of prototyping to the other. Such mapping may require computational toolboxes using parameters such as promoter strength and binding coefficients derived in this work.[38] Additionally, one would need increased understanding of experimental variation in TX-TL. For example, with plasmid DNA we have noticed expression differences dependent on the strain used for amplification, and with linear DNA expression differences between samples that were not processed in the same batch. Part of the difference is explained by exogenous steps, such as salt content post-miniprep using different columns.[14] We hypothesize other differences may be intrinsic to the DNA used, either through biochemical modifications or through conformational differences which have been shown *in vivo* to affect gene

expression.[39] Some variation can be compensated for by controls, such as harvesting all plasmid DNA used in a single batch. Such approaches are analogous to those addressing ubiquitous variation in *in vivo* systems.[29]

Ultimately, one would like to prototype circuits in TX-TL or a comparable *in vitro* environment for functionality *in vivo*. This could be challenging in light of the lack of correlation of results *in vivo* to those of TX-TL plasmid DNA data in our dataset. While promoter strengths could be calibrated individually between TX-TL and *in viv*o, it is unclear how to (or if it is necessary to) calibrate complex circuits with multiple interconnecting relationships. Encouragingly, there are examples of circuits prototyped *in vitro* for *in vivo* demonstration – namely a negative feedback gene and a logic gate.[40, 41] Future work can focus on important parameters in the transition, and on the transition of complex circuits of three or more promoters or those not based on known *in vivo* motifs.

In vitro systems in general and TX-TL in specific form a strong basis for the testing of novel circuits. For applications using T7 promoters or for simple assays, finely controlled T7-based reconstituted systems without linear DNA degradation can be used.[12] However, TX-TL and S30 based systems have the additional ability to strongly express sigma-70 and alternate sigma promoters, as well as provide nucleic acid degradation. There is also a wealth of data from previous S30 extract studies and from recent studies allowing for long-term expression[42], small-scale expression[43, 44], and novel control techniques.[45] Rapid prototyping techniques explored in this work, when tied into other existing technologies and to characterization research, are a compelling and rapid alternative to *in vivo* systems for circuit design and testing.

Methods

Cell-free expression preparation and execution

Preparation of the cell-free TX-TL expression system was done according to previously described protocols, resulting in extract with conditions: 8.9-9.9 mg/mL protein, 4.5 mM-10.5 mM Mg-glutamate, 40-160 mM K-glutamate, 0.33-3.33 mM DTT, 1.5 mM each amino acid except leucine, 1.25 mM leucine, 50 mM HEPES, 1.5 mM ATP and GTP, 0.9 mM CTP and UTP, 0.2 mg/mL tRNA, 0.26 mM CoA, 0.33 mM NAD, 0.75 mM cAMP, 0.068 mM folinic acid, 1 mM spermidine, 30 mM 3-PGA, and 2% PEG-8000.[14] Unless otherwise specified, one extract set "eZS1" was used consistently throughout the experiments to prevent variation from batch to batch. Extract "e10" was similarly prepared for toxicity assays. Extract "e13" was prepared using above conditions, but grew only at 29°C with a 12-hour second incubation. TX-TL reactions were conducted in a volume of 10 μL in a 384-well plate (Nunc) at 29°C, using a three tube system: extract, buffer, and DNA. When possible, inducers such as IPTG or purified proteins such as gamS were added to a mix of extract and buffer to ensure uniform distribution. For deGFP, samples were read in a Synergy H1 plate reader (Biotek) using settings for excitation/emission: 485 nm/ 525 nm, gain 61. For deCFP, settings were 440 nm/ 480 nm, gain 61. All samples were read in the same plate reader, and for deGFP rfu units were converted to μM of protein using a purified deGFP-His6 standard. Unless otherwise stated, endpoint measurements are after 8 hours of expression at 29°C.

GamS protein purification

The composition of buffers used was buffer L: 50 mM Tris-Cl pH 8, 500 mM NaCl, 5mM imidazole, 0.1% Triton X; buffer W: 50 mM Tris-Cl pH 8, 500 mM NaCl, 25 mM imidazole; buffer E: 50 mM Tris-Cl pH 8, 500 mM NaCl, 250 mM imidazole; buffer S: 50 mM Tris-Cl pH 7.5, 100mM NaCl, 1mM DTT, 1mM EDTA, and 2% DMSO. A frozen stock of P_araBAD-gamS in a BL21-DE3 *E. coli* strain was grown overnight in LB-carbenicillin media. 100 mL was used to inoculate 1 L LB-carbenicillin to an OD 600 nm of 0.4-0.6 at 37°C, 220 rpm. Cells were then incubated to 0.25% arabinose (final concentration) and grown for four additional hours at 25 C, 220 rpm, before being pelleted and frozen at -80°C. Cells were resuspended in buffer L, mechanically lysed, and incubated with Ni-NTA agarose (Qiagen). Ni-NTA agarose was washed twice with 15 column volumes of buffer W and eluted in buffer E. Fractions with a ~13 kD band were concentrated and dialyzed into buffer S overnight, and further purified on a 26/60 Sephadex 75 column. Protein concentration was verified by Bradford, concentrated to 3 mg/ml using an Ultra-0.5 3K MWCO Centrifugal Filter (Ambion), and stored in buffer S at -80°C. Protein purity was verified by gel. Purification steps were verified by SDS-PAGE gel electrophoresis.

Plasmid DNA and PCR product preparation

Plasmids used in this study were constructed using standard cloning procedures and maintained in a KL740 strain if using an OR2-OR1 promoter (29°C), a MG1655Z1 strain if using a Pl-tetO1 or Pl-lacO1 promoter, a BL21-DE3 strain for protein purification, a BL21 strain for promoter characterization, or a JM109 strain for all other constructs. KL740 upregulates a temperature sensitive lambda cI repressor, and

MG1655Z1 upregulates tetR and lacI. PCR products were amplified using Pfu Phusion Polymerase (New England Biolabs) for all constructs except for those labeled with AlexaFluor-588-5-dUTP, which used Taq Polymerase (New England Biolabs), and were DpnI digested. Plasmids were either miniprepped using a PureYield column (Promega) or midiprepped using a NucleoBond Xtra Midi column (Macherey-Nagel). All plasmids were processed at stationery phase. Before use in the cell-free reaction, both plasmids and PCR products underwent an additional PCR purification step using a QiaQuick column (Qiagen) which removed excess salt detrimental to TX-TL, and were eluted and stored in 10 mM Tris-Cl solution, pH 8.5 at 4°C for short term storage and -20°C for long term storage.

Sequences used for steric protection

Three sets of sequences were used for steric protection assays. One set was based on the vector backbone of previously published pBEST-OR2-OR1-Pr-UTR1-deGFP-T500 (Addgene #40019). Another set, used only in Figure 2d and referred to as "Sequence 2", was derived from the coding sequence of *gltB* and *lhr*. These sequences were found by parsing the NCBI GenBank MG1655 record in BioPython for all known coding sequences and sorting by size. A final set, used in Figure 4, was based on the vector backbone of pBEST-p15A-OR2-OR1-Pr-UTR1-deGFP-T500. Sequences were analyzed using Geneious 6.0 (Biomatters Ltd).

***In vitro* linear DNA assembly**

Linear DNA fragments were amplified using Pfu Phusion Polymerase (New

England Biolabs), DpnI digested for 5 minutes at 37°C (New England Biolabs) while verified with agarose gel electrophoresis, and PCR purified using previously described procedures. Fragments were then assembled *in vitro* using either Isothermal assembly or Golden Gate assembly. For Isothermal assembly, Gibson Assembly Master Mix (New England Biolabs) was used according to manufacturer instructions with 1:3 molar ratio vector:insert, and reacted at 1 hour at 50°C. [2] For Golden Gate assembly, a 15 μL reaction was set up consisting of equimolar amounts of vector and insert, 1.5 μL 10x NEB T4 Buffer (New England Biolabs), 1.5 μL 10x BSA (New England Biolabs), 1 μL BsaI (New England Biolabs), and 1 μL T4 Ligase at 2 million units/mL (New England Biolabs) [34]. Reactions were run in a thermocycler at 10 cycles of 2min/37°C, 3min/20°C, 1 cycle 5min/50°C, 5min/80°C. For Golden Gate assembly, constructs with internal BsaI cut sites were silently mutated beforehand using a QuikChange Lightning Multi Site-Directed Mutagenesis Kit (Agilent). For the Lambda Exonuclease / Exonuclease digest assay, we followed the assembly procedure up to assembly completion but using twice the amount of assembly mix. Then, a 20 μL reaction was prepared with 12 μL assembly product, 2 μL 10x ExoI reaction buffer (New England Biolabs), 2 μL 10x BSA (New England Biolabs), 0.5 μL Lambda Exonuclease (New England Biolabs), 0.5 μL Exonuclease I (New England Biolabs), and 3 μL water. The control was not digested. Reaction was run for 1 hour at 37°C and PCR purified using previously described procedures.

Rapid assembly product protocol

The *in vitro* linear DNA assembly protocol was followed. Overlap primers were

then designed to bind over the vector:promoter and vector:terminator junctions such that while the Tm of the final primer was above 60°C, the Tm of binding on each junction side was below 40°C. Then, 1 μL of the resulting assembly product was PCR amplified for 35 cycles in a 50 μL PCR reaction, and verified by agarose gel electrophoresis. If the resulting band was 80% or more pure, the DNA was PCR purified using previously described procedures and used directly in TX-TL. Simultaneously, 2 μL of the assembly product was transformed into cells using standard chemically competent or electrically competent procedures. The cells were grown, miniprepped, and sequenced. PCR products off of the resulting plasmids were used as a positive control.

Linear DNA degradation assay

To form linear DNA with AlexaFluor distributed on the dUTP, template DNA producing deGFP was amplified using a Taq Polymerase (New England Biolabs) and AlexaFluor-594-5-dUTP (Invitrogen) according to manufacturer standards with a 1:3:4:4:4 ratio of AlexaFluor-5-dUTP:dTTP:dCTP:dATP:dGTP (New England Biolabs), DpnI digested, and PCR purified using previously described procedures. Successful labeling was verified through comparison of pre-stained and SybrSafe post-stained agarose gel electrophoresis (Invitrogen). To form linear DNA with AlexaFluor on the 5' end, AlexaFluor 594 was covalently linked on the 5' end to both forward and reverse synthetic primers (Integrated DNA Technologies) and used for PCR amplificaton. For the 2 nM assay, DNA was then added to a 105 μL TX-TL reaction in triplicate with or without gamS protein, and incubated at 29°C. A negative control with no DNA was done in parallel. Aliquots of 10 μL were removed at indicated time points and immediately

added to 50 μL of PB buffer (Qiagen) and flash-frozen in liquid nitrogen. In parallel, 2 μL of sample was read for deGFP fluorescence on a Synergy H1 Take3 Plate (Biotek). After all samples were collected, samples were PCR-purified to remove degraded components and measured on a 384-well plate (Nunc) using setting excitation/emission: 590 nm/617 nm, gain 100. Negative control values were subtracted per data point. GFP signal was normalized to endpoint fluorescence and AlexaFluor-594 signal was normalized to DNA present at time 0. For the 250 ng assay, similar procedures were followed except 20 nM of DNA was added to 40 μL TX-TL reactions for teach condition in triplicate and aliquots of 5 μL were removed and added to 25 μL of PB buffer (Qiagen).

In vivo promoter characterization

Twelve promoters and a random control sequence of DNA were cloned in front of UTR1-deGFP-T500 on a p15A low copy plasmid using standard cloning procedures and propagated at 29°C in BL21 *E. coli* (New England Biolabs). Growth at 37°C or cloning on a high-copy colE1 plasmid resulted in a significant mutation rate. Single colonies were simultaneously sequenced and mixed with glycerol for storage at -80°C. Specific sequences can be found in Supplemental S2. Frozen stocks were used to inoculate 300 mL of culture in MOPS-glycerol-carbenicillin media (MOPS EZ Rich Defined Medium Kit, Teknova, using 0.4% glycerol working concentration in lieu of glucose and adding 100 μg/ml of carbenicillin) in a 96 DeepWell polypropylene plate (Fisher Scientific). The Pl-lacO1 sample was grown with 0.5mM of IPTG in addition. Plate was covered with a BreatheEasy gas-permeable membrane (Sigma-Aldrich) and grown overnight at 29°C on

a Symphony Incubating Microplate Shaker (VWR), shaking at 900 rpm. Cultures were then diluted 1:50 in triplicate, grown for 4 hours at 29°C, and diluted to an OD 600 nm of 0.1 – 0.2 in triplicate depending on growth rate. Cultures were then grown for 90 minutes at 29°C, and transferred to a CulturPlate 96-well plate (PerkinElmer) for OD 600 nm and fluorescent measurement at excitation/emission 485 nm/520 nm on a Synergy H1 plate reader. Background fluorescence from media was subtracted, and each sample was normalized to OD 600 nm. The normalized value for the random control was then subtracted. Each sample was then normalized to J23101.

TX-TL promoter characterization on linear and plasmid DNA

Sequenced cultures from frozen stocks were used to inoculate 20 mL of LB-carbenicillin media and grown in parallel to stationery phase. For each sample, 4 x 3 mL of sample was miniprepped using previously described procedures. The miniprep products were PCR purified into one 30 μL sample, and re-sequenced. To generate linear DNA for each sample with 250 bp of non-coding DNA at each end, the resulting plasmid was PCR amplified in 4 x 50 μL reactions, DpnI digested, and PCR purified into one 30 μL sample. Plasmid and linear DNA were quantified by spectrophotometry. For each promoter, DNA was diluted 1:2 from 4-32 nM for linear DNA or 2–6 nM for plasmid DNA in water or 0.5 mM IPTG for Pl-lacO1. To generate relative strength to J23101, background fluorescence and random control sequence fluorescence were subtracted per promoter sample, and endpoint data was normalized to J23101. To generate saturation

curves, background fluorescence was subtracted per promoter sample, and correlation and slope for each promoter (including the random control sequence) was determined.

TX-TL promoter induction curves

DNA was prepared as previously mentioned. For Pl-lacO1, 1 nM of a Pl-tetO1-lacI plasmid and 2 nM of either linear or plasmid Pl-lacO1-deGFP were combined with varying amounts of IPTG in the presence of gamS and endpoint fluorescence was read. For Pl-tetO1, the same was done but with 1 nM of a Pl-lacO1-tetR plasmid, 2 nM of either linear or plasmid Pl-tetO1-deGFP, and 0.5 mM of IPTG in addition to aTc and gamS to inactivate any lacI present in the extract. Data was subtracted from background fluorescence for those containing aTc.

Acknowledgements

We thank Shaobin Guo, Dan Siegal-Gaskins, Anu Thubagere, Jongmin Kim, and Patrik Lundin for assistance testing initial methods of linear DNA assembly and protection, Emmanuel de Los Santos for advice on protein purification, Victoria Hsiao for assistance on *in vivo* assays, Angela Ho and Jost Vielmetter for protein purification through the Caltech Protein Expression Center and contribution of Figure S3a, and Clare Chen and Barclay Lee for assistance in the early stages of the project. This material is based upon work supported in part by the Defense Advanced Research Projects Agency (DARPA/MTO) Living Foundries program, contract number HR0011-12-C-0065 (DARPA/CMO). Z.Z.S. is also supported by a UCLA/Caltech Medical Scientist Training Program fellowship and Z.Z.S and E.Y are supported by National Defense Science and Engineering Graduate fellowships. The views and conclusions contained in this document are those of the authors and should not be interpreted as representing officially policies, either expressly or implied, of the Defense Advanced Research Projects Agency or the U.S. Government.

Author Contributions

Z.Z.S., E.Y., and C.A.H., designed the experiments with guidance from V.N and R.M.M. Z.Z.S performed the experiments. All analyzed the data. Z.Z.S wrote the manuscript. The authors declare no competing financial interest.

Figure 1

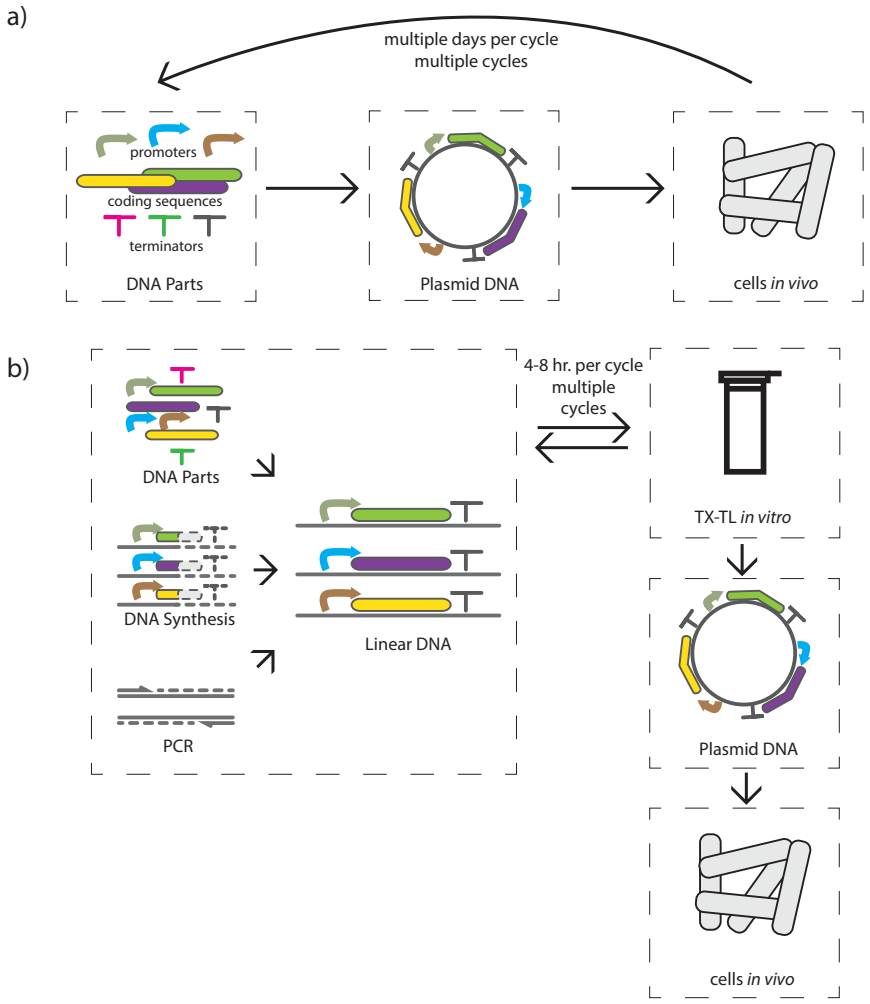

Figure 1. Overview of rapid prototyping procedure of gene circuits. a) Traditional testing of circuits, where parts are cloned onto a single plasmid or sets of complementary plasmids, tested in vivo, and cycled back to construction. b) Rapid prototyping procedure, where circuits are cycled between construction on linear DNA and testing in TX-TL. When a final circuit prototype is completed, only 1 cycle occurs of plasmid DNA construction and circuit implementation in vivo.

Figure 2

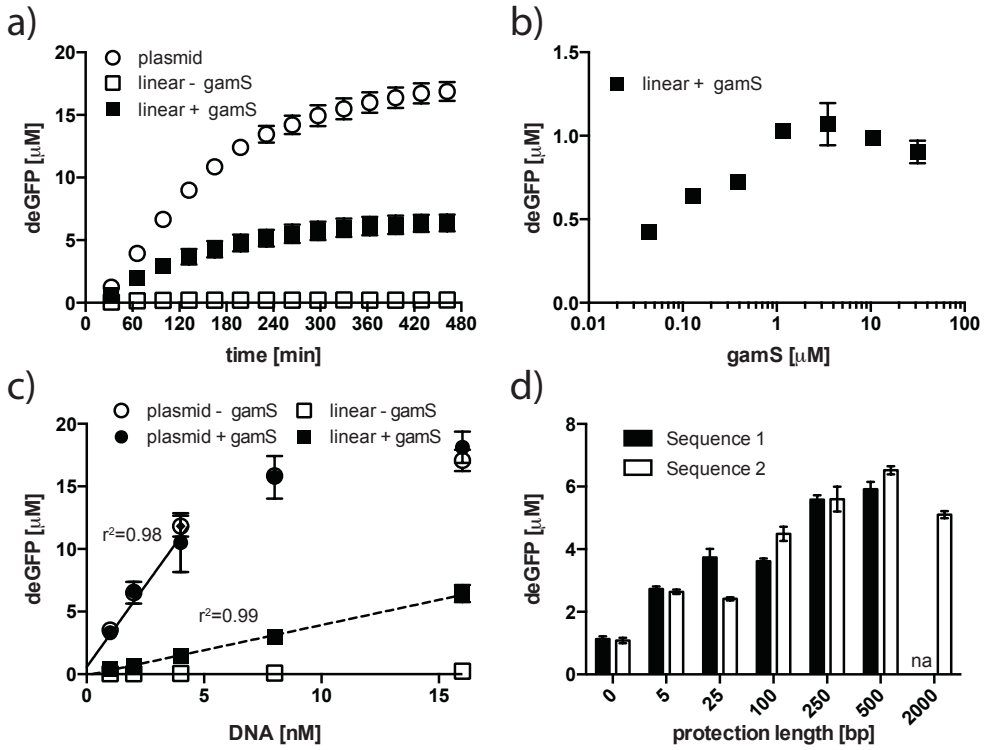

Figure 2. Protection of linear DNA from degradation in TX-TL. a) Comparison of deGFP time-series fluorescence for plasmid DNA, linear DNA without gamS protection, and linear DNA with gamS protection. Plasmid DNA used is pBEST-OR2-OR1-Pr-UTR1-deGFP-T500, linear DNA is an 810 bp PCR product with no steric protection ends, and each is supplied at 16 nM. b) Endpoint deGFP expression after 8 hours of 2 nM of linear DNA plotted against signal for different working concentrations of gamS, without prior incubation of the protein with crude extract. c) Endpoint deGFP expression from plasmid and linear DNA with or without gamS protein, at increasing DNA concentrations. Correlation of 0.98 on plasmid DNA is for 0 nM – 4 nM values only; correlation of 0.99 on linear DNA is for 0 nM – 16 nM. d) Protection of 2 nM of linear DNA using different amounts of non-coding DNA at template ends. Each length corresponds to an amount of non-coding base pairs at each end of the linear DNA, and Sequence 1 is independent of Sequence 2. Readout is endpoint deGFP fluorescence after 8 hours, and experiment is in the presence of gamS protein. Error bars represent one standard deviation from three independent experiments.

Figure 3

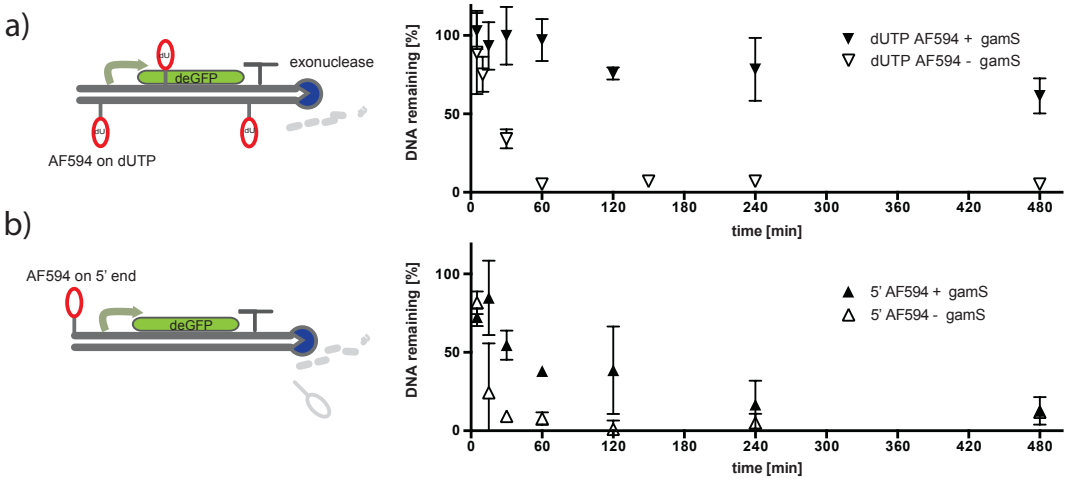

Figure 3. Time-series of DNA degradation in TX-TL at typical working concentrations. a) DNA degradation of 2 nM (25 ng) of DNA with or without 3.5 μM of gamS. DNA is labeled throughout by an AlexaFluor-594-5-dUTP incorporated by PCR. Percentage of DNA remaining is based on 25 ng present at time 0. b) Same experiment as panel a), but with AlexaFluor-594 incorporated at the 5' end on a PCR primer. Error bars represent one standard deviation from three independent experiments.

Figure 4

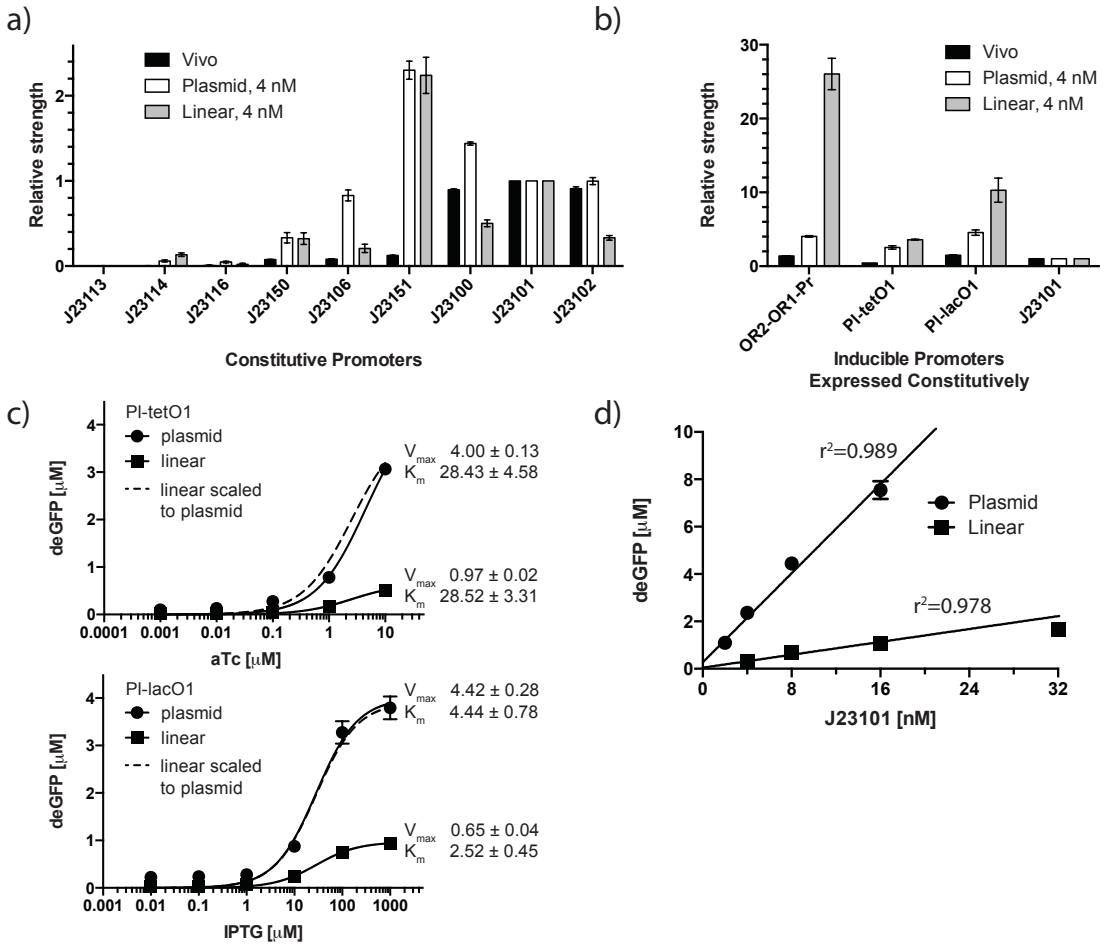

Figure 4. Comparison of different promoter strengths in TX-TL and in vivo. a) Nine commonly used BioBrick promoters are cloned in front of a strong RBS and expressed in either mid-log phase *in vivo*, on plasmids in TX-TL, or on linear DNA pieces in TX-TL. Relative endpoint expression of a 4 nM non-saturating amount of linear and plasmid DNA is scaled to the strength of J23101, with signal from a random promoter sequence subtracted. b) Three inducible promoters expressed constitutively are similarly analyzed, scaled to the strength of J23101. For Pl-lacO1, 0.5 mM of IPTG is added both to the *in vivo* and the TX-TL data to sequester any native lacI repressor. c) Hill functions for Pl-lacO1 and Pl-tetO1 on linear and on plasmid to varying amounts of IPTG and aTc, respectively. 1 nM of a plasmid constitutively producing tetR or lacI is combined with 2 nM of a linear or plasmid reporter. d) Saturation curve for J23101, plotting endpoint fluorescence to concentration of linear or plasmid DNA. Both r^2 and linear regression line are derived from 0 – 16 nM data points. Linear DNA is protected with 250 bp of steric protection and with gamS. Error bars represent one standard deviation from three independent experiments.

Figure 5

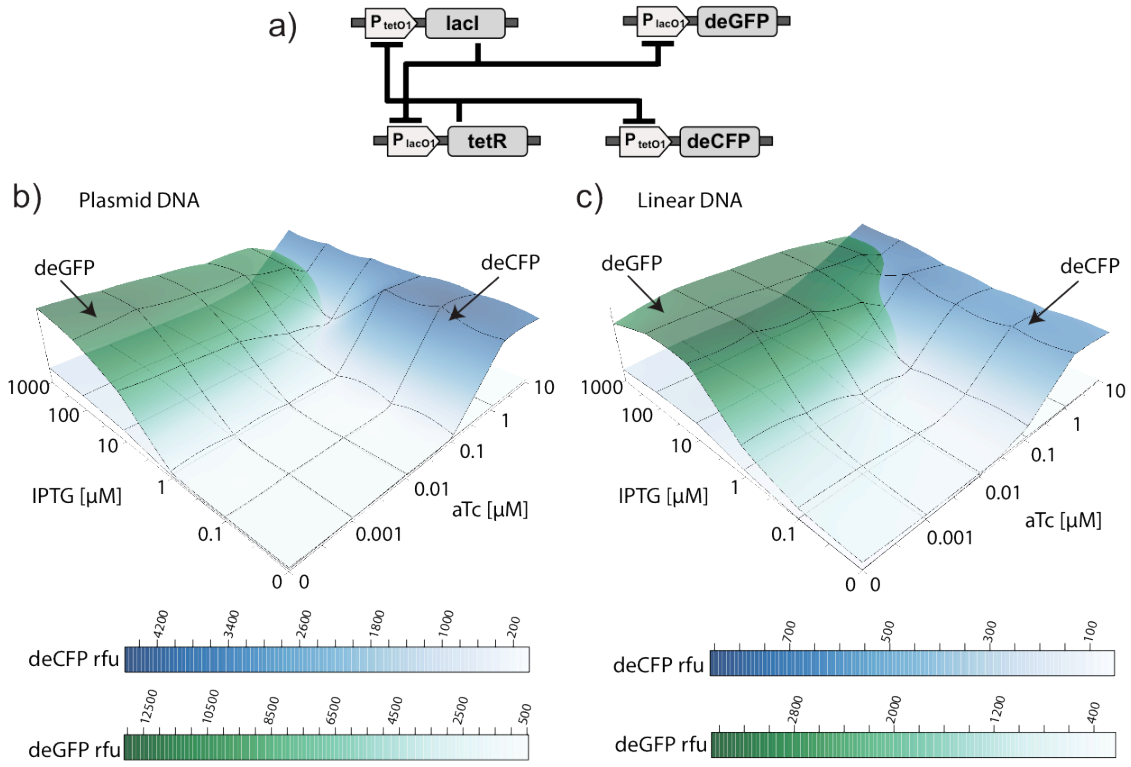

Figure 5. Comparison of a genetic switch made from linear vs. plasmid DNA. a) Diagram of the genetic switch. b) Endpoint fluorescence of deGFP and deCFP for plasmid DNA at various IPTG and aTc inducer concentrations. Four plasmid DNA pieces are used at 2 nM reporter and 1nM repressor. Due to the logarithmic scale, 0 μM is represented as 0.01 μM for IPTG and 0.001 μM for aTc. c) Endpoint fluorescence for four linear DNA pieces at the same concentration. Linear DNA is protected with 31 bp of steric protection and with gamS.

Figure 6

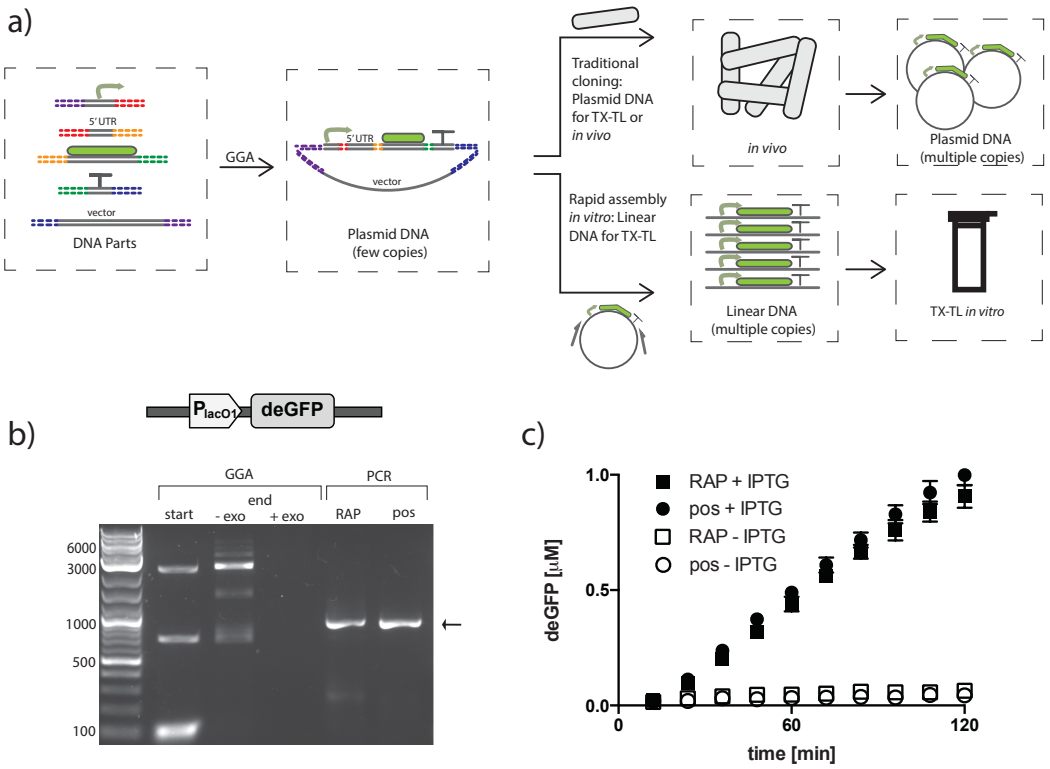

Figure 6. Rapid *in vitro* assembly and prototyping in TX-TL. a) Overview of the rapid assembly and prototyping procedure, where DNA parts are assembled using Golden Gate assembly ("GGA") to create a plasmid, which is then directly used as a PCR template to create linear DNA at high concentrations suitable for TX-TL. In parallel, the assembly product can also be propagated *in vivo* to yield more copies of clonal plasmid. Time comparisons for both methods can be found in Table S2. b) Agarose gel of a gene assembled from 5 standard pieces of 66 bp, 103 bp, 110 bp, 707 bp, and 2376 bp. Shown are 50 ng each of starting fragments (except 66 bp), fragments post-assembly before and after exonuclease digestion ("exo"), and rapid assembly PCR product ("RAP") compared to post-cloned PCR product ("pos"). Arrow indicates expected size of 892 bp. c) Functional testing of 4 nM of rapid assembly or post-cloned products, with or without 0.5 mM IPTG inducer. Experiment conducted in the presence of 2 nM Pl-tetO1-lacI linear DNA. Linear DNA is protected with 31 bp of steric protection and with gamS. Error bars represent one standard deviation from three independent experiments.

Figure 7

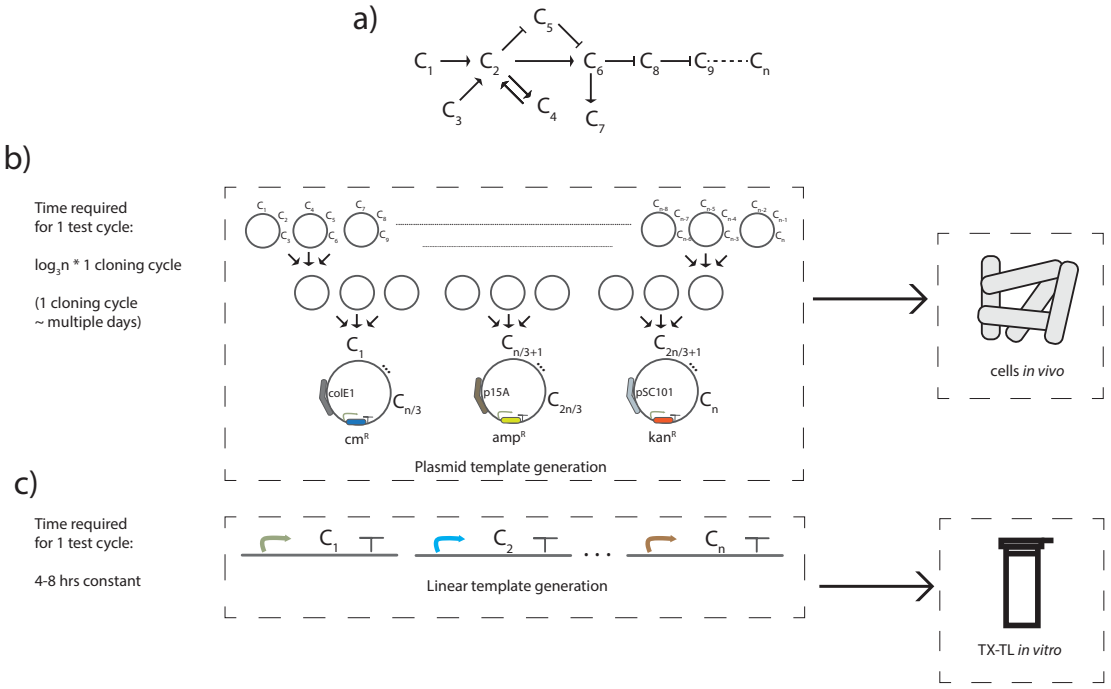

Figure 7. Linear DNA prototyping of large synthetic circuits in TX-TL. a) A large circuit composed of *n* components is to be prototyped *in vivo* or in TX-TL. b) Prototyping *in vivo* requires the reduction of *n* components to three plasmids, which can then be transformed into a cell. c) Prototyping using rapid assembly of linear DNA requires 4-8 hours, as each component can be assembled and tested in parallel.

Table 1

Calibration data for different promoters in TX-TL. Twelve promoters are tested at different concentrations in linear (4-32 nM) and plasmid (2-16 nM) DNA form and a linear regime is determined based on a cutoff of $r^2 > 0.975$. The slopes (m) are of the resulting linear regression, in units of μM deGFP/nM DNA. P:L ratio is the ratio of the slopes. "nd": signal not detectable, "na": not applicable. Error represents one standard deviation from three independent experiments.

Promoter name	Plasmid DNA (P)			Linear DNA (L)			P:L ratio
	linear regime DNA [nM]	r^2	m	linear regime DNA [nM]	r^2	m	
OR2-OR1-Pr	0-4	0.998	2.211 ± 0.058	0-8	0.979	1.582 ± 0.018	1.40
Pl-tetO1	0-8	0.980	1.187 ± 0.029	0-16	0.993	0.228 ± 0.029	5.21
Pl-lacO1	0-4	0.990	2.666 ± 0.111	0-8	0.998	0.722 ± 0.085	3.69
J23113	nd	na	na	0-8	0.976	0.003	na
J23114	0-16	0.985	0.025 ± 0.001	0-16	0.981	0.012	2.08
J23116	0-16	0.975	0.022 ± 0.001	0-16	0.984	0.004	5.50
J23150	0-16	0.986	0.187 ± 0.009	0-16	0.982	0.022 ± 0.001	8.50
J23106	0-8	0.992	0.420 ± 0.007	0-16	0.996	0.018	23.33
J23151	0-8	0.982	1.091 ± 0.108	0-8	0.995	0.186 ± 0.017	5.87
J23100	0-8	0.995	0.761 ± 0.049	0-8	0.998	0.041 ± 0.006	18.56
J23101	0-16	0.989	0.470 ± 0.017	0-16	0.978	0.068 ± 0.005	6.91
J23102	0-16	0.976	0.398 ± 0.018	0-16	0.986	0.024 ± 0.003	16.58

References

1. Green, M. R., Sambrook, J., and Sambrook, J. (2012) *Molecular cloning : a laboratory manual*, 4th ed., Cold Spring Harbor Laboratory Press, Cold Spring Harbor, N.Y.
2. Gibson, D. G., Young, L., Chuang, R. Y., Venter, J. C., Hutchison, C. A., 3rd, and Smith, H. O. (2009) Enzymatic assembly of DNA molecules up to several hundred kilobases, *Nature methods 6*, 343-345.
3. Alzari, P. M., Berglund, H., Berrow, N. S., Blagova, E., Busso, D., Cambillau, C., Campanacci, V., Christodoulou, E., Eiler, S., Fogg, M. J., Folkers, G., Geerlof, A., Hart, D., Haouz, A., Herman, M. D., Macieira, S., Nordlund, P., Perrakis, A., Quevillon-Cheruel, S., Tarandeau, F., van Tilbeurgh, H., Unger, T., Luna-Vargas, M. P., Velarde, M., Willmanns, M., and Owens, R. J. (2006) Implementation of semi-automated cloning and prokaryotic expression screening: the impact of SPINE, *Acta crystallographica. Section D, Biological crystallography 62*, 1103-1113.
4. Ro, D. K., Paradise, E. M., Ouellet, M., Fisher, K. J., Newman, K. L., Ndungu, J. M., Ho, K. A., Eachus, R. A., Ham, T. S., Kirby, J., Chang, M. C., Withers, S. T., Shiba, Y., Sarpong, R., and Keasling, J. D. (2006) Production of the antimalarial drug precursor artemisinic acid in engineered yeast, *Nature 440*, 940-943.
5. Kwok, R. (2010) Five hard truths for synthetic biology, *Nature 463*, 288-290.
6. Forster, A. C., and Church, G. M. (2007) Synthetic biology projects in vitro, *Genome Res 17*, 1-6.
7. Noireaux, V., Bar-Ziv, R., and Libchaber, A. (2003) Principles of cell-free genetic circuit assembly, *P Natl Acad Sci USA 100*, 12672-12677.
8. Hockenberry, A. J., and Jewett, M. C. (2012) Synthetic in vitro circuits, *Current opinion in chemical biology 16*, 253-259.
9. Kim, J., White, K. S., and Winfree, E. (2006) Construction of an in vitro bistable circuit from synthetic transcriptional switches, *Molecular systems biology 2*, 68.
10. Kim, J., and Winfree, E. (2011) Synthetic in vitro transcriptional oscillators, *Molecular systems biology 7*, 465.
11. Saito, H., Kobayashi, T., Hara, T., Fujita, Y., Hayashi, K., Furushima, R., and Inoue, T. (2010) Synthetic translational regulation by an L7Ae-kink-turn RNP switch, *Nature chemical biology 6*, 71-78.
12. Shimizu, Y., Inoue, A., Tomari, Y., Suzuki, T., Yokogawa, T., Nishikawa, K., and Ueda, T. (2001) Cell-free translation reconstituted with purified components, *Nat Biotechnol 19*, 751-755.
13. Nirenberg, M. W., and Matthaei, J. H. (1961) The dependence of cell-free protein synthesis in E. coli upon naturally occurring or synthetic polyribonucleotides, *Proceedings of the National Academy of Sciences of the United States of America 47*, 1588-1602.
14. Sun, Z. Z., Hayes, C. A., Shin, J., Caschera, F., Murray, R. M., and Noireaux, V. (2013) Protocols for Implementing an Escherichia Coli Based TX-TL Cell-Free Expression System for Synthetic Biology, *Journal of Visualized Experiments e50762*.

15. Shin, J., and Noireaux, V. (2010) Study of messenger RNA inactivation and protein degradation in an Escherichia coli cell-free expression system, *Journal of biological engineering 4*, 9.
16. Shin, J., and Noireaux, V. (2010) Efficient cell-free expression with the endogenous E. Coli RNA polymerase and sigma factor 70, *Journal of biological engineering 4*, 8.
17. Karzbrun, E., Shin, J., Bar-Ziv, R. H., and Noireaux, V. (2011) Coarse-grained dynamics of protein synthesis in a cell-free system, *Physical review letters 106*, 048104.
18. Shin, J., and Noireaux, V. (2012) An E. coli cell-free expression toolbox: application to synthetic gene circuits and artificial cells, *ACS synthetic biology 1*, 29-41.
19. Shin, J., Jardine, P., and Noireaux, V. (2012) Genome Replication, Synthesis, and Assembly of the Bacteriophage T7 in a Single Cell-Free Reaction, *Acs Synth Biol 1*, 408-413.
20. Murphy, K. C. (1991) Lambda Gam protein inhibits the helicase and chi-stimulated recombination activities of Escherichia coli RecBCD enzyme, *Journal of bacteriology 173*, 5808-5821.
21. Sitaraman, K., Esposito, D., Klarmann, G., Le Grice, S. F., Hartley, J. L., and Chatterjee, D. K. (2004) A novel cell-free protein synthesis system, *Journal of biotechnology 110*, 257-263.
22. Chappell, J., Jensen, K., and Freemont, P. S. (2013) Validation of an entirely in vitro approach for rapid prototyping of DNA regulatory elements for synthetic biology, *Nucleic acids research 41*, 3471-3481.
23. Lin, C. H., Chen, Y. C., and Pan, T. M. (2011) Quantification bias caused by plasmid DNA conformation in quantitative real-time PCR assay, *PloS one 6*, e29101.
24. Ott, J., and Eckstein, F. (1987) Protection of oligonucleotide primers against degradation by DNA polymerase I, *Biochemistry 26*, 8237-8241.
25. Murphy, K. C. (2007) The lambda Gam protein inhibits RecBCD binding to dsDNA ends, *Journal of molecular biology 371*, 19-24.
26. Mosberg, J. A., Gregg, C. J., Lajoie, M. J., Wang, H. H., and Church, G. M. (2012) Improving lambda red genome engineering in Escherichia coli via rational removal of endogenous nucleases, *PloS one 7*, e44638.
27. Dillingham, M. S., and Kowalczykowski, S. C. (2008) RecBCD enzyme and the repair of double-stranded DNA breaks, *Microbiology and molecular biology reviews : MMBR 72*, 642-671, Table of Contents.
28. Seki, E., Matsuda, N., Yokoyama, S., and Kigawa, T. (2008) Cell-free protein synthesis system from Escherichia coli cells cultured at decreased temperatures improves productivity by decreasing DNA template degradation, *Analytical biochemistry 377*, 156-161.
29. Kelly, J. R., Rubin, A. J., Davis, J. H., Ajo-Franklin, C. M., Cumbers, J., Czar, M. J., de Mora, K., Glieberman, A. L., Monie, D. D., and Endy, D. (2009) Measuring the activity of BioBrick promoters using an in vivo reference standard, *Journal of biological engineering 3*, 4.

30. Lutz, R., and Bujard, H. (1997) Independent and tight regulation of transcriptional units in Escherichia coli via the LacR/O, the TetR/O and AraC/I1-I2 regulatory elements, *Nucleic acids research 25*, 1203-1210.
31. Gardner, T. S., Cantor, C. R., and Collins, J. J. (2000) Construction of a genetic toggle switch in Escherichia coli, *Nature 403*, 339-342.
32. Litcofsky, K. D., Afeyan, R. B., Krom, R. J., Khalil, A. S., and Collins, J. J. (2012) Iterative plug-and-play methodology for constructing and modifying synthetic gene networks, *Nature methods 9*, 1077-1080.
33. Pachuk, C. J., Samuel, M., Zurawski, J. A., Snyder, L., Phillips, P., and Satishchandran, C. (2000) Chain reaction cloning: a one-step method for directional ligation of multiple DNA fragments, *Gene 243*, 19-25.
34. Engler, C., Kandzia, R., and Marillonnet, S. (2008) A one pot, one step, precision cloning method with high throughput capability, *PloS one 3*, e3647.
35. Rosenfeld, N., Elowitz, M. B., and Alon, U. (2002) Negative autoregulation speeds the response times of transcription networks, *Journal of molecular biology 323*, 785-793.
36. Sarrion-Perdigones, A., Falconi, E. E., Zandalinas, S. I., Juarez, P., Fernandez-del-Carmen, A., Granell, A., and Orzaez, D. (2011) GoldenBraid: an iterative cloning system for standardized assembly of reusable genetic modules, *PloS one 6*, e21622.
37. Moon, T. S., Lou, C., Tamsir, A., Stanton, B. C., and Voigt, C. A. (2012) Genetic programs constructed from layered logic gates in single cells, *Nature 491*, 249-253.
38. Tusa, Z. A., Singhal, V., Kim, J., and Murray, R. M. (2013) An In Silico Modeling Toolbox for Rapid Prototyping of Circuits in a Biomolecular "Breadboard" System, In *2013 Conference on Decision and Control*, IEEE, Florence, Italy.
39. Higgins, C. F., Dorman, C. J., Stirling, D. A., Waddell, L., Booth, I. R., May, G., and Bremer, E. (1988) A physiological role for DNA supercoiling in the osmotic regulation of gene expression in S. typhimurium and E. coli, *Cell 52*, 569-584.
40. Karig, D. K., Iyer, S., Simpson, M. L., and Doktycz, M. J. (2012) Expression optimization and synthetic gene networks in cell-free systems, *Nucleic acids research 40*, 3763-3774.
41. Iyer, S., Karig, D. K., Norred, S. E., Simpson, M. L., and Doktycz, M. J. (2013) Multi-input regulation and logic with t7 promoters in cells and cell-free systems, *PloS one 8*, e78442.
42. Niederholtmeyer, H., Stepanova, V., and Maerkl, S. J. (2013) Implementation of cell-free biological networks at steady state, *Proceedings of the National Academy of Sciences of the United States of America 110*, 15985-15990.
43. Okano, T., Matsuura, T., Suzuki, H., and Yomo, T. (2013) Cell-free Protein Synthesis in a Microchamber Revealed the Presence of an Optimum Compartment Volume for High-order Reactions, *ACS synthetic biology*.
44. Okano, T., Matsuura, T., Kazuta, Y., Suzuki, H., and Yomo, T. (2012) Cell-free protein synthesis from a single copy of DNA in a glass microchamber, *Lab on a chip 12*, 2704-2711.

45. Iyer, S., and Doktycz, M. J. (2013) Thrombin mediated transcriptional regulation using DNA aptamers in DNA based cell free protein synthesis, *ACS synthetic biology*.

Supplemental Information

Included are Supplemental S1 – S3, Table S1 – S2, Figures S1 – S13, and Supplemental References.

Supplemental S1

We required a method to accurately quantify broad ranges of DNA, and tested both spectrophotometry and fluorometry. Both have known advantages and disadvantages: in particular, spectrophotometry is known to be inaccurate at low DNA concentrations, while fluorometry can produce biased plasmid DNA results due to conformational changes.[1] Comparing spectrophotometry (Nanodrop 2000) to fluorometry (Qubit 2.0 dsDNA HS and BR Assay), we found that linear DNA and plasmid DNA were most accurate and precise on the Nanodrop when at concentrations above 30 ng/μL, incurring at most 5.17% error (Figure S1, Table S1). However, for linear DNA from 2-30 ng/μL both of the dsDNA HS and BR Assays had superior accuracy and precision, incurring at most 12.02% error. For plasmid DNA from 2-30 ng/μL only the dsDNA BR Assay using a linear standard was accurate and precise, incurring 5.07% error. Based on these results, for subsequent data we quantified all constructs above 30 ng/μL on the Nanodrop, end-working concentration linear DNA from 2-30 ng/μL using the Qubit dsDNA HS Assay, and end-working concentration plasmid DNA from 2-30 ng/μL either from diluted Nanodrop stocks above 30 ng/μL or using the dsDNA BR Assay.

DNA Quantification Materials and Methods

A Nanodrop 2000 UV-Vis spectrophotometer (Thermo Fisher Scientific) and a Qubit 2.0 fluorometer (Invitrogen) were used to measure dsDNA concentration. Per run, either 500 ng/μL of 1 kb DNA ladder (New England Biolabs) or 500 ng/μL of supercoiled DNA ladder (New England Biolabs) were diluted 1:2 down to 0.98 ng/μL in TE buffer and used as experimental samples. For the Nanodrop, 2 μL of sample was used

to determine concentration. For the Qubit, 2 μL of sample was combined with 198 μL of supplied reagent:buffer to determine concentration. Different standards were tested for the Qubit, depending on the assay (dsDNA BR or dsDNA HS) and the type of DNA quantified (linear or plasmid). Linear standards were supplied by the manufacturer; plasmid standards consisted of pUC19 vector at 1000 ng/μL (New England Biolabs) diluted 1:10 in TE for the dsDNA BR assay or 1:100 for the dsDNA HS assay.

Supplemental S2

The following plasmids, relevant DNA pieces, and primers were used in the study, along with Addgene Plasmid Depository Information and sequence data (if applicable).

Plasmids

Name	Short ID	Addgene	Notes
pBEST-p15A-Pl-tetO1-UTR1-lacI-T500	1	45784	
pBEST-p15A-Pl-tetO1-UTR1-deGFP-T500	2	45392	
pBEST-p15A-Pl-lacO1-UTR1-TetR-T500	3		Derived from 2 with replacement of "deGFP" with "tetR" coding sequence
pBEST_OR2-OR1-Pr_UTR1_deCFP_T500	18		Derived from 21 with replacement of "deGFP" with "deCFP" coding sequence
pBEST_OR2-OR1-Pr_UTR1_deGFP-T500	21	40019	
pBADmod1-linker2-gamS	22	45833	
pBEST_OR2-OR1-Pr-UTR1_ClpX-T500	48		Derived from 21 with "ClpX" coding sequence from Genbank U00096.3 substituted for "deGFP" – used as T500 template for 134-137.
pBEST-colE1-Pl-tetO1-UTR1-deGFP-T500	58		Derived from 21 with replacement of "OR2-OR1-Pr" with "Pl-tetO1"
pBEST-2kblhr2-OR2-OR1-Pr_UTR1_deGFP_T500-1gltB2kb	87		Derived from gltB and lhr genes from Genbank U00096.3 cloned into 21 - directly after T500 from <3354960 (AAAACTA…):3356959 (…GTGCTTC)> and directly before OR2-OR1-Pr from <1731632(ACGGTGG…):1733631(…GGTCCGG). G->A silent mutation in T500
pBEST_OR2-OR1-Pr_UTR1-deGFP-T500 BsaI, BbsI-safe	105		Derived from 21 with silent mutations to make BsaI, BbsI compatible
pBEST-Pl-tetO1-tetR-linker-deGFP-T500	109		Post cloned 4-piece from Isothermal/Golden Gate assembly (GGA), using sequences from 2 (Pl-tetO1-UTR1), 3 (tetR+linker from primer extension), 21 (linker from primer extension + deGFP), and 105 (vector backbone).
pBEST-p15A-Pl-tetO1-UTR1-lacI-T500 BsaI, BbsI-safe	113		Derived from 1 with silent mutations to make BsaI, BbsI compatible

pBEST-p15A-OR2-OR1-Pr-UTR1-deGFP-T500	121		Derived from 1 with promoter replacement
pBEST-p15A-Pl-tetO1-deGFP-T500	122		“
pBEST-p15A-Pl-lacO1-deGFP-T500	123		“
pBEST-p15A-J23113-deGFP-T500	124		“
pBEST-p15A-J23114-deGFP-T500	125		“
pBEST-p15A-J23116-deGFP-T500	126		“
pBEST-p15A-J23150-deGFP-T500	127		“
pBEST-p15A-J23106-deGFP-T500	128		“
pBEST-p15A-J23151-deGFP-T500	129		“
pBEST-p15A-J23100-deGFP-T500	130		“
pBEST-p15A-J23101-deGFP-T500	131		“
pBEST-p15A-J23102-deGFP-T500	132		“
pBEST-p15A-pNull-deGFP-T500	133		“
P3U2C7T2-v1-1 (Pl-lacO1-deGFP)	134		Post cloned 5-piece GGA using sequences from 105 (backbone), 3 (Pl-lacO1), 21 (UTR1), 21 (deGFP), and 48 (T500).
P4U2C8T2-v1-1 (Pl-tetO1-deCFP)	135		Post cloned 5-piece GGA using sequences from 105 (backbone), 2 (Pl-tetO1), 21 (UTR1), 18 (deCFP), and 48 (T500).
P3U2C5T2-v1-2 (Pl-lacO1-tetR)	136		Post cloned 5-piece GGA using sequences from 105 (backbone), 3 (Pl-lacO1), 21 (UTR1), 3 (tetR), and 48 (T500).
P4U2C6T2-v1-2 (Pl-tetO1-lacI)	137		Post cloned 5-piece GGA using sequences from 105 (backbone), 2 (Pl-tetO1), 21 (UTR1), 113 (lacI), and 48 (T500).

Promoters, Regulatory Elements, and Coding Sequences

Name	Sequence
OR2-OR1-Pr	TGAGCTAACACCGTGCGTGTTGACAATTTTACCTCTGGCGGTGATAATGGTTGCA
Pl-tetO1	TCCCTATCAGTGATAGAGATTGACATCCCTATCAGTGATAGAGATACTGAGCACA
Pl-lacO1	ATAAATGTGAGCGGATAACATTGACATTGTGAGCGGATAACAAGATACTGAGCACA
J23113	CTGATGGCTAGCTCAGTCCTAGGGATTATGCTAGC
J23114	TTTATGGCTAGCTCAGTCCTAGGTACAATGCTAGC
J23116	TTGACAGCTAGCTCAGTCCTAGGGACTATGCTAGC
J23150	TTTACGGCTAGCTCAGTCCTAGGTATTATGCTAGC
J23106	TTTACGGCTAGCTCAGTCCTAGGTATAGTGCTAGC
J23151	TTGATGGCTAGCTCAGTCCTAGGTACAATGCTAGC
J23100	TTGACGGCTAGCTCAGTCCTAGGTACAGTGCTAGC
J23101	TTTACAGCTAGCTCAGTCCTAGGTATTATGCTAGC
J23102	TTGACAGCTAGCTCAGTCCTAGGTACTGTGCTAGC
pNull	ATTCTGGGATTATACAGTAGTAATCACTAATTTAC
UTR1	AATAATTTTGTTTAACTTTAAGAAGGAGATATA
T500	CAAAGCCCGCCGAAAGGCGGGCTTTTCTGT
deGFP	ATGGAGCTTTTCACTGGCGTTGTTCCCATCCTGGTCGAGCTGGACGGCGACG

	TAAACGGCCACAAGTTCAGCGTGTCCGGCGAGGGCGAGGGCGATGCCACCT ACGGCAAGCTGACCCTGAAGTTCATCTGCACCACCGGCAAGCTGCCCGTGC CCTGGCCCACCCTCGTGACCACCCTGACCTACGGCGTGCAGTGCTTCAGCCG CTACCCCGACCACATGAAGCAGCACGACTTCTTCAAGTCCGCCATGCCCGA AGGCTACGTCCAGGAGCGCACCATCTTCTTCAAGGACGACGGCAACTACAA GACCCGCGCCGAGGTGAAGTTCGAGGGCGACACCCTGGTGAACCGCATCGA GCTGAAGGGCATCGACTTCAAGGAGGACGGCAACATCCTGGGGCACAAGCT GGAGTACAACTACAACAGCCACAACGTCTATATCATGGCCGACAAGCAGAA GAACGGCATCAAGGTGAACTTCAAGATCCGCCACAACATCGAGGACGGCAG CGTGCAGCTCGCCGACCACTACCAGCAGAACACCCCCATCGGCGACGGCCC CGTGCTGCTGCCCGACAACCACTACCTGAGCACCCAGTCCGCCCTGAGCAA AGACCCCAACGAGAAGCGCGATCACATGGTCCTGCTGGAGTTCGTGACCGC CGCCGGGATCTAA
deCFP	ATGGAGCTTTTCACTGGCGTTGTTCCCATCCTGGTCGAGCTGGACGGCGACG TAAACGGCCACAAGTTCAGCGTGTCCGGCGAGGGCGAGGGCGATGCCACCT ACGGCAAGCTGACCCTGAAGTTCATCTGCACCACCGGCAAGCTGCCCGTGC CCTGGCCCACCCTCGTGACCACCCTGACCTGGGGCGTGCAGTGCTTCAGCCG CTACCCCGACCACATGAAGCAGCACGACTTCTTCAAGTCCGCCATGCCCGA AGGCTACGTCCAGGAGCGCACCATCTTCTTCAAGGACGACGGCAACTACAA GACCCGCGCCGAGGTGAAGTTCGAGGGCGACACCCTGGTGAACCGCATCGA GCTGAAGGGCATCGACTTCAAGGAGGACGGCAACATCCTGGGGCACAAGCT GGAGTACAACTACATCAGCCACAACGTCTATATCACCGCCGACAAGCAGAA GAACGGCATCAAGGCCAACTTCAAGATCCGCCACAACATCGAGGACGGCAG CGTGCAGCTCGCCGACCACTACCAGCAGAACACCCCCATCGGCGACGGCCC CGTGCTGCTGCCCGACAACCACTACCTGAGCACCCAGTCCGCCCTGAGCAA AGACCCCAACGAGAAGCGCGATCACATGGTCCTGCTGGAGTTCGTGACCGC CGCCGGGATCTAA
lacI_GGA_safe	ATGAAACCAGTAACGTTATACGATGTCGCAGAGTATGCCGGTGTCTCTTATC AGACCGTTTCCCGCGTGGTGAACCAGGCCAGCCACGTTTCTGCGAAAACGC GGGAAAAAGTGGAAGCGGCGATGGCGGAGCTGAATTACATTCCCAACCGCG TGGCACAACAACTGGCGGGCAAACAGTCGTTGCTGATTGGCGTTGCCACCT CCAGTCTGGCCCTGCACGCGCCGTCGCAAATTGTCGCGGCGATTAAATCTCG CGCCGATCAACTGGGTGCCAGCGTGGTGGTGTCGATGGTAGAACGAAGCGG CGTCGAAGCCTGTAAAGCGGCGGTGCACAATCTTCTCGCGCAACGCGTCAG TGGGCTGATCATTAACTATCCGCTGGATGACCAGGATGCCATTGCTGTGGAA GCTGCCTGCACTAATGTTCCGGCGTTATTTCTTGATGTCTCTGACCAGACAC CCATCAACAGTATTATTTTCTCCCATGAGGACGGTACGCGACTGGGCGTGGA GCATCTGGTCGCATTGGGTCACCAGCAAATCGCGCTGTTAGCGGGCCCATTA AGTTCTGTCTCGGCGCGTCTGCGTCTGGCTGGCTGGCATAAATATCTCACTC GCAATCAAATTCAGCCGATAGCGGAACGGGAAGGCGACTGGAGTGCCATGT CCGGTTTTCAACAAACCATGCAAATGCTGAATGAGGGCATCGTTCCCACTGC GATGCTGGTTGCCAACGATCAGATGGCGCTGGGCGCAATGCGCGCCATTAC CGAGTCCGGGCTGCGCGTTGGTGCGGATATCTCGGTAGTGGGATACGACGA TACCGAGGACAGCTCATGTTATATCCCGCCGTTAACCACCATCAAACAGGAT TTTCGCCTGCTGGGGCAAACCAGCGTGGACCGCTTGCTGCAACTCTCTCAGG GCCAGGCGGTGAAGGGCAATCAGCTGTTGCCCGTCTCACTGGTGAAAAGAA AAACCACCCTGGCGCCCAATACGCAAACCGCCTCTCCCCGCGCGTTGGCCG ATTCATTAATGCAGCTGGCACGACAGGTTTCCCGACTGGAAAGCGGGCAGT GA
tetR	ATGTCTAGATTAGATAAAAGTAAAGTGATTAACAGCGCATTAGAGCTGCTT AATGAGGTCGGAATCGAAGGTTTAACAACCCGTAAACTCGCCCAGAAGCTA GGTGTAGAGCAGCCTACATTGTATTGGCATGTAAAAAATAAGCGGGCTTTG CTCGACGCCTTAGCCATTGAGATGTTAGATAGGCACCATACTCACTTTTGCC CTTTAGAAGGGGAAAGCTGGCAAGATTTTTTACGTAATAACGCTAAAAGTTT TAGATGTGCTTTACTAAGTCATCGCGATGGAGCAAAAGTACATTTAGGTACA CGGCCTACAGAAAAACAGTATGAAACTCTCGAAAATCAATTAGCCTTTTTAT

	GCCAACAAGGTTTTTCACTAGAGAATGCATTATATGCACTCAGCGCTGTGGG GCATTTTACTTTAGGTTGCGTATTGGAAGATCAAGAGCATCAAGTCGCTAAA GAAGAAAGGGAAACACCTACTACTGATAGTATGCCGCCATTATTACGACAA GCTATCGAATTATTTGATCACCAAGGTGCAGAGCCAGCCTTCTTATTCGGCC TTGAATTGATCATATGCGGATTAGAAAAACAACTTAAATGTGAAAGTGGGT CTTAA
linker sequence for tetR-deGFP fusion	GGTGAAAACCTGTACTTCCAGTCTGGTGGTGCT

Primers to make linear sequences and other plasmids

CHA-R	TTTTATCTAATCTAGACATGTGGTATATCTC CTTCTTAAAGTTAA	Isothermal assembly piece 1 to make 109, 2 w/ ZS30432f
CHB	TTTAAGAAGGAGATATACCACATGTCTAGA TTAGATAAAAGTAAAGTGAT	Isothermal assembly piece 2 to make 109, 3 w/ CHB-R
CHB-R	ACCAGACTGGAAGTACAGGTTTTCACCAGA CCCACTTTCACATTTAAGT	Isothermal assembly piece 2 to make 109, 3 w/ CHB
CHC	AACCTGTACTTCCAGTCTGGTGGTGCTATGG AGCTTTTCACTGGC	Isothermal assembly piece 3 to make 109, 21 w/ CHC-R
CHC-R	CTTTGAGTGAGCTGATACCGCAGTCATAAG TGCGGCGA	Isothermal assembly piece 3 to make 109, 21 w/ CHC
CHD	CGTCGCCGCACTTATGACTGCGGTATCAGCT CACTCAAAG	Isothermal assembly piece 4 to make 109, 105 w/ ZS30432r
ZS3033f	TGAGCTAACACCGTGCGT	0 bp protection, 21 w/ ZS3033rb
ZS3033rb	ACAGAAAAGCCCGCCTTTCGGCGGGCTTTG CTCGAGTTAGATC	0 bp protection, 21 w/ ZS3033f
ZS3034f	CATGCTGAGCTAACACCG	5 bp protection, 21 w/ ZS3034ra
ZS3034ra	TCGACACAGAAAAGCCCG	5 bp protection, 21 w/ ZS3034f
ZS3035f	GTGTGTGCTGTTCCGCT	25 bp protection, 21 w/ ZS3035r
ZS3035r	AAGGCTCTCAAGGGCATC	25 bp protection, 21 w/ ZS3035f
ZS3036f	AAAACCGAATTTTGCTGG	100 bp protection, 21 w/ ZS3036r
ZS3036r	ATGATAAAGAAGACAGTCATAAGTGCG	100 bp protection, 21 w/ ZS3036f
ZS3037f	TGGCGAATCCTCTGACC	250 bp protection, 21 w/ ZS3037r or 121-133 w/ ZS30610r or 58, 134-137 w/ ZS3037r
ZS3037r	TCTTTCCTGCGTTATCCC	250 bp protection, 21 w/ ZS3037f or 134-137 w/ ZS3037f
ZS3038f	AAAGGGAATAAGGGCGACA	500 bp protection, 21 w/ ZS3038r
ZS3038r	AGCGCCACGCTTCCC	500 bp protection, 21 w/ ZS3038f
ZS30412f	TCCGGTGAGCTAACACC	0 bp protection, 87 w/ ZS303412r
ZS30412r	GTTTTACAGAAAAGCCCGC	0 bp protection, 87 w/ ZS303412f
ZS30413f	AGAAGTGAATGATCTACCGGTC	5 bp protection, 87 w/ ZS303413r
ZS30413r	AAGAGCATCCCGACAGC	5 bp protection, 87 w/ ZS303413f
ZS30414f	ATTACTCGCCCCAGAGGTT	25 bp protection, 87 w/ ZS303414r
ZS30414r	GACAAGGTTTCGCGTTG	25 bp protection, 87 w/ ZS303414r
ZS30415f	GTGGGGAAATCTTCTGCC	100 bp protection, 87 w/ ZS303415r
ZS30415r	CGGCGGGCGATAAAC	100 bp protection, 87 w/ ZS303415f
ZS30416f	GCTACGGCATCATCAGTC	250 bp protection, 87 w/ ZS303416r
ZS30416r	GGTGATGGTGTTGATTTCAC	250 bp protection, 87 w/ ZS303416f
ZS30417f	ACGGTGGCGAAATTCA	500 bp protection, 87 w/ ZS303417r
ZS30417r	GAAGCACAGGCCCACTAC	500 bp protection, 87 w/ ZS303417f

ZS30432f	ATGACTATCGCACCATCAGCTAACGATATC CGCCTGAT	Isothermal assembly piece 1 to make 109, 2 w/ CHA-R
ZS30432r	GCATCAGGCGGATATCGTTAGCTGATGGTG CGATAGTCA	Isothermal assembly piece 4 to make 109, 21 w/ CHD
ZS30433f	ATCTAGGTCTCTAACGATATCCGCCTGAT	GGA piece 1 to make 109, 2 w/ ZS30433r
ZS30433r	GTTATGGTCTCGACATGTGGTATATCTCCTT CTTAAAGTTAA	GGA piece 1 to make 109, 2 w/ ZS30433f
ZS30434f	GATACGGTCTCCATGTCTAGATTAGATAAA AGTAAAGTGAT	GGA piece 2 to make 109, 3 w/ ZS3081r
ZS30435r	GTGCCGGTCTCATACCGCAGTCATAAGTGC GGCGA	GGA piece 3 to make 109, 21 w/ ZS3081f
ZS30436f	GGTTTGGTCTCCGGTATCAGCTCACTCAAAG	GGA piece 4 to make 109, 105 w/ ZS30436r
ZS30436r	ACGTTGGTCTCTCGTTAGCTGATGGTGCGAT AGTC	GGA piece 4 to make 109, 105 w/ ZS30436f
ZS30512f	AACAGGGTCTCACATGGAGCTTTTCACTGG	GGA “C7”, “C8”, 21 w/ ZS30523r or 18 w/ ZS30523r
ZS30513r	GTCCGGGTCTCACGACTCTCAAGGGCATCG GT	GGA “T2”, 21 w/ ZS30524f
ZS30514f	GTCCTGGTCTCTATGCGTGGTTGTCTTCGTA CGTCCGTCACGTTC	GGA “v1-1”, 105 w/ ZS30514r
ZS30514r	ATATAGGTCTCTGTCGGGCATTGTCTTCGCT CCTTCCGGTGG	GGA “v1-1”, 105 w/ ZS30514f
ZS30515f	TAGCGGGTCTCTGTCGTGCCTTGTCTTCGTT ACGTCCGTCACGTTC	GGA “v1-2”, 105 w/ ZS30528r
ZS30521r	CGTAAGGTCTCAGCTTGCTGTGCTCAGTATC TCT	GGA “P4”, 2 w/ ZS3057f
ZS30522f	AGCCAGGTCTCAAAGCAATAATTTTGTTTA ACTT	GGA “U2”, 21 w/ ZS3059r
ZS30523r	TTAGTGGTCTCATTCATTAGATCCCGGCGGC	GGA “C7”, “C8”, 21 w/ ZS30512f or 18 w/ ZS30512f
ZS30524f	GGCTCGGTCTCATGAAGCATCTGGTGAATA ACTCGAG	GGA “T2”, 21 w/ ZS30513r
ZS30528r	AGGTGGGTCTCTATGCTATGTTGTCTTCGCT CCTTCCGGTGG	GGA “v1-2”, 105 w/ ZS30515f
ZS30534r	CGTAAGGTCTCAGCTTGCTGTGCTCAGTATC TTGT	GGA “P3”, 3 w/ ZS3057f
ZS3057f	AGAACGGTCTCAGCATTGCTGTTCCGCTGG	GGA “P3”, “P4”, 3 w/ ZS30534r or 2 w/ ZS30521r
ZS3059r	TCCCCGGTCTCACATGGTATATCTCCTTCTT A	GGA “U2”, 21 w/ ZS30522f
ZS30610r	GAAGATCATCTTATTAATCAGATAAAATAT	250 bp protection, 121-133 w/ ZS3037f
ZS30611f	ACGAGGCCCTTTCGTCT	250 bp protection, 109 w/ ZS30611r
ZS30611r	ACGAGGCCCTTTCGTCT	250 bp protection, 109 w/ ZS30611f
ZS3064f	T*G*AGCTAACACCGTGCGT	0 bp protection, 2 TS, 21 w/ ZS3064r
ZS3064r	A*C*AGAAAAGCCCGCCTTTCGGCGGGCTTT GCTCGAGTTAGATC	0 bp protection, 2 TS, 21 w/ ZS3064f
ZS3065f	T*G*A*G*C*TAACACCGTGCGT	0 bp protection, 5 TS, 21 w/ ZS3065r
ZS3065r	A*C*A*G*A*AAAGCCCGCCTTTCGGCGGGC TTTGCTCGAGTTAGATC	0 bp protection, 5 TS, 21 w/ ZS3065f
ZS3066f	C*A*TGCTGAGCTAACACCG	5 bp protection, 2 TS, 21 w/ ZS3066r
ZS3066r	T*C*GACACAGAAAAGCCCGCCTTTCGGCGG	5 bp protection, 2 TS, 21 w/ ZS3066f

	GCTTTGCTCG	
ZS3067f	C*A*T*G*C*TGAGCTAACACCG	5 bp protection, 5 TS, 21 w/ ZS3067r
ZS3067r	T*C*G*A*C*ACAGAAAAGCCCGCCTTTCGG CGGGCTTTGCTCG	5 bp protection, 5 TS, 21 w/ ZS3067f
ZS3068f	T*G*GCGAATCCTCTGACC	250 bp protection, 2 TS, 21 w/ ZS3068r
ZS3068r	T*C*TTTCCTGCGTTATCCC	250 bp protection, 2 TS, 21 w/ ZS3068f
ZS3069f	T*G*G*C*G*AATCCTCTGACC	250 bp protection, 5 TS, 21 w/ ZS3069r
ZS3069r	T*C*T*T*T*CCTGCGTTATCCC	250 bp protection, 5 TS, 21 w/ ZS3069f
ZS3071f	/5Alex594N/TGGCGAATCCTCTGACC	250 bp protection, 5' AF594, 21 w/ ZS3071r
ZS3071r	/5Alex594N/TCTTTCCTGCGTTATCCC	250 bp protection, 5' AF594, 21 w/ ZS3071f
ZS30810f	CAACCACGCATTGCTGTT	Overlap primers on "v1-1", 134-135 w/ ZS30810r
ZS30810r	CAATGCCCGACTCTCAAG	Overlap primers on "v1-1", 134-135 w/ ZS30810f
ZS30811f	CAAGGCACGACTCTCAAG	Overlap primers on "v1-2", 136-137 w/ ZS30811f
ZS30811r	ACAACATAGCATTGCTGTTC	Overlap primers on "v1-2", 136-137 w/ ZS30811r
ZS3081f	TCCTTGGTCTCGCTTCCAGTCTGGTGGTGCT ATGGAGCTTTTCACTGGC	GGA piece 3 to make 109, 21 w/ ZS30435r
ZS3081r	TAACCGGTCTCAGAAGTACAGGTTTTCACC AGACCCACTTTCACATTTAAGT	GGA piece 2 to make 109, 3 w/ ZS30434f

Supplemental S3

Inducible promoters Pl-tetO1 and Pl-lacO1 in linear and plasmid DNA were fit to a standard Hill function to approximate Michaelis-Menten dynamics using Prism 6.0 software (GraphPad Software, Inc.), which assumes a hill slope of 1.0:

$$[\boldsymbol{deGFP}] = \frac{\boldsymbol{V_{max}}[\boldsymbol{inducer}]}{\boldsymbol{K_m} + [\boldsymbol{inducer}]}$$

Table S1

Comparing absorbance and fluorometric quantifications of linear and plasmid DNA. (numerical). Data from Figure S1 in numerical form, with percent error from expected value included.

Linear	**Nanodrop**		**BR linear standard**		**HS linear standard**	
Expected (ng/μL)	Actual (ng/μL)	% Error	Actual (ng/μL)	% Error	Actual (ng/μL)	% Error
500	490.8 +/ 4.2	1.84%	471.7 +/- 41.3	5.67%		
250	251.3 +/- 2.1	0.53%	229.7 +/- 2.5	8.13%		
125	126.7 +/- 3.6	1.36%	114.7 +/- 1.2	8.27%	55	56.00 %
62.5	63.80 +/- 3.10	2.08%	53.63 +/- 2.24	10.99 %	55.33 +/- 1.15	11.47 %
31.25	32.87 +/- 2.61	5.17%	27.73 +/- 2.00	11.25 %	28.07 +/- 2.38	10.19 %
15.625	17.33 +/- 1.99	10.93%	13.97 +/- 1.40	10.61 %	13.77 +/- 1.76	11.89 %
7.8125	9.60 +/- 1.84	22.88%	6.97 +/- 0.92	10.74 %	7.02 +/- 1.09	10.14 %
3.90625	5.67 +/- 1.50	45.07%	3.51 +/- 0.82	10.06 %	3.44 +/- 0.69	12.02 %
1.953125	3.70 +/- 0.82	89.44%	1.77 +/- 0.54	9.38%	1.78 +/- 0.32	8.86%
0.976563	2.50 +/- 1.13	156.00 %	1.17 +/- 0.05	19.30 %	0.91 +/- 0.15	6.65%

Plasmid	**Nanodrop**		**BR linear standard**		**HS linear standard**		**BR plasmid standard**		**HS plasmid standard**	
Expected (ng/μL)	Actual (ng/μL)	% Error	Actual (ng/μL)	% Error	Actual (ng/μL)	% Error	Actual (ng/μL)	% Error	Actual (ng/μL)	% Error
500	494.2 +/- 7.1	1.15%	516.0 +/- 24.3	3.20%			556.7 +/- 47.3	11.33 %		
250	255.7 +/- 4.6	2.28%	244.7 +/- 6.4	2.13%			260.7 +/- 18.0	4.27%		
125	128.9 +/- 5.3	3.15%	122.0 +/- 7.5	2.40%			124.0 +/- 3.5	0.80%		
62.5	64.87 +/- 4.02	3.79%	59.90 +/- 4.16	4.16%	46.43 +/- 6.93	25.71 %	61.10 +/- 3.47	2.29%		
31.25	32.83 +/- 3.32	5.07%	29.43 +/- 3.40	5.81%	19.10 +/- 0.72	38.88 %	29.37 +/- 1.01	6.03%	27.13 +/- 1.93	13.17 %
15.625	16.83 +/- 2.50	7.73%	14.83 +/- 2.11	5.07%	8.57 +/- 0.85	45.13 %	14.53 +/- 0.74	6.99%	12.77 +/- 1.50	18.29 %
7.8125	8.67 +/- 2.23	10.93%	7.54 +/- 1.19	3.49%	4.02 +/- 0.28	48.50 %	7.32 +/- 0.31	6.26%	5.70 +/- 0.75	27.04 %
3.90625	4.57 +/- 1.70	16.91%	3.75 +/- 0.87	4.00%	1.99 +/- 0.20	49.14 %	3.52 +/- 0.26	9.97%	2.90 +/- 0.22	25.76 %
1.953125	2.80 +/- 1.73	43.36%	1.88 +/- 0.57	3.57%	0.99 +/- 0.06	49.33 %	1.84 +/- 0.17	5.96%	1.44 +/- 0.07	26.27 %
0.976563	1.60 +/- 1.40	63.84%	1.17 +/- 0.11	19.81 %	0.50 +/- 0.04	48.77 %	1.12	14.69 %	0.72 +/- 0.08	26.48 %

Table S2
Time Estimates of a Test Cycle in TX-TL. Time needed for rapid assembly in vitro versus traditional cloning, corresponding to Figure 6, is presented.

	Rapid Assembly[1]	Conventional Techniques (plasmid generation)
PCR of segments	na	1 h 15 min
DpnI digest[2, 3]	na	5 min
Assembly reaction[4]	1 h	1 h
Transformation and Recovery	na	1 h 30 min
Overnight growth on plates	na	16 h
Colony isolation and liquid media growth	na	8 h
Miniprep	na	30 min
PCR of rapid assembly product	1 h 15 min	
PCR Cleanup[3]	15 min	15 min
Setup TX-TL	15 min	15 min
TOTAL pre-TX-TL	2 h 45 min	1 d +
TOTAL post-TX-TL	4 h – 8 h	1 d +

[1] Rapid Assembly assumes the use of premade, re-usable modular parts – if these are not available, add 1 h 20 min to predicted time and follow beginning of "Conventional Techniques" protocol.

[2] Assumes the use of a fast-digest enzyme.

[3] During digest, run the previous reaction on an agarose gel to determine purity and reaction completion.

[4] Golden Gate Assembly has multiple protocols, from 1h to 3h20min in length. Protocol listed here assumes 10 cycles of 2min/37°C, 3min/20°C, 1 cycle 5min/50°C, 5min/80°C. Difficult assemblies can be accomplished by increasing cycling steps or by doing a constant at 37°C. Isothermal assembly can also be used in lieu.

Figure S1

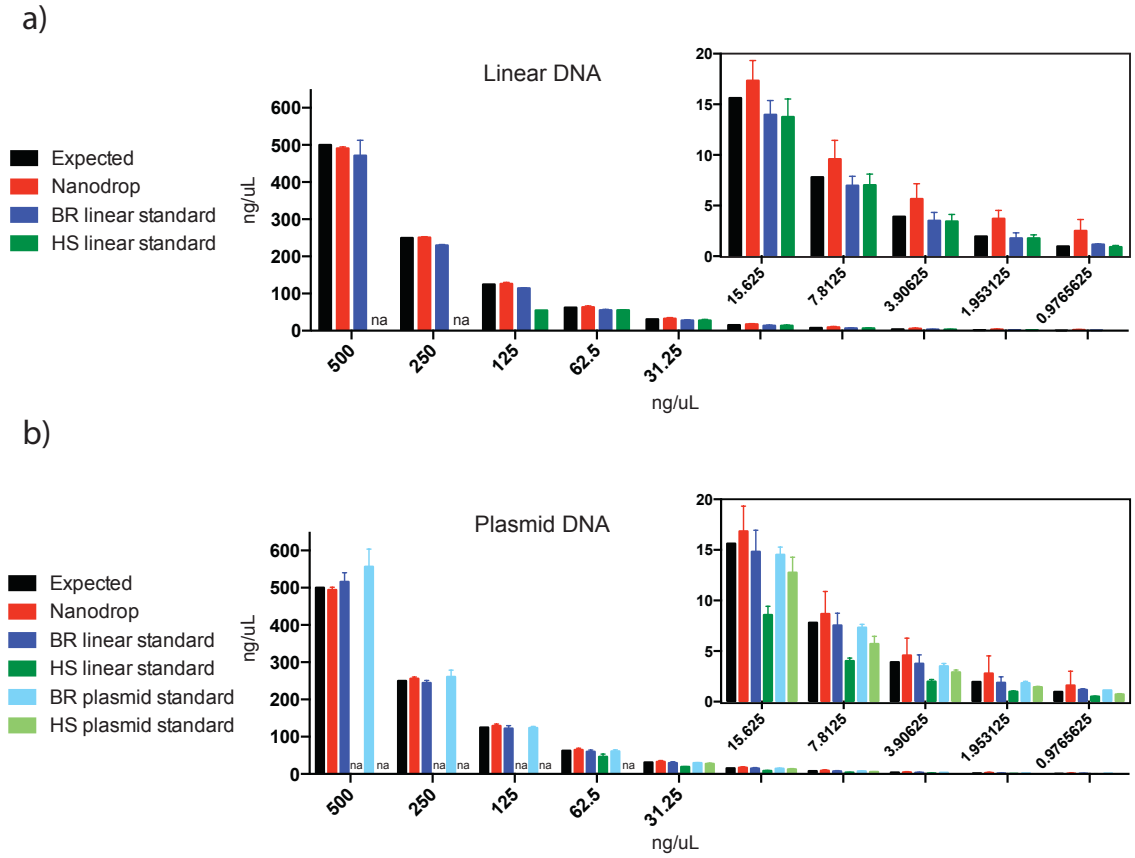

Figure S1. Comparing spectrophotomeric and fluorometric quantifications of linear and plasmid DNA. (graphic). a) 2 μL of 1kb linear ladder DNA at the expected ng/μL is either measured in the Nanodrop or the Qubit fluorometer using the dsDNA BR assay or dsDNA HS assay. Error bars represent a standard deviation from three independent samples, and "na" indicates out of range of the machine. b) Same process as a), but with supercoiled plasmid ladder DNA. BR linear standard: supplied with Qubit dsDNA BR Assay kit; HS linear standard: supplied with Qubit dsDNA HS Assay kit; BR plasmid standard: pUC19 plasmid DNA of known concentration at 0 ng/μL and 100 ng/μL in TE buffer; HS plasmid standard: pUC19 at 0 ng/μL and 10 ng/μL in TE buffer.

Figure S2

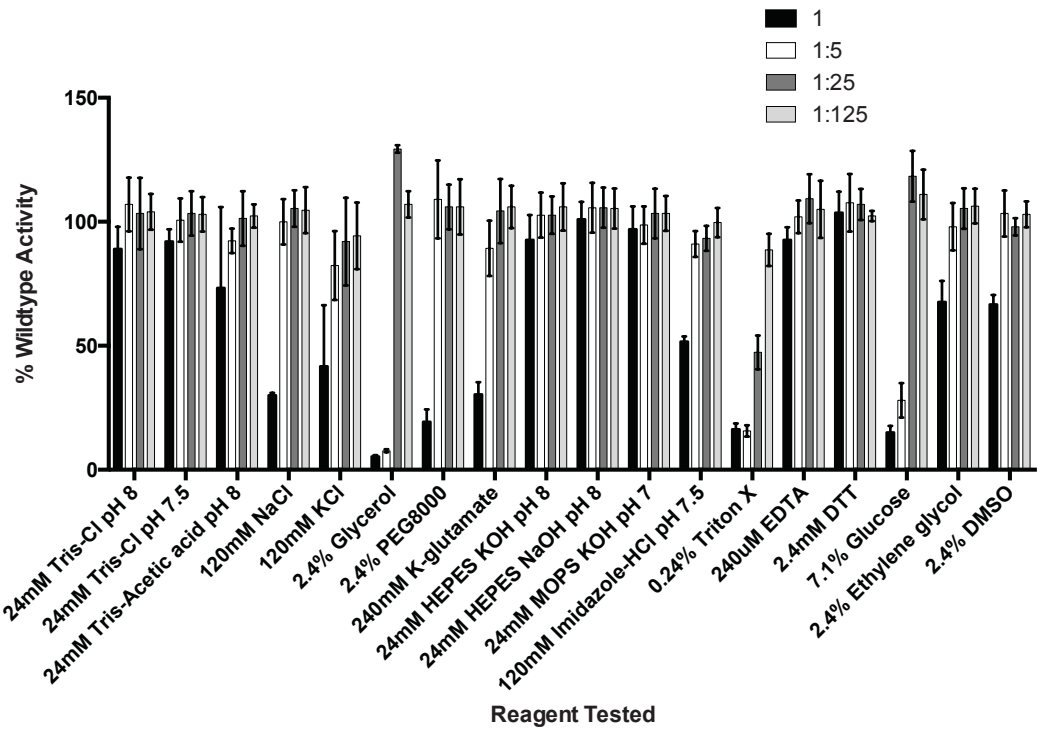

Figure S2. Effects of different additives on TX-TL efficiency. A variety of different additives commonly used in protein buffers are tested for toxicity. Endpoint fluorescence after 8 hours is determined for 1nM of pBEST-OR2-OR1-Pr-UTR1-deGFP-T500 at the final working concentrations listed in TX-TL or at 1:5 dilutions. Percent wildtype activity is against a control with no additive. Error bars represent one standard deviation from three independent experiments. Experiment is done in extract "e10."

Figure S3

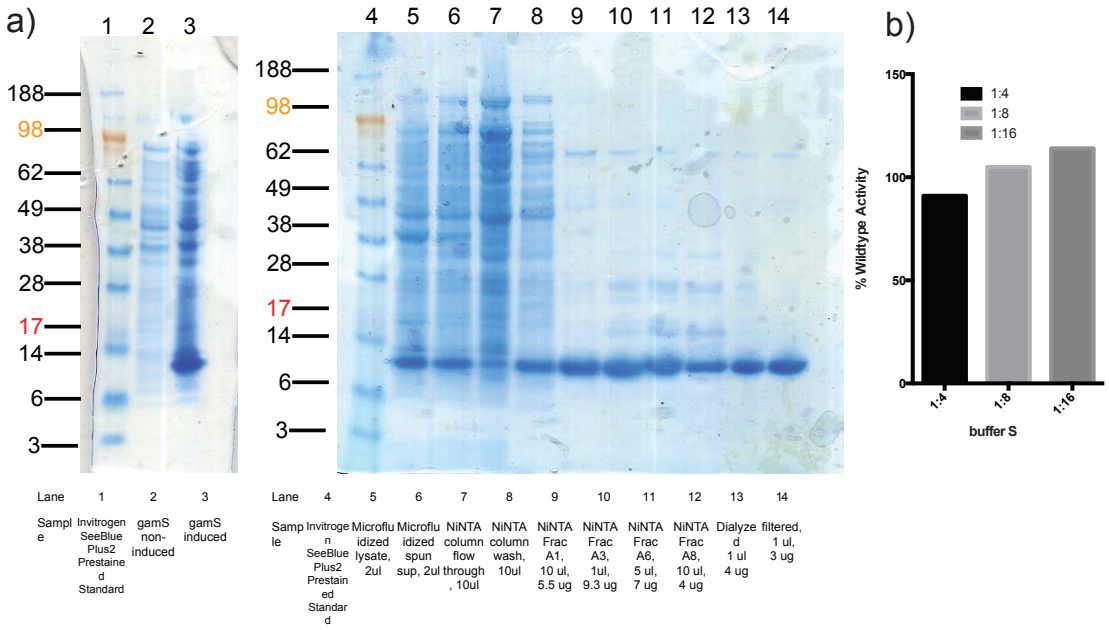

Figure S3. Purification of gamS protein into gamS storage buffer S. a) GamS protein is purified, expressed, and concentrated into 3 mg/ml as described in "Materials and Methods." Shown is the Coomassie Brilliant Blue stain of the purification procedure. b) Buffer toxicity of gamS storage buffer in TX-TL at different dilutions. Storage buffer composition ("buffer S") is 50 mM Tris-Cl pH 7.5, 100 mM NaCl, 1 mM DTT, 1 mM EDTA, 2% DMSO. Experiment is done in extract "e10."

Figure S4

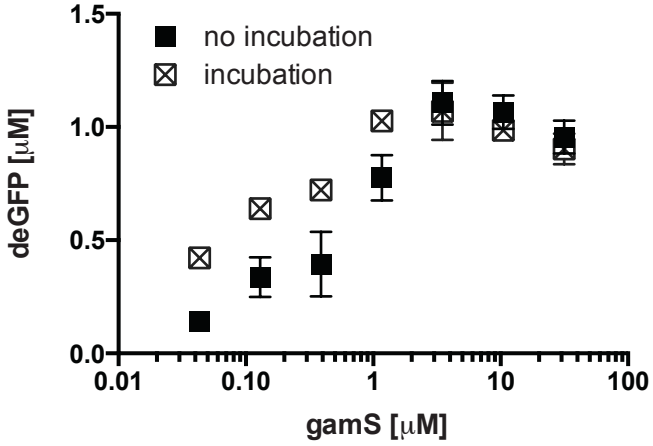

Figure S4. Effect of incubation time of gamS protein on linear protection. GamS protein to the listed concentration is added either directly to the crude cell extract for 30 minutes at room temperature ("incubation," square-x) or directly to the DNA ("no incubation," black-x). In the "incubation" case, crude cell extract incubated with gamS protein is then moved to 4°C and added to DNA. In the "no incubation" case, crude cell extract at 4°C is added directly to a mix of DNA and gamS protein. Reaction is run with 2 nM of linear DNA with no protection, and deGFP endpoint signal is measured. Error bars represent one standard deviation from three independent experiments.

Figure S5

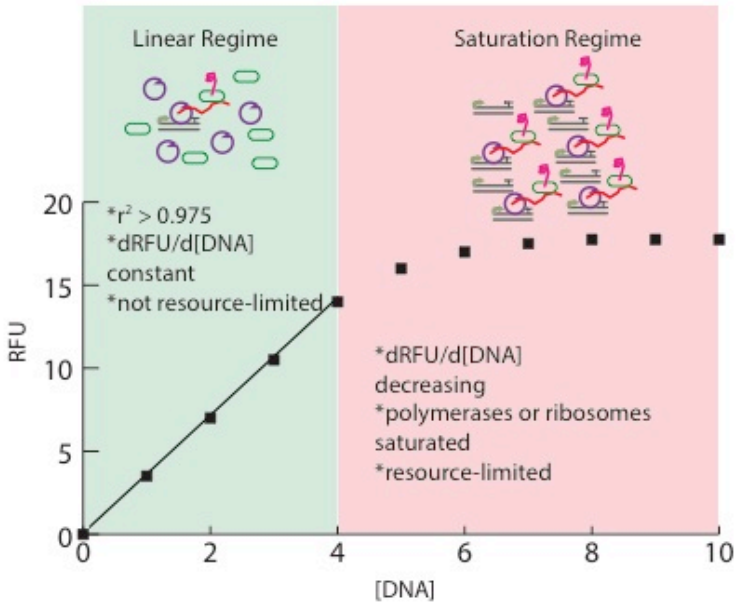

Figure S5. Definition of linear regime and saturation regime in TX-TL. Cartoon diagram shows hypothetical reaction with reporter protein, where rate of signal increase with DNA is constant up to 4 nM ("linear regime", green), begins to slow from 4 nM to 7 nM before becoming 0 above 7 nM ("saturation regime," red). The linear regime is not resource-limited, while the saturation regime is resource limited. Purple semicircle: RNA polymerase; green oval: ribosome; grey lines: DNA; red line: mRNA; pink squiggly: protein.

Figure S6

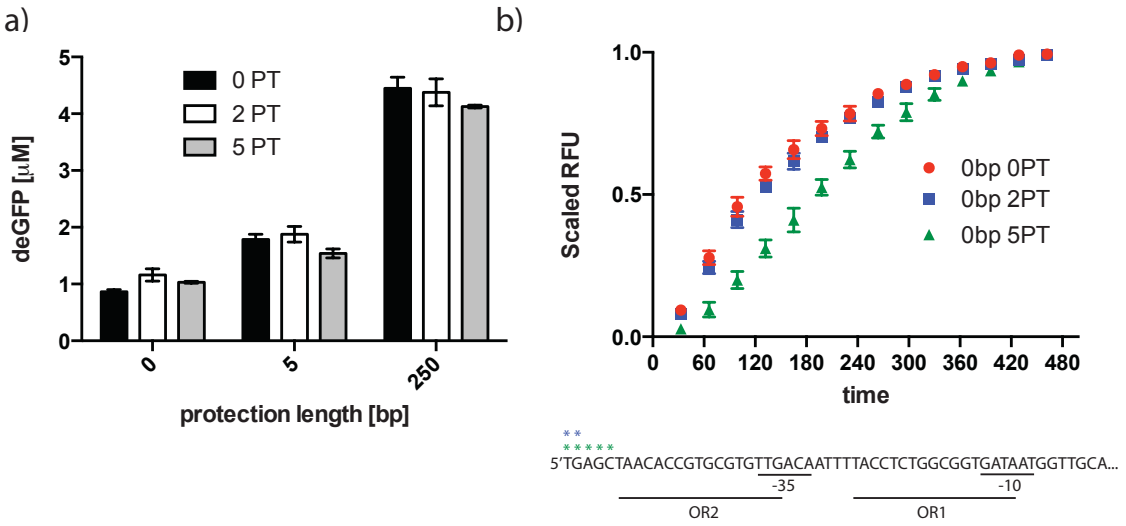

Figure S6. Protection of linear constructs with varying amounts of phosphorothioates. a) Endpoint expression of 2 nM linear DNA with 0, 2, or 5 phosphorothioates ("PT") on the 5" end on constructs with 0 bp, 5 bp, or 250 bp of non-coding DNA protection. b) Top, time-series data of expression from 2nM of a linear DNA construct with no non-coding sequence protection on either side of promoter OR2-OR-Pr and of terminator. All data series are scaled to an endpoint expression of 1.0 after 8 hours. Below, nucleotide sequence of the left side of the construct, with operator, promoter -35 and -10, and phosphorothioate sites notated.[2] Error bars represent one standard deviation from three independent experiments. Linear DNA is protected with gamS.

Figure S7

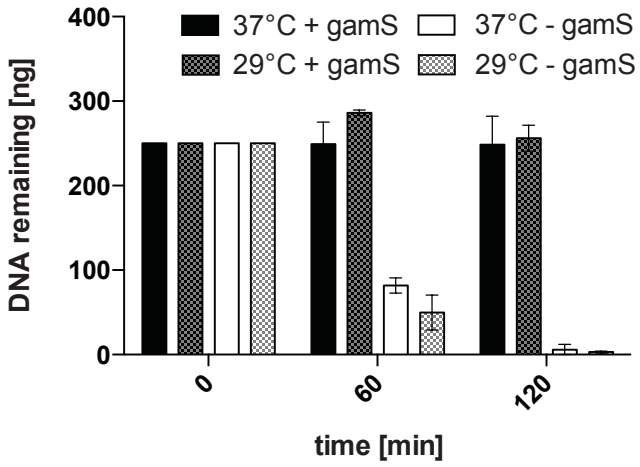

Figure S7. Degradation of saturating amounts of DNA in extracts prepared at different temperatures with and without gamS protein. Degradation rates of 250 ng (20 nM) of linear DNA with AlexaFluor-584 labeled dUTPs over time in extract produced at 37°C (extract "eZS1") or 29°C (extract "e13"). Signal is scaled to maximum DNA levels at time t=0. Error bars represent one standard deviation from three independent experiments.

Figure S8

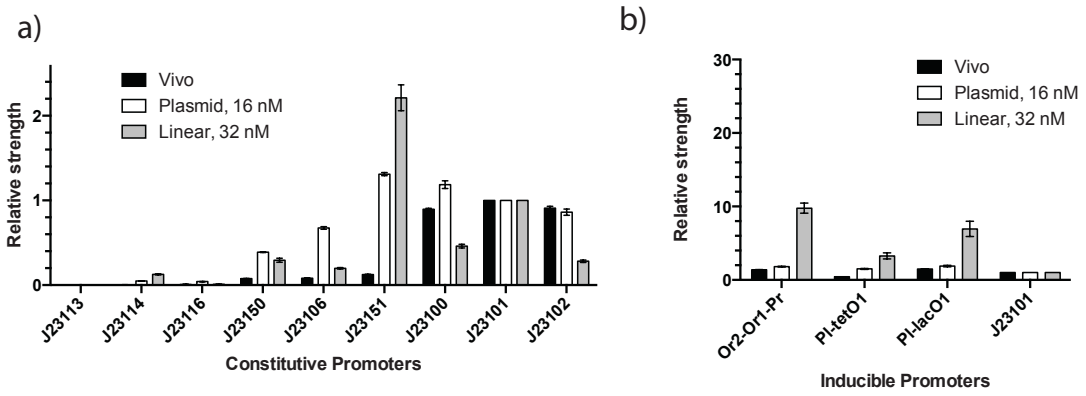

Figure S8. Comparison of strengths of different promoters using maximum measured amounts of DNA in TX-TL. a) Figure 4a is repeated for constitutive promoters but using maximum measured amounts of plasmid and linear DNA. b) Figure 4b is repeated for inducible promoters expressed constitutively.

Figure S9

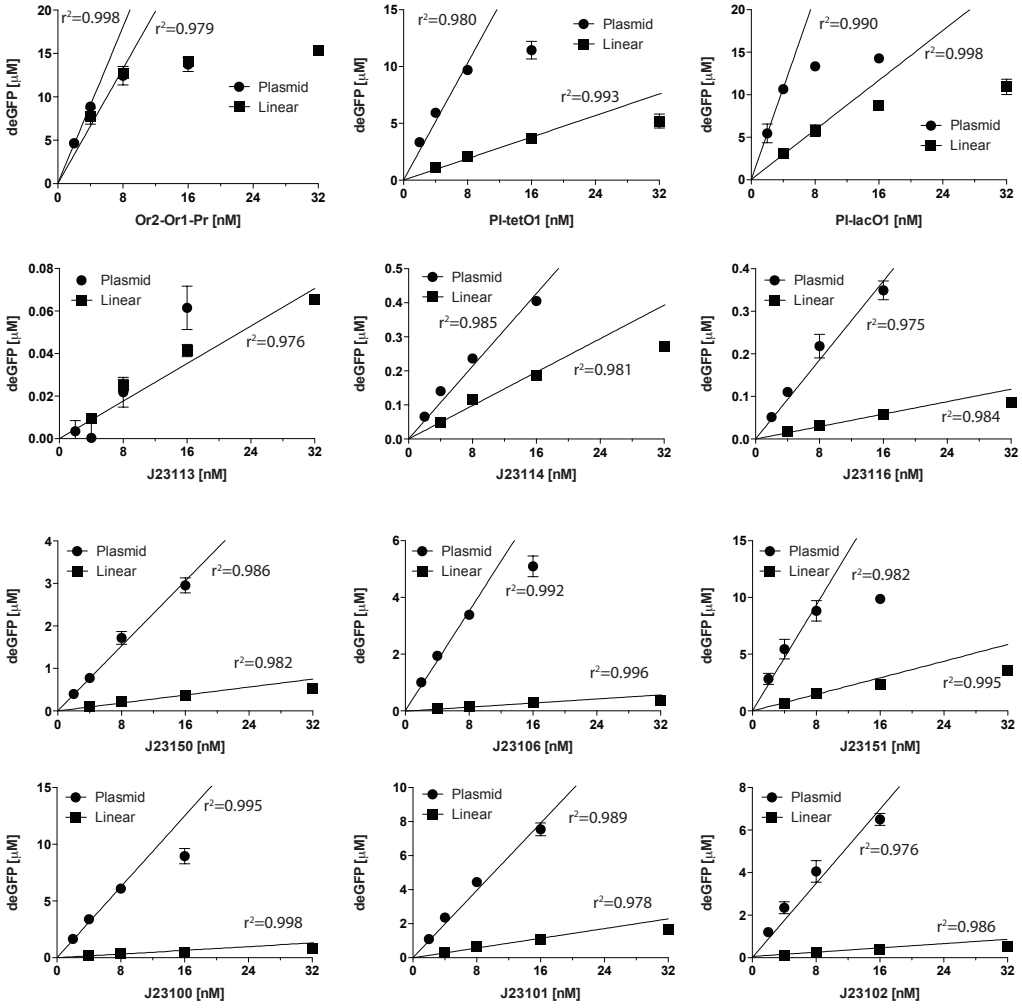

Figure S9. Individual traces of saturation curves. Saturation curves similar to Figure 4d, plotted for all promoters. r^2 and linear regression line are based on a cutoff of 0.975 and correspond to data from Table 1. Linear DNA is protected with 250bp of steric protection and with gamS. Error bars represent one standard deviation from three independent experiments.

Figure S10

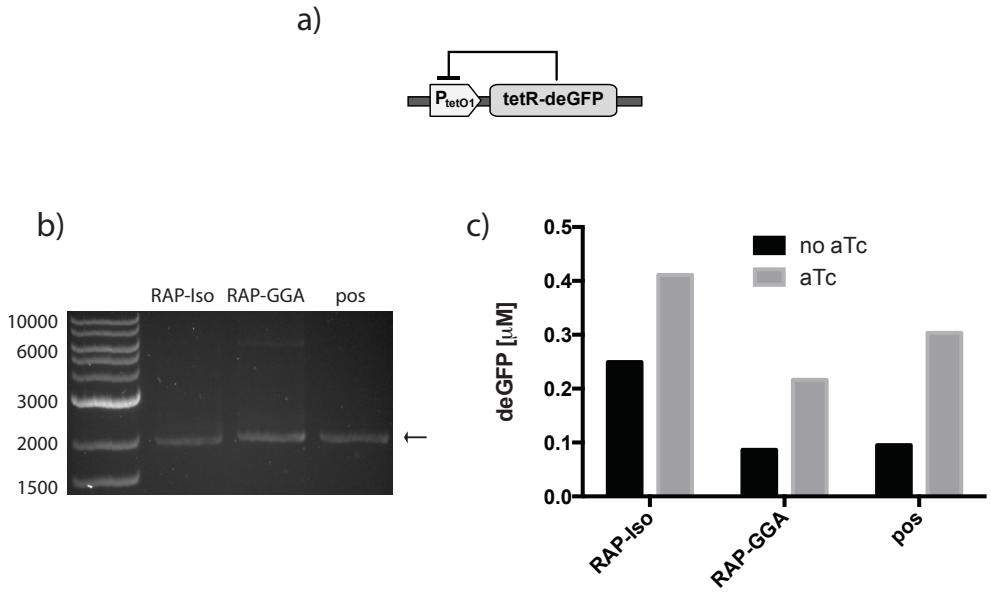

Figure S10. Rapid assembly and testing of a negative feedback gene. a) A four-piece negative feedback gene is assembled from standard pieces. b) Comparison by agarose gel electrophoresis of rapid assembly product made by Isothermal assembly ("RAP-iso"), rapid assembly product made by Golden Gate assembly ("RAP-GGA"), and post-cloned PCR product ("pos"). Arrow indicates expected band. Linear DNA is protected with 250 bp of steric protection and with gamS. c) Functional testing of 6 nM of rapid assembly products compared to post-cloned PCR product with or without 10 μM aTc.

Figure S11

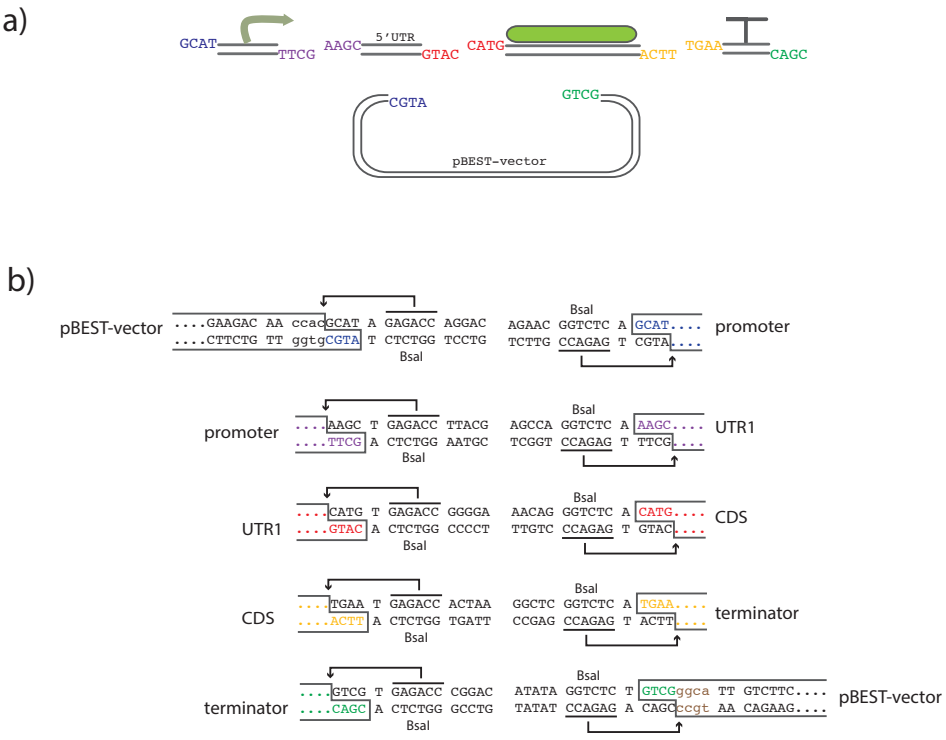

Figure S11. Overview of standard cloning procedure. a) A five-piece standard adopted with specific ligation ends for a promoter, 5' UTR, coding sequence, terminator, and vector based on the previously used pBEST backbone. b) Diagram of sequences for ligation at each site.

Figure S12

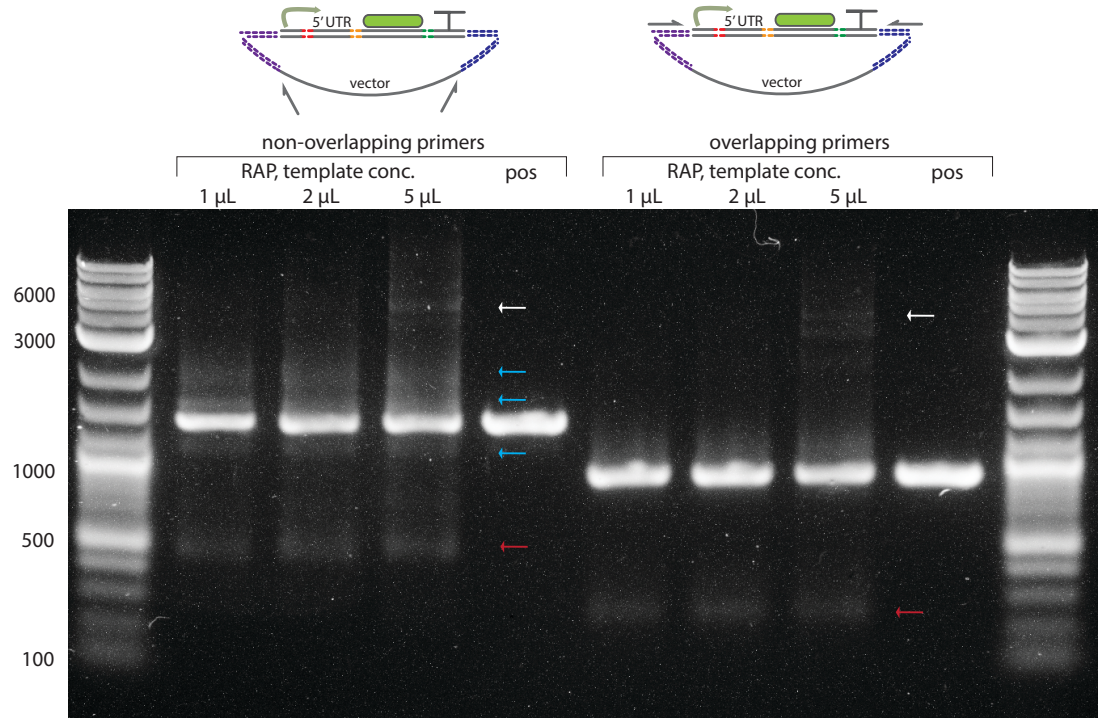

Figure S12. Purity of rapid assembly product as a function of template concentration and of overlapping primers. For a standard 5-piece assembly, the rapid assembly product ("RAP") is amplified off 1 µL, 2 µL, or 5 µL of template in a 50 µL PCR reaction. A post-cloned PCR product ("pos") is also produced. Non-overlapping primers refer to binding sites that do not cross the assembly junction between the vector and promoter and the vector and terminator; overlapping primers cross this junction. White arrow: template DNA; Blue arrows: Non-specific products removed by overlapping primers; Red arrow: non-specific products retained by overlapping primers. Red arrow is presumed to be self-ligated vector based on size.

Figure S13

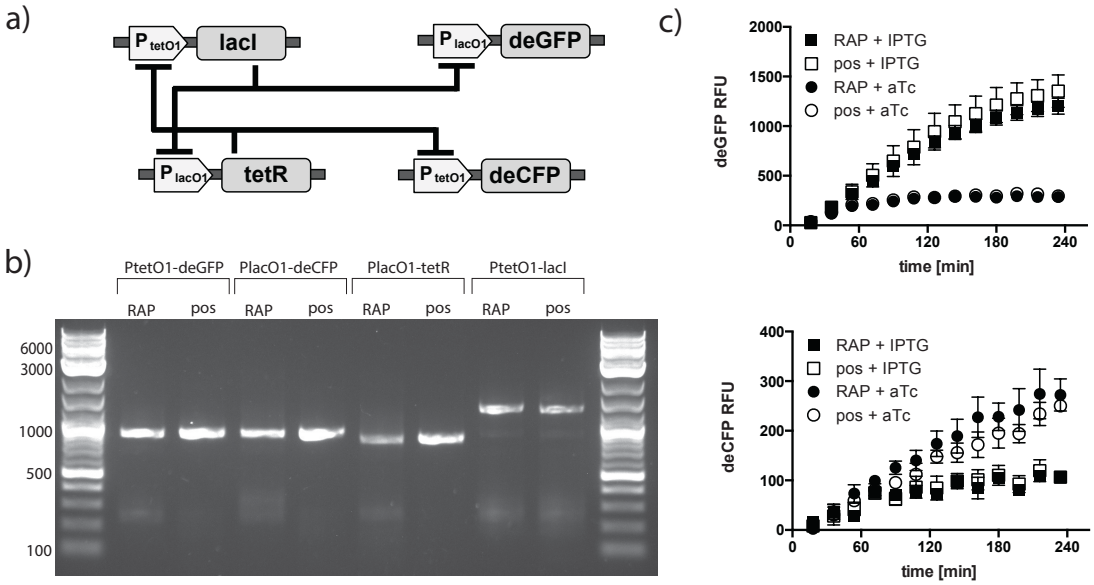

Figure S13. Rapid assembly of genetic switch. a) A four-piece genetic switch, identical to that in Figure 5a. b) Comparison of rapid assembly product ("RAP") to post-cloned PCR product ("pos") for four linear pieces formed, using overlap primers. c) Functional assay of RAP products versus post-cloned PCR products for "on" or "off" states of genetic switch. 2 nM of reporter and 1 nM of repressor is tested, and "+ IPTG" indicates the 0.5 mM IPTG, 0 μM aTc state while "- IPTG" indicates the 0 mM IPTG, 10 μM aTc state. Linear DNA is protected with 31 bp of steric protection and with gamS. Error bars represent one standard deviation from three independent experiments.

Supplementary Information References

1. Labarca, C., and Paigen, K. (1980) A simple, rapid, and sensitive DNA assay procedure, *Analytical biochemistry 102*, 344-352.
2. Meyer, B. J., Maurer, R., and Ptashne, M. (1980) Gene regulation at the right operator (OR) of bacteriophage lambda. II. OR1, OR2, and OR3: their roles in mediating the effects of repressor and cro, *Journal of molecular biology 139*, 163-194.

Chapter 4: Characterizing dynamics in the breadboard

Preprint as:
Sun ZZ, Kim J, Singhal V, Murray RM. Protein degradation in a TX-TL cell-free expression system using ClpXP protease. *bioRxiv,* doi: 10.1101/019695 (2015)

Introduction

An *in vitro* S30-based *Escherichia coli* expression system ("Transcription-Translation", or "TX-TL") has been developed as an alternative prototyping environment to the cell for synthetic circuits [1-5]. Basic circuit elements, such as switches and cascades, have been shown to function in TX-TL, as well as bacteriophage assembly [2, 6]. Circuits can also be prototyped from basic parts within 8 hours, avoiding cloning and transformation steps [7]. However, most published results have been obtained in a "batch mode" reaction, where factors that play an important role for *in vivo* circuit dynamics – namely protein degradation and protein dilution – are severely hindered or are not present. This limits the complexity of circuits built in TX-TL without steady-state or continuous-flow solutions [8-10]. However, alternate methods that enable dilution either require extra equipment and expertise or demand lower reaction throughput.

We explored the possibility of supplementing TX-TL with ClpXP, an AAA+ protease pair that selectively degrades tagged proteins [11], to provide finely-tuned degradation. The mechanism of ClpXP degradation has been extensively studied both *in vitro* and *in vivo* [12-15]. However, it has not been characterized for use in synthetic circuits – metrics such as toxicity, ATP usage, degradation variation over time, and cellular loading need to be determined. In particular, TX-TL in batch mode is known to be resource limited [16], and ClpXP is known to require significant amounts of ATP to unfold different protein targets [17, 18]. We find that ClpXP's protein degradation dynamics is dependent on protein identity, but can be determined experimentally. Degradation follows Michaels-Menten kinetics, and can be fine tuned by ClpX or ClpP concentration. Added purified ClpX is also not toxic to TX-TL reactions. Therefore,

ClpXP provides a controllable way to introduce protein degradation and dynamics into synthetic circuits in TX-TL.

Results and Discussion

There are two methods to supplement ClpXP into TX-TL: by expressing the proteins off of plasmid DNA or by adding purified protein. We first attempted to express both ClpX and ClpP off of DNA, and found that ClpX when expressed was able to degrade fluorescent ssrA-tagged reporters at a rate independent of ClpP concentration (data not shown). However, expressing ClpX posed two difficulties: degradation was rate-limited and time-delayed based on production rate of ClpX, and the load of ClpX expression reduced the expression of other synthetic circuits. To avoid these problems, we tried to purify a N-terminal His-tagged version of ClpX using a standard Ni-NTA procedure; however, we found that this version of ClpX lost activity after the purification procedure when stored in a previously developed glycerol-free buffer compatible with TX-TL [7]. We hypothesized that a linked-hexametric form previously developed would be more stable in solution [13]. With the His-tagged linked-hexameric N-terminal deletion form of ClpX, we were able to retain activity (**Fig. 1ab**). We refer to this as the ClpX form hereafter. To quantify degradation rates, we also purified fluorescent proteins with and without –ssrA tags (**Fig. 1c**).

We first verified the ability of purified ClpX to selectively degrade ssrA-tagged versions of deGFP, mRFP, and Venus over non-tagged versions (**Fig. 2**). ClpX is selective for ssrA-tagged versions over non-ssrA tagged versions, and has a degradation rate dependent on protein identity. This is similar to findings *in vitro*, where ClpX is known to have different unfolding rates and ATP hydrolysis rates depending on the target difficulty [17, 19]. We also determined the concentration dependence of ClpX to

degradation rate and throughput (**Fig. 3ab**). Initially, we made a simple Michelis-Menten model:

$$\frac{d[GFP]}{dt} = \frac{-k_{cat}[ClpXP][GFP]}{[GFP] + K_m}$$

$$[ClpXP] = \min([ClpX], [ClpP])$$

We set K_m to 1.1 μM, k_{cat} to 0.9 min^{-1} based on previously published parameters [14], and estimated initial (native) concentrations of 20 nM ClpX and of 250 nM ClpP in TX-TL extract. We also ran a TX-TL experiment varying added ClpX concentrations from 0 nM to 400 nM. Comparing the modeling data to the experimental data, ClpXP degradation closely follows Michaelis-Menten kinetics as described. We also determined concentration dependence of ClpX to Venus-ssrA and mRFP-ssrA, and then plotted the degradation rate vs. time **(Fig. 3c)**. Since the degradation rate changes over time as the concentration of substrate decreases, we plotted degradation rate vs. added ClpX concentration at t = 16.5 min, which we took as an initial degradation rate **(Fig. 3d)**. In this figure, the dependence of fluorescent reporter to added ClpX concentration can be clearly discerned, with a saturation point between 200-400 nM of additional ClpX added to the system, suggesting a rate-limiting native ClpP concentration. The decreased degradation rate of Venus-ssrA relative to deGFP-ssrA and mRFP-ssrA can also be seen. Based on this figure, additional ClpX is able to increase deGFP-ssrA degradation rates by 5-fold, mRFP-ssrA degradation rates by 4.2-fold, and Venus-ssrA degradation rates by 1.8-fold.

We additionally tried to supplement TX-TL with ATP and Mg, based on the known heavy usage of ClpX for protein unfolding (500 ATP per titin I27 subunit, ~100 aa) [19]. With 200 nM of added ClpX in TX-TL, there was a clear effect on the degradation of Venus-ssrA over deGFP-ssrA and mRFP-ssrA, indicating that at working concentrations of proteins likely achievable in a typical TX-TL reaction ATP concentration was not rate-limiting except on hard-to-degrade proteins (**Fig. 4**).

In order for supplemented ClpX to be a useful tool for controlled protein degradation, either the addition of ClpX or the ClpX storage buffer must not be toxic to expression of proteins off of DNA in TX-TL. We diagnosed this by diluting purified ClpX into a TX-TL reaction driving the production of deGFP off of a strong promoter, and saw no effect at saturating ClpX levels to DNA expression (**Fig. 5**). We also verified that ATP was not rate-limiting to ClpXP degradation and DNA expression by treating the degradation of mRFP-ssrA as a "background process" running during a TX-TL reaction producing deGFP (**Fig. 6**). As 10 μM of mRFP-ssrA is approaching the maximum protein concentration producible by TX-TL, this result suggests that ATP is at a saturating level in a typical TX-TL reaction. However, we did not test the combination of a difficult-to-degrade protein such as Venus-ssrA combined with the expression of saturating amounts of mRFP, which would support this conclusion.

We also explored increasing the amount of ClpP in a saturated ClpX TX-TL reaction to verify that ClpP was a limiting reagent. For simplicity, we expressed ClpP off of a strong promoter instead of adding purified amounts of ClpP. In the main extract used, "eZS6" derived from an ExpressIQ strain (New England Biolabs), ClpP was able to marginally increase degradation of deGFP-ssrA in the presence of 200 nM of ClpX (**Fig.**

7a). However, the ability to increase degradation was more pronounced in an alternate extract, “e8”, made from a BL21 Rosetta2 strain (Novagen) (**Fig. 7b**). This indicates that ClpXP degradation dynamics can be different depending on strain and on preparation, which could vary the amount of native ClpX or ClpP already present.

Conclusion

We explored the use of supplementing the ClpXP system inherent in TX-TL with purified ClpX protease to provide fine-tunable degradation to run synthetic dynamic circuits. ClpXP degradation closely follows Michaelis-Menten kinetics, but has varying degradation rates depending on substrate. Degradation can also be controlled by ClpX concentration, allowing for up to 5-fold increased degradation rates over non-tagged variants. Degradation does not limit the running of synthetic circuits when purified ClpX is added, and rates can be further increased by adding ClpP when ClpX reaches saturated conditions between 200-400 nM.

While ClpXP provides tunable degradation, it may not be an ideal substitute for protein dilution, as degradation is neither linear nor stepwise. However, due to the fact that degradation closely follows Michaelis-Menten kinetics, degradation can be included in a "biological breadboard"-type model [20] to predict amounts needed to implement circuit dynamics. This can be easily done for fluorescent proteins, but may require indirect assays for other commonly used circuit components such as activators or repressors. However, once substrate degradation rates are characterized supplementing ClpX is easy to accomplish and fairly predictable when adjusting for concentration.

Acknowledgements

We thank Jan Kostecki for protein purification and size exclusion chromatography assistance, Rohit Sharma for initial testing of AAA+ degradation mechanisms, Robert Sauer and Karl Schmitz for advice in purifying ClpX, and Kyle Martin for laboratory assistance. This material is based upon work supported in part by the Defense Advanced Research Projects Agency (DARPA/MTO) Living Foundries program, contract number HR0011-12-C-0065 (DARPA/CMO). Z.Z.S. is also supported by a UCLA/Caltech Medical Scientist Training Program fellowship, and a National Defense Science and Engineering Graduate fellowship. The views and conclusions contained in this document are those of the authors and should not be interpreted as representing officially policies, either expressly or implied, of the Defense Advanced Research Projects Agency or the U.S. Government.

Materials and Methods

Cell-free extract preparation and execution

Preparation and execution of TX-TL was according to previously described protocols [1], with a modification in strain to ExpressIQ (New England Biolabs) and lysis according to work by Jewett et al. (personal communication). This resulted in extract "eZS6" with conditions: 9.9 mg/mL protein, 9.5 mM Mg-glutamate, 95 mM K-glutamate, 0.33 mM DTT, 1.5 mM each amino acid except leucine, 1.25 mM leucine, 50 mM HEPES, 1.5 mM ATP and GTP, 0.9 mM CTP and UTP, 0.2 mg/mL tRNA, 0.26 mM CoA, 0.33 mM NAD, 0.75 mM cAMP, 0.068 mM folinic acid, 1 mM spermidine, 30 mM 3-PGA, 2% PEG-8000. Only "eZS6" is used to prevent extract-to-extract variation, except in the final figure where "e8" prepared from BL21 Rosetta2 (Novagen) using previously described protocols [1] was used. Reactions were conducted in 15 μL in a 384-well plate (Nunc) at 29°C, and read in a Synergy H1/MF or H4 plate reader (Biotek). Settings used were: deGFP, 485 nm/515 nm gain 61; Venus, 505 nm/ 535 nm, gain 61; mRFP, 580 nm/ 610 nm, gain 100.

Protein purification

For fluorescent proteins eGFP, mRFP, and Venus and variants eGFP-ssrA, mRFP-ssrA, and Venus-ssrA, coding sequences were cloned into a T7-lacO inducible vector containing a N-terminus His6 tag using standard techniques and propagated in a BL21-DE3 strain (New England Biolabs). Proteins were purified following a similar protocol as in [7], but were grown in TB broth in lieu of LB broth, induced with 1 mM IPTG (final concentration), and selected for a band between 25 kDa – 35 kDa

corresponding to the fluorescent protein in question. Fluorescent proteins were further processed in a Supradex 20 10/300 column to select for pure, active proportions, and flash-frozen at -80°C in a storage buffer consisting of: 50 mM Tris-Cl pH 7.5, 100 mM NaCl, 1 mM DTT, 1 mM EDTA, 2% DMSO shown previously to be amenable to usage in TX-TL [7]. Final concentrations were: deGFP-ssrA, 164.8 μM; deGFP, 184.8 μM; mRFP-ssrA, 185.6 μM; mRFP, 170.6 μM; Venus-ssrA, 87.9 μM; Venus, 147.5 μM.

For ClpX, a monomeric N-terminal deletion variant Flag-clpXdeltaNLinkedHexamer-His6 was used [13] (Addgene #22143), as purifying the wildtype with a N-terminal His-tag using general Ni-NTA purification techniques resulted in a loss of activity. We followed a Ni-NTA purification procedure listed in [12], followed by Supradex 20 10/300 and functional testing for pure, active proportions above 250 kDa. Active proportions were flash frozen in the same buffer used for fluorescent proteins. Final concentration of ClpX was 1.95 μM.

Figure 1

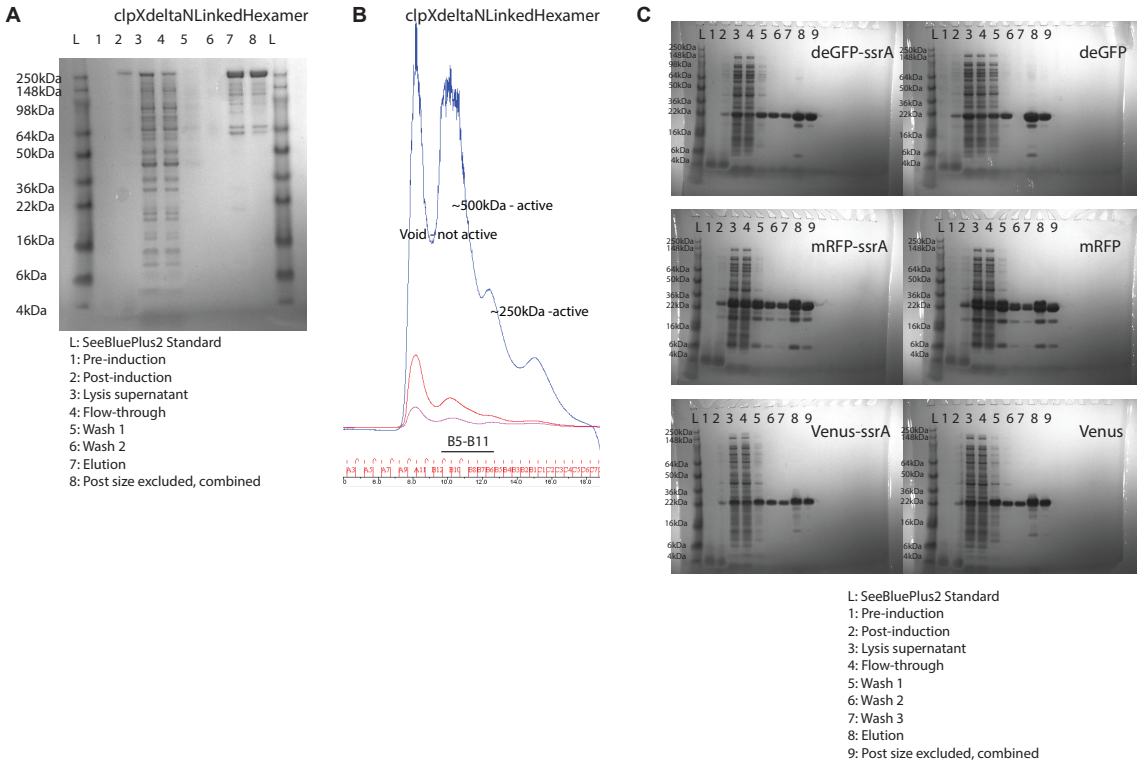

Figure 1. Purification of clpXdeltaNLinkedHexamer ("ClpX") and fluorescent proteins. a) ClpX with a His6 tag is purified in a Ni-NTA column and run on denaturing SDS-PAGE gel. b) Size excluded chromatography of elute product on a Superdex 200 10/300 column, with a functionality test of active species. B5-B11 are fractions combined for forward use. c) Three fluorescent proteins (deGFP, mRFP, Venus), with or without ssrA tags, with a His6 tag are purified in a Ni-NTA column and run on denaturing SDS-PAGE gel. Last column is active, purified fractions combined for forward use.

Figure 2

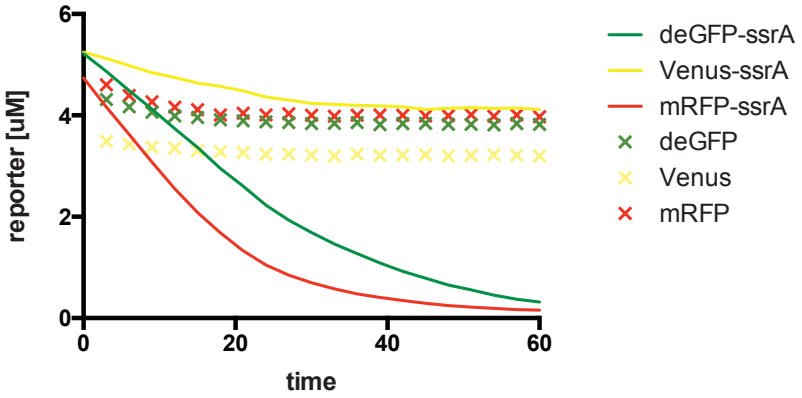

Figure 2. Degradation of deGFP, Venus, and mRFP by added ClpX. 400 nM of purified ClpX is combined with approximately 5 μM of purified fluorescent proteins with and without ssrA degradation tags in TX-TL.

Figure 3

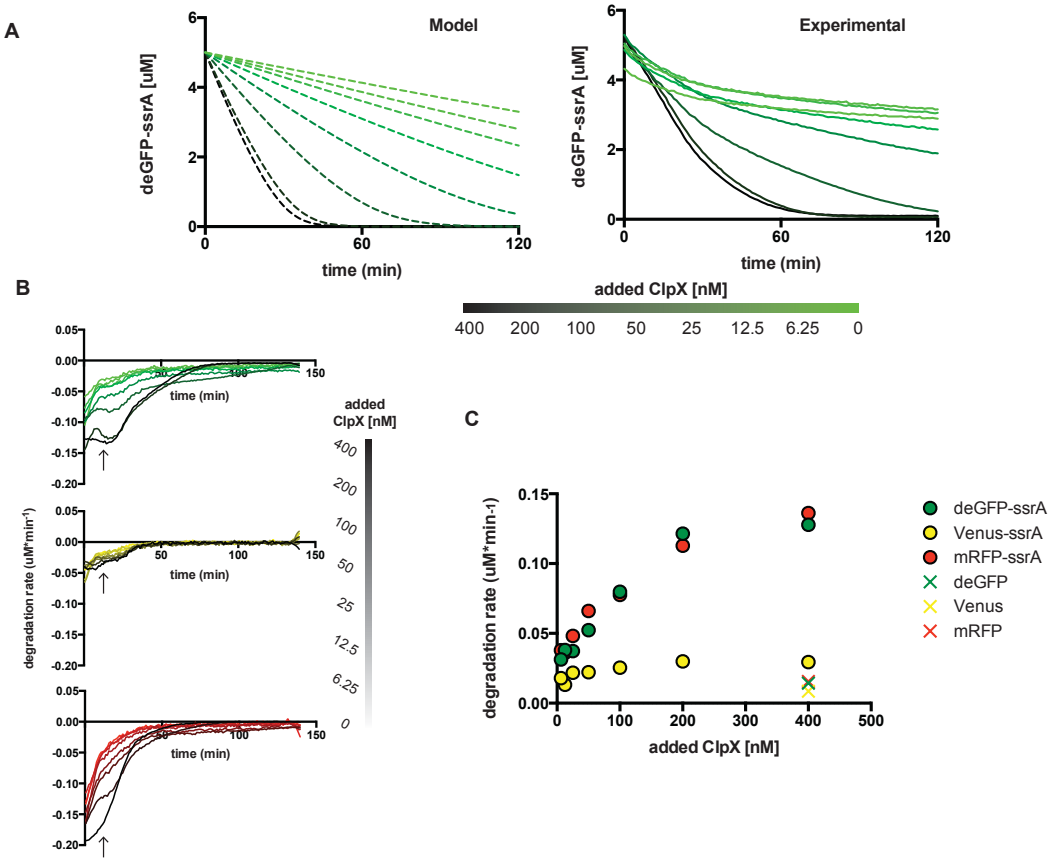

Figure 3. Dependence of degradation on ClpX concentration. A) Shown to the left is a Michaelis-Menten kinetics model of degradation of fluorescent GFP-ssrA over time, using K_m 1.1 μM, k_{cat} 0.9 min^{-1}, similar to literature values [14]. Added ClpX is varied from 400nM to 0nM. Showing to the right is experimental data demonstrating similar results as modeling data for deGFP-ssrA. B) Degradation rate of deGFP-ssrA, Venus-ssrA, and mRFP-ssrA over time with varied ClpX concentration. At the arrow is t = 16.5 min. C) Degradation rate plotted at t = 16.5 min as a function of added ClpX, for both ssrA tagged and non-ssrA tagged fluorescent proteins.

Figure 4

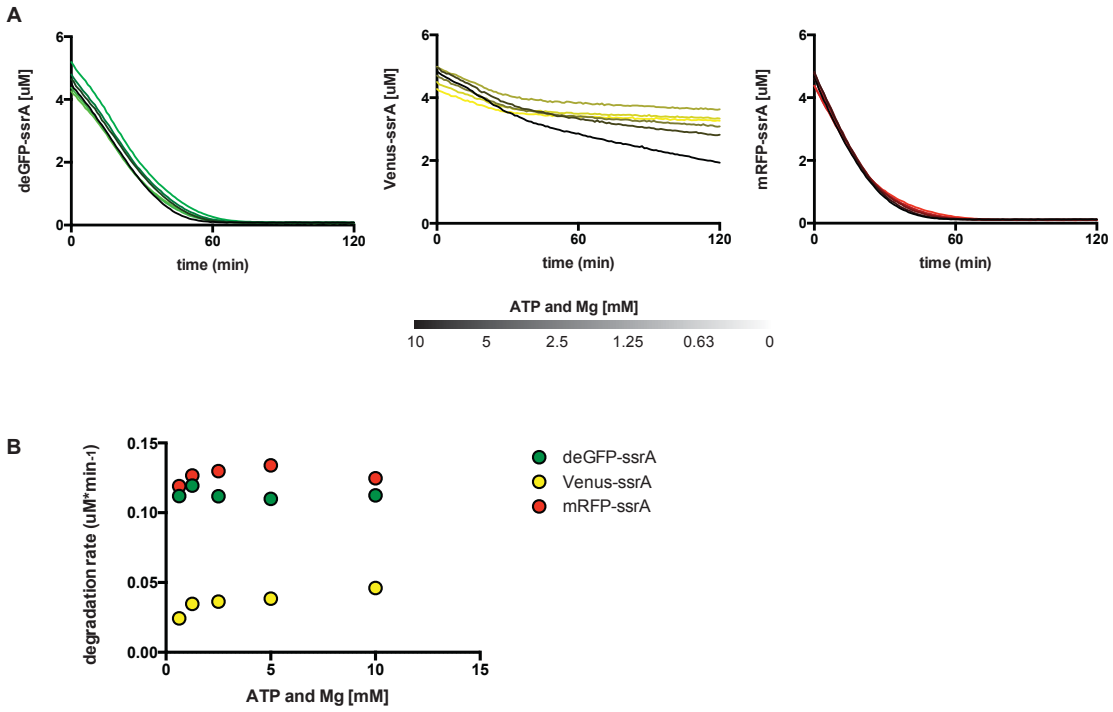

Figure 4. Dependence of degradation on added ATP and Mg. A) With added ClpX set to 200 nM, degradation of fluorescent ssrA tagged proteins is plotted as a function of time and additional ATP and Mg added to each reaction. B) Degradation rate at t = 16.5 min from above data is plotted as a function of additional ATP and Mg.

Figure 5

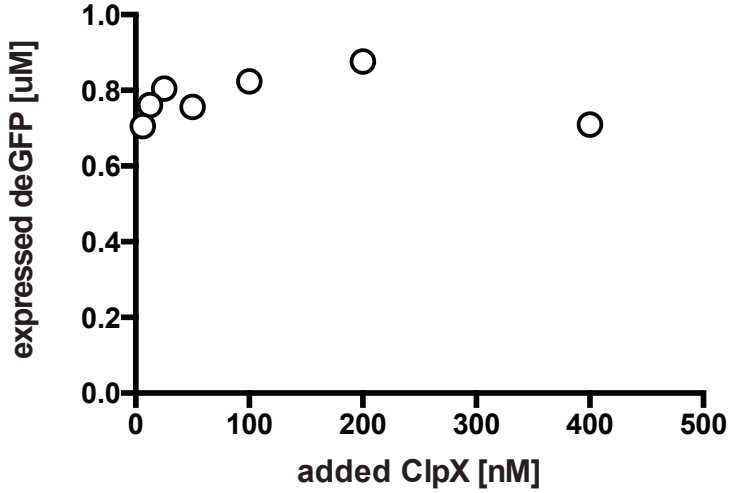

Figure 5. Toxicity of added ClpX to TX-TL expression. A plasmid expressing deGFP off of a strong promoter-UTR is added to a TX-TL reaction at 1 nM, and endpoint expression after 8 hours is plotted as a function of added, purified ClpX protein.

Figure 6

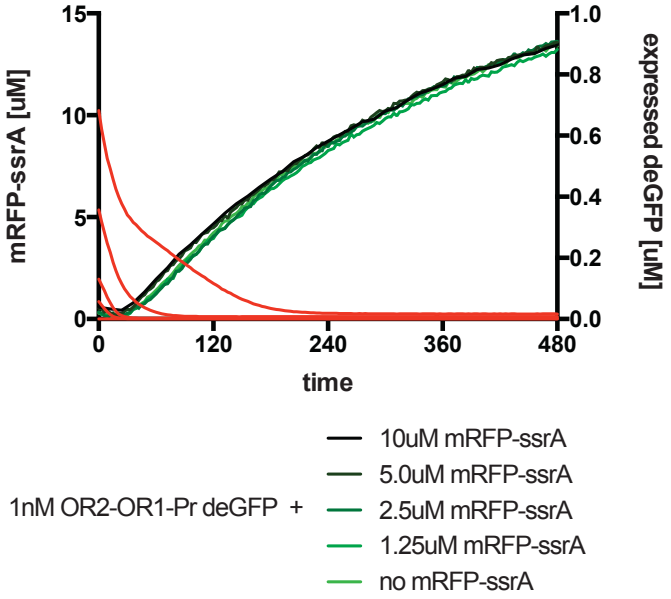

Figure 6. Effect of background degradation processes to TX-TL expression. A plasmid expressing deGFP off of a strong promoter-UTR is added to a TX-TL reaction at 1nM. In the same reaction, purified mRFP-ssrA is being degraded by 200 nM of added ClpX. No additional ATP or Mg is added to the reaction. Five different concentrations of mRFP-ssrA are tested. Both remaining mRFP-ssrA and deGFP expression are measured in real time.

Figure 7

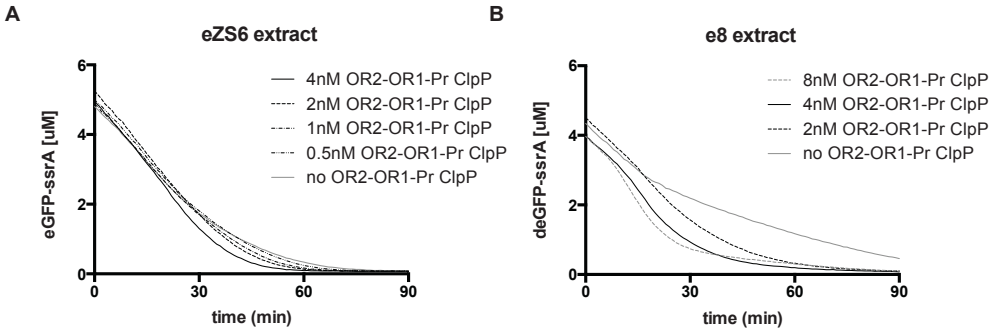

Figure 7. Effect of ClpP expression on degradation. A) In eZS6 extract, a plasmid expressing ClpP off of a strong promoter-UTR is added to a TX-TL reaction at varying concentrations in the presence of 200 nM of added purified ClpX. Degradation of deGFP-ssrA is plotted versus time. B) The same experiment as A), but in a different extract.

References

1. Sun, Z.Z., et al., *Protocols for Implementing an Escherichia Coli Based TX-TL Cell-Free Expression System for Synthetic Biology.* Journal of Visualized Experiments, 2013. **e50762**.
2. Shin, J. and V. Noireaux, *An E. coli cell-free expression toolbox: application to synthetic gene circuits and artificial cells.* ACS Synth Biol, 2012. **1**(1): p. 29-41.
3. Shin, J. and V. Noireaux, *Study of messenger RNA inactivation and protein degradation in an Escherichia coli cell-free expression system.* J Biol Eng, 2010. **4**: p. 9.
4. Shin, J. and V. Noireaux, *Efficient cell-free expression with the endogenous E. Coli RNA polymerase and sigma factor 70.* J Biol Eng, 2010. **4**: p. 8.
5. Noireaux, V., R. Bar-Ziv, and A. Libchaber, *Principles of cell-free genetic circuit assembly.* Proceedings of the National Academy of Sciences of the United States of America, 2003. **100**(22): p. 12672-12677.
6. Shin, J., P. Jardine, and V. Noireaux, *Genome Replication, Synthesis, and Assembly of the Bacteriophage T7 in a Single Cell-Free Reaction.* Acs Synthetic Biology, 2012. **1**(9): p. 408-413.
7. Sun, Z.Z., et al., *Linear DNA for rapid prototyping of synthetic biological circuits in an Escherichia coli based TX-TL cell-free system.* ACS Synth Biol, 2013.
8. Siuti, P., S.T. Retterer, and M.J. Doktycz, *Continuous protein production in nanoporous, picolitre volume containers.* Lab Chip, 2011. **11**(20): p. 3523-9.
9. Khnouf, R., D.J. Beebe, and Z.H. Fan, *Cell-free protein expression in a microchannel array with passive pumping.* Lab Chip, 2009. **9**(1): p. 56-61.
10. Niederholtmeyer, H., V. Stepanova, and S.J. Maerkl, *Implementation of cell-free biological networks at steady state.* Proc Natl Acad Sci U S A, 2013.
11. Gottesman, S., et al., *The ClpXP and ClpAP proteases degrade proteins with carboxy-terminal peptide tails added by the SsrA-tagging system.* Genes Dev, 1998. **12**(9): p. 1338-47.
12. Davis, J.H., T.A. Baker, and R.T. Sauer, *Engineering synthetic adaptors and substrates for controlled ClpXP degradation.* J Biol Chem, 2009. **284**(33): p. 21848-55.
13. Martin, A., T.A. Baker, and R.T. Sauer, *Rebuilt AAA + motors reveal operating principles for ATP-fuelled machines.* Nature, 2005. **437**(7062): p. 1115-20.
14. Hersch, G.L., T.A. Baker, and R.T. Sauer, *SspB delivery of substrates for ClpXP proteolysis probed by the design of improved degradation tags.* Proc Natl Acad Sci U S A, 2004. **101**(33): p. 12136-41.
15. Kim, Y.I., et al., *Dynamics of substrate denaturation and translocation by the ClpXP degradation machine.* Mol Cell, 2000. **5**(4): p. 639-48.
16. Siegal-Gaskins, D., et al., *Gene circuit performance characterization and resource usage in a cell-free "breadboard".* ACS Synth Biol, 2014. **3**(6): p. 416-25.
17. Kenniston, J.A., et al., *Linkage between ATP consumption and mechanical unfolding during the protein processing reactions of an AAA+ degradation machine.* Cell, 2003. **114**(4): p. 511-20.

18. Burton, R.E., T.A. Baker, and R.T. Sauer, *Energy-dependent degradation: Linkage between ClpX-catalyzed nucleotide hydrolysis and protein-substrate processing.* Protein Sci, 2003. **12**(5): p. 893-902.
19. Baker, T.A. and R.T. Sauer, *ClpXP, an ATP-powered unfolding and protein-degradation machine.* Biochim Biophys Acta, 2012. **1823**(1): p. 15-28.
20. Tusa, Z.A., et al., *An In Silico Modeling Toolbox for Rapid Prototyping of Circuits in a Biomolecular "Breadboard" System*, in *2013 Conference on Decision and Control*. 2013, IEEE: Florence, Italy.

Chapter 5: Applying the breadboard on a complex synthetic circuit

Published as, in modified form:
Niederholtmeyer H*, Sun ZZ*, Hori Y, Yeung E, Verpoorte A, Murray RM. Rapid cell-free forward engineering of novel genetic ring oscillators. *eLife*, doi: 10.7554/eLife.09771 (2015).

*Equal contribution

Abstract

While complex dynamic biological networks control gene expression in all living organisms, engineering comparable synthetic networks remains time-consuming and challenging. Cell-free environments can speed up engineering, but it remains questionable whether complex synthetic networks behave similarly *in vivo* and *in vitro*. We characterized *in vitro* the "repressilator," a three-node synthetic oscillator. We then used our cell-free framework to engineer novel three, four, and five-node synthetic architectures from characterization of circuit components to rapid analysis of complete networks. We validated our cell-free approach by transferring these novel three-node and five-node oscillators to *Escherichia coli*, resulting in robust oscillations reflecting the *in vitro* results. A cell-free framework can thus drastically speed up design-build-test cycles in biological engineering and enable the quantitative characterization of synthetic and natural networks.

Main Text

A central tenet of engineering involves characterizing and verifying prototypes by conducting rapid design-build-test cycles in a simplified environment (*1*). Electronic circuits are tested on a breadboard to verify circuit design and aircraft prototypes are tested in a wind tunnel to characterize their aerodynamics. A simplified environment does not exist for engineering biological systems, nor is accurate software based design possible, requiring design-build-test cycles to be conducted *in vivo* (*2*). Conducting extensive, quantitative and rapid characterization *in vivo* is severely limited due to cumbersome molecular cloning and the difficulties associated with measuring parts, components, and systems in cellular hosts.

In vitro systems promise to be efficient and effective tools to rapidly develop novel biological systems and understand their operating regimes (*3*-*5*) but whether they reflect the cellular environment sufficiently well to be of significance to biological engineering has remained questionable. We devised a cell-free framework consisting of *E. coli* lysate ("TX-TL") (*3*, *6*) and a microfluidic device capable of emulating cellular growth and division (*4*) (**Fig. 1**). Almost all prototyping can be done on linear DNA, which requires less than 8 hours to assemble and test. Here, we demonstrate that a cell-free environment can fill the gap between theoretical network design and *in vivo* implementation of biological systems and thus provide a simplified and controlled environment that drastically reduces the design-build-test cycle (*7*).

We first asked whether our cell-free framework could be used to run and characterize an existing synthetic *in vivo* circuit and chose to test the repressilator (*8*) as a model circuit. We successfully implemented the original repressilator network in our cell-

free framework and observed long-term sustained oscillations with periods matching the *in vivo* study (**Fig 2, Movie S1**). We compared the original repressilator to a modified version containing a point mutation in one of the CI repressor binding sites in the promoter regulating LacI (**Fig. 2A**). This mutation increases the repressor concentration necessary for half-maximal repression (K_M), and reduces cooperativity (*9*). At long dilution times (t_d) both circuits oscillated, but with shifted absolute reporter protein concentrations (**Fig. 2B**). At decreasing dilution times amplitudes decreased and periods became faster with a linear dependence on t_d. Faster dilution times, however, did not support oscillations for the modified network (**Fig. 2B-C**). Experimentally, the range of dilution times supporting oscillations can serve as a measure for robust oscillator function, which generally diminishes with decreasing synthesis rates or when binding of one repressor to its promoter is weakened as in the O_R2* mutant (**Fig. S1**). To give another example for an experimental characterization that would be challenging to perform in a cellular environment we analyzed the repressilator network in phase space showing limit cycle oscillations and invariance to initial conditions (**Fig. 2D**).

The cell-free framework also allows rapid characterization of individual network components. We measured the transfer functions of repressor-promoter pairs in the repressilator network (**Fig. 3A, Fig. S2A,B, Table S1**) and found that the network is symmetric in terms of transfer functions. In the CI promoter O_R2* mutant we observed the expected shift in K_M and decreased steepness of the transfer function. We also characterized TetR repressor homologs as building blocks for novel negative feedback circuits (**Fig. 3A**) and with the exception of QacR observed similar transfer functions as observed *in vivo* (*10*) (**Fig. S2C**).

Using three new repressors, BetI, PhlF and SrpR, we constructed a novel 3-node (3n) circuit (3n1) and observed high-amplitude oscillations over a broad range of dilution times with the same dependence of amplitude and period on t_d as for the repressilator (**Fig. 3B**). In our characterization of the repressilator network and the 3n1 oscillator we found dilution rates to be critical for the existence, period, and amplitude of oscillations. Protein degradation is similar to dilution in that it results in removal of repressor proteins. In order to study the effect of degradation we constructed a second 3n network (3n2) using TetR, PhlF, and SrpR repressors on linear DNA. One version of the circuit used strong ssrA ClpXP degradation tags, while the second used untagged repressors. We observed oscillations for both circuits (**Fig 3C**). However, the circuit without ssrA-tag mediated protein degradation exhibited slower oscillations, which extended to lower dilution times, showing that protein degradation, just like dilution, affects oscillator function and period. Effects of ClpXP-mediated protein degradation, which have been shown to be important for existence and frequency of oscillations *in vivo* (*11*, *12*), can thus be emulated in a cell-free environment.

Theory predicts that ring architectures built from an odd number of repressors oscillate, while even-numbered architectures have stable steady states (*13*, *14*). We experimentally built and tested a 4-node circuit from LacI, TetR, PhlF, and SrpR on linear DNA. Initial pulses of LacI inducer IPTG or TetR inducer aTc allowed us to switch expression into either one of the two stable steady states (**Fig. 3D**).

Encouraged by the robust oscillations observed in the 3n networks, we built two 5-node ring oscillators (5n) to test our prototyping environment on a novel synthetic network architecture (**Fig. 3E**). Despite their considerable complexity both circuits

oscillated over a broad range of dilution times with the expected period lengthening, which could be as long as 19h. Comparing all ssrA-tagged 3n and 5n ring architectures, we show that the observed periods could be accurately predicted for all four networks by computational simulations (**Fig. 3F**). Our cell-free framework allows testing and characterization of complex networks including verifying networks cloned onto a single plasmid, which is the closest approximation to *in vivo* implementation (**Fig. S3**).

To validate our cell-free approach *in vivo* we cloned the 3n1 and 3n2 networks onto low-copy plasmids and co-transformed each with a medium-copy reporter plasmid into *lacI*- JS006 *E. coli* (*15*). When tested on a microfluidic device (mother machine (*16*)), both 3n oscillators showed regular oscillations with periods of 6 ±1 hours for at least 30 hours (**Fig. 4A, Movies S2,3**). Both oscillators were surprisingly robust as all cells undergoing healthy cellular division oscillated (n = 71) (**Fig. S4**, **Movie S4**).

We next tested our 5n oscillators *in vivo*. Due to loading effects (*17*), 5n1 was not viable when co-transformed with a strong reporter. When tested with a low expression strength reporter both 5n oscillators showed robust oscillations that were maintained for at least 70 hours, and over 95% of all analyzed traps containing healthy cells oscillated (n = 104). In addition, both 5n networks oscillated with similar periods: 8 hours for 5n1, and 9 hours for 5n2 (**Fig. 4B, Fig. S4, Movies S5-7)**.

We also tested both 3n oscillators on a CellASIC system, which allows planar single-layer colony formation. In this system we observed a striking population level synchronization of daughter cells inheriting the oscillator state from their mother cells (**Fig. 4C**, **Fig. S5A, Movies S8,9**). Synchronization was also apparent when using three different fluorescent reporters simultaneously (**Fig. S5B, Movie S10**). We did not

observe population level synchronization in the original repressilator, the O_R2* mutant (**Fig. S5C**) nor the 5n networks. Synchronized oscillations were not reported with the original repressilator (*8*), and have only been observed in oscillators using intercellular communication (*18*, *19*). We hypothesize that the 3n1 and 3n2 synchronization is due to increased repressor concentrations as compared to the original repressilator network (**Fig. S5D**), which increases the inheritance of the period phenotype and minimizes the rapid de-synchronization expected from stochastic cellular protein fluctuations (*20*). However, a quantitative characterization of the synchronization phenotype requires more in-depth understanding of stochastic effects *in vivo*.

Because cells were synchronized, we were able to analyze the population as a whole to make general conclusions of oscillator behavior. We varied dilution time by using different media conditions and media flow rates, and found a direct relationship between division times and period, consistent with the *in vitro* data collected. Oscillation periods of the 5n oscillators were also consistent with our *in vitro* results and showed a similar dependence on doubling time (**Fig. 4D**).

Finally, we compared 3n1 and 5n2 with weak and strong reporters *in vivo* to analyze the effect of protein degradation on the oscillator period. We theorized that given a constant concentration of ClpXP, stronger reporters would result in more ClpXP loading, thereby slowing the period of oscillation. ClpXP is thought to influence oscillation dynamics *in vivo* in this manner (*11*). We found that in the mother machine, both the period distributions of 3n1 and 5n2 showed this characteristic (**Fig. 4E**), which reflects our *in vitro* findings of differential –ssrA tag dependent period length (**Fig. 3C**).

We showed that synthetic dynamic networks can be readily implemented, characterized, and engineered in a cell-free framework and consequently transferred to cellular hosts and demonstrated the utility of our approach for biological systems engineering and component characterization. We observed some differences between the *in vitro* and cellular environment, particularly in the difficulty of predicting cellular toxicity and loading effects of the 5n oscillators *in vivo*. While more work is necessary describing and explaining differences between *in vitro* and *in vivo* environments (*7*, *21*), the observed behavior of complex networks in our cell-free environment reflected network behavior *in vivo* well. The cell-free framework is thus a powerful emulator of the cellular environment allowing precise control over experimental conditions and enabling studies that are difficult or time consuming to perform in cells. With further developments in cell-free lysate systems and supporting technologies, the *in vitro* approach is posed to play an increasing role in biological systems engineering and provides a unique opportunity to design, build, and analyze biological systems.

Materials and Methods

DNA and strain construction

DNA was constructed using either Golden Gate Assembly or Isothermal Assembly. For linear DNA, all DNA was constructed using previously published Rapid Assembly protocols on a "v1-1" vector (*7*). Linear DNA constructs are summarized in **Table S2**. The original repressilator plasmid, pZS1 (*8*) was used as a template for initial characterization and for construction of the O_R2* mutant. Transfer function plasmids were constructed by Transcriptic, Inc. For other plasmids, partial sequences were either obtained from Addgene (*10*) or synthesized on gBlocks or ssDNA annealed oligonucleotides (Integrated DNA Technologies). Specific plasmids required secondary-structure free segments, which were designed by R2oDNA (*22*). JS006 (*15*) was co-transformed with origin-of-replication compatible plasmids to create engineered strains. Specifically, negative-feedback oscillator units were cloned onto pSC101* low copy plasmids (ampR or kanR), while reporters were cloned onto colE1 medium copy plasmids (kanR or cmR) (**Tables S3 and S4**). To modulate the reporter copy number, all experiments were conducted below 37°C (*23*). Strain passage was minimized to avoid plasmid deletions due to the *recA*+ nature of JS006 and the high complexity of oscillator plasmids or triple-reporter plasmid. Based on the *in vitro* and *in silico* results, we used strong transcriptional and translational (*24*) units to maximize gain.

TX-TL reactions

Preparation of TX-TL was conducted as described previously (*6*), but using strain "JS006" co-transformed with Rosetta2 plasmid and performing a 1:2:1

extract:DNA:buffer ratio. This resulted in extract "eZS4" with 8.7 mg/mL protein, 10.5 mM Mg-glutamate, 100 mM K-glutamate, 0.25 mM DTT, 0.75 mM each amino acid except leucine, 0.63 mM leucine, 50 mM HEPES, 1.5 mM ATP and GTP, 0.9 mM CTP and UTP, 0.2 mg/mL tRNA, 0.26 mM CoA, 0.33 mM NAD, 0.75 mM cAMP, 0.068 mM folinic acid, 1 mM spermidine, 30 mM 3-PGA, and 2% PEG-8000. For experiments utilizing linear DNA GamS was added to a final concentration of 3.5 μM (*7*).

Steady-state reactions

Experiments were performed in a microfluidic nano-reactor device as described previousely (*4*, *6*) with some modifications to optimize the conditions for the lysate-based TX-TL mix. Reaction temperature was 33°C. Lysate was diluted to 2x of the final concentration in 5 mM HEPES 5 mM NaCl buffer (pH 7.2). The reaction buffer mix was combined with template DNA and brought to a final concentration of 2x. For a 24 h experiment 30 μl of these stocks were prepared. During the experiment, lysate and buffer/DNA solutions were kept in separate tubing feeding onto the chip, cooled to approximately 6ºC, and combined on-chip. We ran experiments with dilution rates (μ) between approximately 2.8 and 0.5 h^{-1}, which corresponds to dilution times, $t_d = \ln(2)\ \mu^{-1}$, between 15 and 85 min. These were achieved with dilution steps exchanging between 7 and 25% of the reactor volume with time intervals of 7 to 10 min, which alternately added fresh lysate stock or fresh buffer/DNA solution into the reactors. Dilution rates were calibrated before each experiment. Initial conditions for the limit cycle analysis of the repressilator network were set by adding pre-synthesized repressor protein at the beginning of each experiment. For this, CI repressor (together with Citrine reporter) and

TetR repressor (together with Cerulean reporter) were expressed for 2.5h in batch. On chip the initial reaction was mixed to be composed of 25% pre-synthesis reaction and 75% fresh TX-TL mix and repressilator template DNA. Then, the experiment was performed at a t_d of 19.2 ± 0.3 min. Initial conditions for the 4-node experiment were 2.5μM aTc or 250μM IPTG, and the experiment was performed at a t_d of 44.5 ± 0.9 min. DNA template concentrations used in steady-state reactions are listed in **Table S5**. Arbitrary fluorescence values were converted to absolute concentrations from a calibration using purified Citrine, Cerulean, and mCherry, which were prepared using previously published protocols utilizing a His6 purification method followed by size-exclusion chromatography and a Bradford assay to determine protein concentration (*7*).

Transfer function measurement

Transfer functions of the repressor – promoter pairs were determined in the nano-reactor device at a minimum of two different dilution times (**Fig. S2**). All tested promoters were cloned into a plasmid in front of a BCD7 ribosomal binding site and the Citrine open reading frame. A non-saturating concentration of 1nM plasmid was used in the experiment. The repressors were expressed from linear templates carrying the J23151 promoter and the BCD7 ribosomal binding site with time-varying concentrations, which were increased from 0 to 2.5nM and decreased back to 0 during the course of the experiment (*4*). Simultaneously we expressed Cerulean as a reporter for the repressor concentration from a linear template at an identical concentration as the repressor template. From the concentration of the Citrine reporter we calculated the synthesis rate

of the fluorescent protein over time using a model of steady state protein synthesis in the nano-reactor device (*4*),

(1) $$P_d(t+\Delta t) = P_d(t) + syn(t)\cdot\Delta t - mat\cdot P_d(t)\cdot\Delta t - dil\cdot P_d(t)$$

(2) $$P_f(t+\Delta t) = P_f(t) + mat\cdot P_d(t)\cdot\Delta t - dil\cdot P_f(t)$$

where P_d and P_f are dark and fluorescent reporter concentration respectively, t is time, Δt is the time interval between dilution steps, *dil* is the volume fraction replaced per dilution step, which was determined during the calibration of the device, and *mat* is maturation rate of the fluorescent protein. Maturation times of Citrine and Cerulean were determined as described previously(*4*) and were 15 ±4 min for Cerulean and 29 ±3 min for Citrine. Dark fluorescent protein was calculated from equation (2):

(3) $$P_d(t) = \frac{P_f(t+\Delta t) - P_f(t) + dil\cdot P_f(t)}{mat\cdot\Delta t}$$

and the synthesis rate was calculated from equation (1):

(4) $$syn(t) = P_d(t+\Delta t) - P_d(t) + mat\cdot P_d(t)\cdot\Delta t + dil\cdot P_d(t)\,.$$

We used the sum of measured fluorescent Cerulean concentration and equation (3) for dark Cerulean as a measure of the total repressor protein present at any time during the experiment. The synthesis rates were normalized to their respective maximal values (v_{max}) and plotted against the concentration of the repressor reporter using only repressor concentrations higher than 1nM. The transfer curves were then fit to a Hill function

(5) $$y = f(x) = y_{\min} + (1 - y_{\min})\frac{K_M^{\,n}}{K_M^{\,n} + x^n}$$

where y is the synthesis rate, $y_{\min}$ is the minimum synthesis rate, n is the Hill coefficient and K_M is the Michaelis Menten constant for half maximal promoter activity. The fitting

was performed in Igor Pro using orthogonal distance regression with ODRPACK95 assuming a 9% error in the measurements of Citrine and Cerulean fluorescence.

V_{max} measurements

Relative promoter strengths (v_{max} values) were determined using the transfer function promoter plasmids. *In vitro* strengths were determined in 5 µl TX-TL reactions at a DNA template concentration of 1nM. Reactions were assembled in 384-well plates, overlaid with 35 µl Chill-Out Liquid wax (BioRad) and analyzed using a Biotek SynergyMx plate reader set to 33ºC reaction temperature, and reading Citrine fluorescence with Exc:510±9nm and Em:540±9nm. For comparison, Citrine fluorescence at 6h was normalized to the value of pLacI. *In vivo* strengths were determined using *E. coli* JS006 transformed with the same plasmids. Cells were grown at 29ºC in MOPS medium supplemented with 0.4% glycerol and 0.2% casaminoacids. For each strain, three independent overnight cultures were diluted 1:50 and grown to mid-log phase. They were then diluted to a starting OD_{600} of 0.15 into 100 µl growth medium in a 96-well plate and grown in the plate reader at 29ºC with periodic shaking measuring Citrine fluorescence. Fluorescence values were normalized to OD resulting in steady state values after 2 h. Average steady state values were normalized to pLacI for comparison with the *in vitro* measurement.

In vivo experiments

Mother machine (*16*) experiments were conducted with custom-made microfluidic chips (mold courtesy of M. Delincé and J. McKinney, EPFL). *E. coli* cells

were trapped in channels of 30 μm length, 2 μm width and 1.2 μm height. Before loading onto the device, cells were grown from a frozen stock to stationery phase. Cells were then concentrated 10-fold and loaded onto the chip. Experiments were performed using LB medium supplemented with 0.075% Tween-20 at a flow rate of 400 μl/h. Oscillation traces were collected from single mother machine traps using the background subtracted average fluorescence intensity of the entire trap.

CellASIC experiments were conducted using B04A plates (Merck Millipore, Darmstadt Germany). Flow rates were varied between 0.25 psi – 2 psi. Cells were grown from frozen stock in media at running temperature to stationery phase. Cells were then diluted 1:100 for 2 hours, and loaded on a equilibrated plate at 1:1000 or less to achieve single-cell loading efficiencies per chamber. To vary cellular doubling times, different growth media were used: LB (BD Biosciences), M9CA (Sigma Aldrich) with 0.2% glucose, 2xYT (MP Bio), and MOPS EZ Rich (Teknova).

Cells were imaged in time series every 10-20 min using a 100x phase objective minimizing both lamp intensity (12% Xcite 120, Excelitas Inc. Waltam MA or 1-2% CoolLED pE-2, Custom interconnected Ltd., UK) and exposure times (<500ms) to limit photo-toxicity.

Analysis of *in vivo* data

Images were processed and stitched (*25*), if necessary, using Fiji/ImageJ (*26*). Fluorescence traces of cell populations with synchronized oscillations were extracted from CellASIC movies using background corrected mean fluorescence intensity from the entire field of view. For cells that were not synchronized over the complete field of view,

we tracked regions of oscillating sister cells at the edge of the microcolony. We used ImageJ to define polygonal regions around those cells and manually shifted the polygonal region to track the front of growing cells. Periods were determined from fluorescence traces derived from mother machine and CellASIC movies by measuring the time from one oscillation peak to the next peak. Doubling times were estimated by averaging over the doubling times of at least ten individual cells.

Acknowledgements

We thank Yin He, Transcriptic, Inc. and Holly Rees for cloning assistance, Jan Kostecki and Stephen Mayo for protein purification and size exclusion chromatography assistance, Rohit Sharma and Marcella Gomez for initial testing and modeling of oscillators *in vitro*, Kyle Martin for laboratory assistance, Adam Abate, Tanja Kortemme, and Charles Craik for laboratory space and equipment, Matthieu Delincé, Joachim De Jonghe, Marc Spaltenstein, John McKinney and Jin Park for mother machine material and assistance, Tim Chang and Benjamin Alderete for CellASIC assistance, and Michael Elowitz for insights and scientific support. This work was supported in part by EPFL and the Defense Advanced Research Projects Agency (DARPA/MTO) Living Foundries program, contract number HR0011-12-C-0065 (DARPA/CMO). Z.Z.S. is also supported by a UCLA/Caltech Medical Scientist Training Program fellowship, Z.Z.S and E.Y by a National Defense Science and Engineering Graduate fellowship, and Y.H. by a JSPS Fellowship for Research Abroad. The views and conclusions contained in this document are those of the authors and should not be interpreted as representing officially policies, either expressly or implied, of the Defense Advanced Research Projects Agency or the U.S. Government.

Figure 1

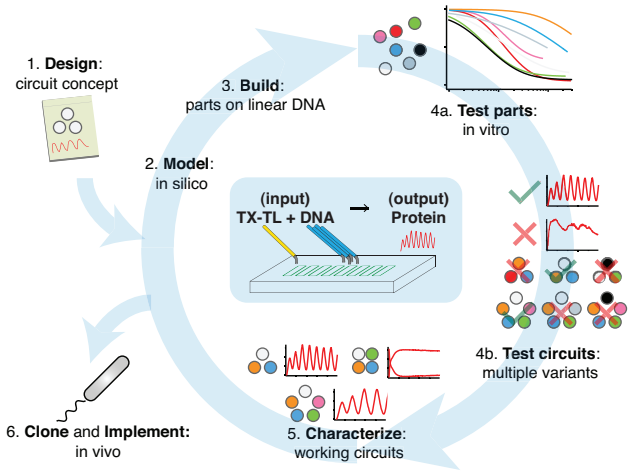

Fig. 1. The cell-free framework allows rapid and extensive characterization of biological systems. Schematic representation of the design-build-test cycle using the cell-free framework. A design is first modeled to obtain intuition about the architecture. Parts are then assembled on linear DNA without cloning, and tested *in vitro*. With functional parts, circuit variants can then be tested and working circuits can be extensively characterized. Final circuits are cloned onto plasmids and implemented *in vivo*. Center shows the microfluidics device used. Input is a circuit encoded by linear or plasmid DNA and TX-TL *in vitro* reagent, which is then translated and transcribed into protein. For a specific example of the cell-free framework applied to engineering a 5-node oscillator network see **Fig. S3**.

Figure 2

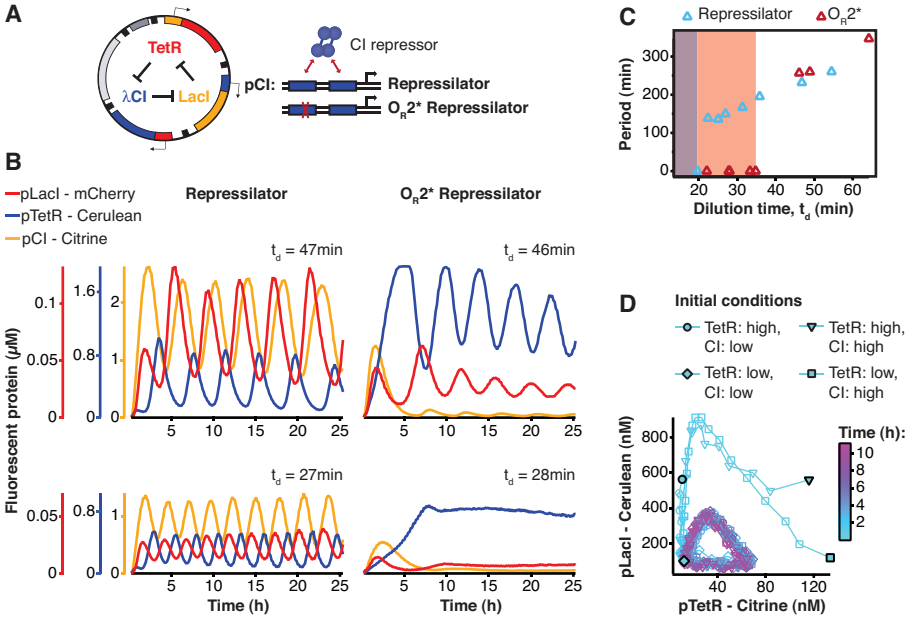

Fig. 2. Cell-free repressilator characterization. (A) Application of the cell-free framework to characterize the original repressilator (*8*) and a modified version with a point mutation in the CI promoter (O_R2^*) located in one of the binding sites of the CI repressor. **(B)** Expression from the three promoters of the repressilator and the O_R2^* version at different dilution times. **(C)** Oscillation periods of the repressilator as a function of dilution time. In the O_R2^* version sustained oscillations were supported in a narrower range of dilution times as compared to the original repressilator network. **(D)** Phase portrait of repressilator oscillations starting from different initial TetR and CI repressor concentrations.

Figure 3

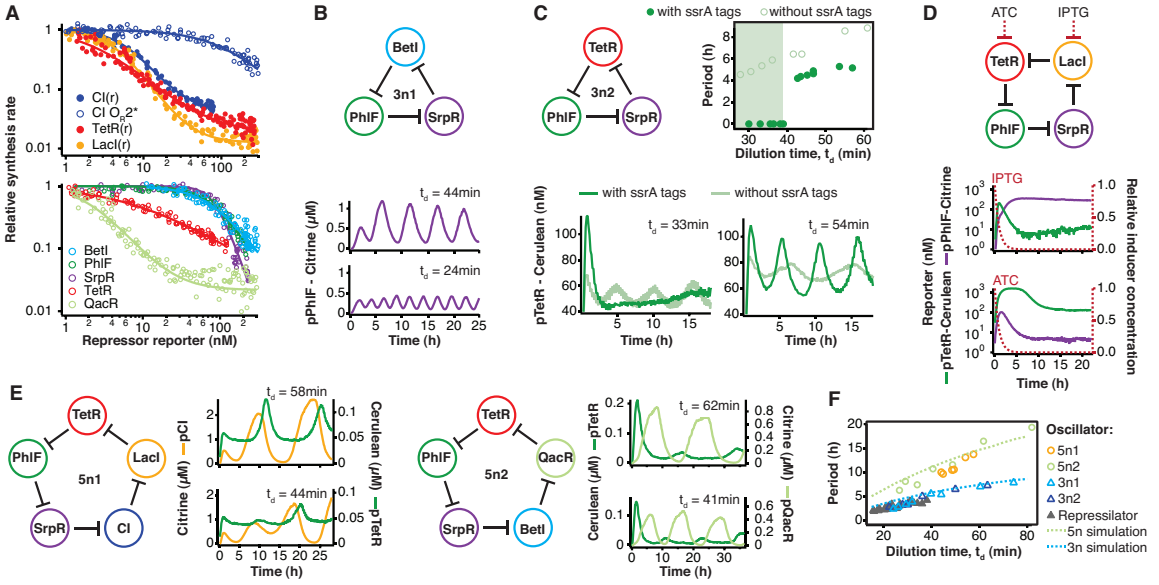

Fig. 3. Cell-free prototyping and characterization of novel negative feedback circuits. (A) Transfer functions of the repressilator repressor-promoter pairs (top) and TetR homologs (bottom). The TetR repressor was tested against two different promoters: the promoter used in the repressilator (top panel) and the J23119-TetR promoter (*10*) (bottom panel). Lines are Hill function fits. **(B)** Oscillations of a novel 3-node ring oscillator (3n1) constructed on plasmid DNA. **(C)** Two versions of a second 3-node ring oscillator (3n2) on linear DNA were used to study the effect of ClpXP degradation on oscillator function. One version was ssrA-tagged on all repressor genes while the other version did not carry degradation tags on the repressors. The same reporter with a medium-strength degradation tag was used in both versions. **(D)** A 4-node cyclic negative feedback network on linear DNA has two stable steady states that depend on the initial conditions. IPTG switched the network into the state where pPhlF was on and pTetR off. An initial pulse of aTc resulted in the opposite stable steady state. **(E)** Two 5-node negative feedback architectures oscillated with longer periods than our 3-node networks as predicted by simulations (Supplemental Model Information) **(F).**

Figure 4

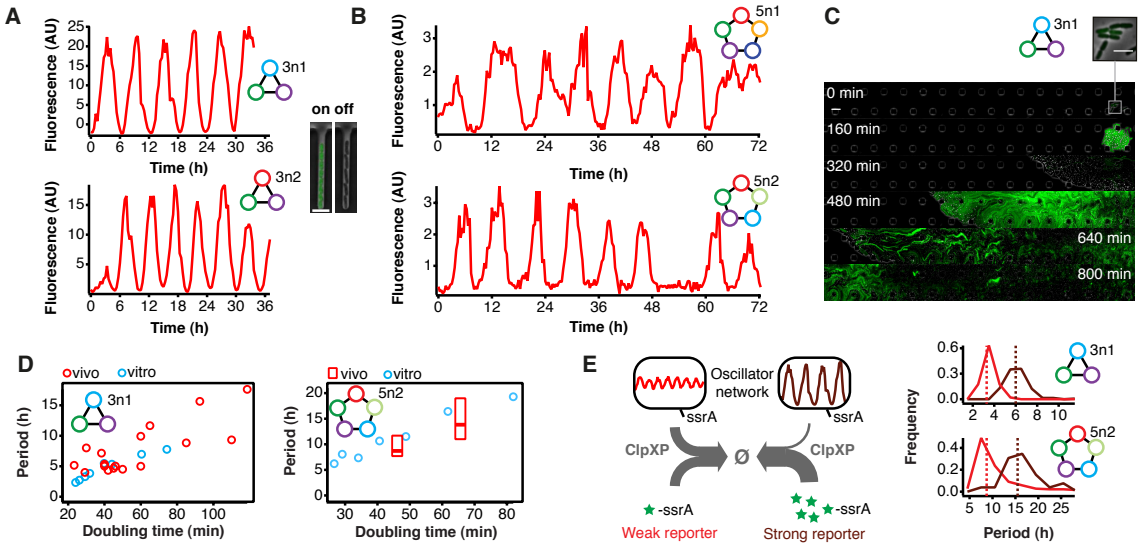

Fig. 4. Novel 3-node and 5-node ring oscillators *in vivo*. (A) Time series traces of 3-node ring oscillators running in *E. coli* (mother machine). Single trap traces of 3n1 and 3n2 observed for 36 h *in vivo* using a strong pPhlF sfGFP-ssrA reporter and a representative image from an "on" and "off" state of oscillation. Scale bar: 5 µm. **(B)** Time series traces of 5-node ring oscillators running in *E. coli* (mother machine). Single trap traces of 5n1 and 5n2 observed for 72 h *in vivo* using a weak pPhlF sfGFP-ssrA reporter. **(C)** 3n1 displays phase synchrony *in vivo* (CellASIC). Time series micrographs of 3n1 under a strong pPhlF sfGFP-ssrA reporter every 160 min; inset shows individual cells of the initial microcolony. Scale bar: 10 µm and 5 µm (inset). **(D)** Relationship between period and division time *in vivo*. Left, 3n1 *in vivo* under a strong pPhlF sfGFP-ssrA reporter. The *in vitro* data is shown for comparison. Each point in the *in vivo* data corresponds to the period and division time from a CellASIC experiment run under different media type and flow rates. Right, 5n2 *in vivo* under a weak pPhlF sfGFP-ssrA reporter. *In vivo* periods determined at 29ºC and 21ºC growth temperature in mother machine experiments. Boxes represent the inner quartile range with the median. **(E)** Influence of reporter concentration on oscillation periods by competing for ClpXP degradation. Left, with constant amounts of ClpXP the reporter concentration affects repressor degradation and thus oscillation period. Histograms of the periods observed with a weak and a strong pPhlF sfGFP-ssrA reporter for both 3n1 and 5n2 run in the mother machine. Dashed lines indicate the medians.

References

1. T. K. Lu, A. S. Khalil, J. J. Collins, Next-generation synthetic gene networks. *Nat Biotechnol* **27**, 1139–1150 (2009).
2. R. Kwok, Five hard truths for synthetic biology. *Nature* **463**, 288–290 (2010).
3. J. Shin, V. Noireaux, An E. coli cell-free expression toolbox: application to synthetic gene circuits and artificial cells. *ACS Synth. Biol.* **1**, 29–41 (2012).
4. H. Niederholtmeyer, V. Stepanova, S. J. Maerkl, Implementation of cell-free biological networks at steady state. *Proceedings of the National Academy of Sciences* **110**, 15985–15990 (2013).
5. E. Karzbrun, A. M. Tayar, V. Noireaux, R. H. Bar-Ziv, Programmable on-chip DNA compartments as artificial cells. *Science* **345**, 829–832 (2014).
6. Z. Z. Sun *et al.*, Protocols for implementing an Escherichia coli based TX-TL cell-free expression system for synthetic biology. *J Vis Exp*, e50762 (2013).
7. Z. Z. Sun, E. Yeung, C. A. Hayes, V. Noireaux, R. M. Murray, Linear DNA for rapid prototyping of synthetic biological circuits in an Escherichia coli based TX-TL cell-free system. *ACS Synth. Biol.* **3**, 387–397 (2013).
8. M. B. Elowitz, S. Leibler, A synthetic oscillatory network of transcriptional regulators. *Nature* **403**, 335–338 (2000).
9. N. Rosenfeld, J. Young, U. Alon, P. Swain, M. Elowitz, Gene Regulation at the Single-Cell Level. *Science* **307**, 1962–1965 (2005).
10. B. C. Stanton *et al.*, Genomic mining of prokaryotic repressors for orthogonal logic gates. *Nature Chemical Biology* **10**, 99–105 (2014).
11. N. A. Cookson *et al.*, Queueing up for enzymatic processing: correlated signaling through coupled degradation. *Mol Syst Biol* **7**, 561 (2011).
12. A. Prindle *et al.*, Rapid and tunable post-translational coupling of genetic circuits. *Nature* **508**, 387–391 (2014).
13. H. Smith, Oscillations and multiple steady states in a cyclic gene model with repression. *Journal of mathematical biology* **25**, 169–190 (1987).
14. Y. Hori, M. Takada, S. Hara, Biochemical oscillations in delayed negative cyclic feedback: Existence and profiles. *Automatica* **49**, 2581–2590 (2013).
15. J. Stricker *et al.*, A fast, robust and tunable synthetic gene oscillator. *Nature* **456**, 516–519 (2008).
16. P. Wang *et al.*, Robust Growth of Escherichia coli. *Current Biology* **20**, 1099–1103 (2010).
17. F. Ceroni, R. Algar, G.-B. Stan, T. Ellis, Quantifying cellular capacity identifies gene expression designs with reduced burden. *Nat Meth* (2015), doi:10.1038/nmeth.3339.
18. T. Danino, O. Mondragón-Palomino, L. Tsimring, J. Hasty, A synchronized quorum of genetic clocks. *Nature* **463**, 326–330 (2010).
19. A. Prindle *et al.*, A sensing array of radically coupled genetic "biopixels." *Nature* **481**, 39–44 (2011).
20. D. J. Kiviet *et al.*, Stochasticity of metabolism and growth at the single-cell level. *Nature* **514**, 376–379 (2014).
21. J. Chappell, K. Jensen, P. S. Freemont, Validation of an entirely in vitro approach for rapid prototyping of DNA regulatory elements for synthetic biology. *Nucleic*

Acids Res. **41**, 3471–3481 (2013).
22. A. Casini *et al.*, R2oDNA Designer: Computational Design of Biologically Neutral Synthetic DNA Sequences. *ACS Synth. Biol.* **3**, 525–528 (2014).
23. T. Fitzwater, X. Y. Zhang, R. Elble, B. Polisky, Conditional high copy number ColE1 mutants: resistance to RNA1 inhibition in vivo and in vitro. *The EMBO Journal* **7**, 3289 (1988).
24. V. K. Mutalik *et al.*, Precise and reliable gene expression via standard transcription and translation initiation elements. *Nat Meth* **10**, 354–360 (2013).
25. S. Preibisch, S. Saalfeld, P. Tomancak, Globally optimal stitching of tiled 3D microscopic image acquisitions. *Bioinformatics* **25**, 1463–1465 (2009).
26. J. Schindelin *et al*., Fiji: an open-source platform for biological-image analysis. **9**, 676–682 (2012).
27. Y. Hori, T.-H. Kim, S. Hara, Existence criteria of periodic oscillations in cyclic gene regulatory networks. *Automatica* **47**, 1203–1209 (2011).
28. R. Lutz, H. Bujard, Independent and tight regulation of transcriptional units in Escherichia coli via the LacR/O, the TetR/O and AraC/I1-I2 regulatory elements. *Nucleic Acids Res.* **25**, 1203–1210 (1997).

Supplemental Information

This includes:

Figs. S1 to S5
Tables S1 to S5
Movies S1 to S10

Figure S1

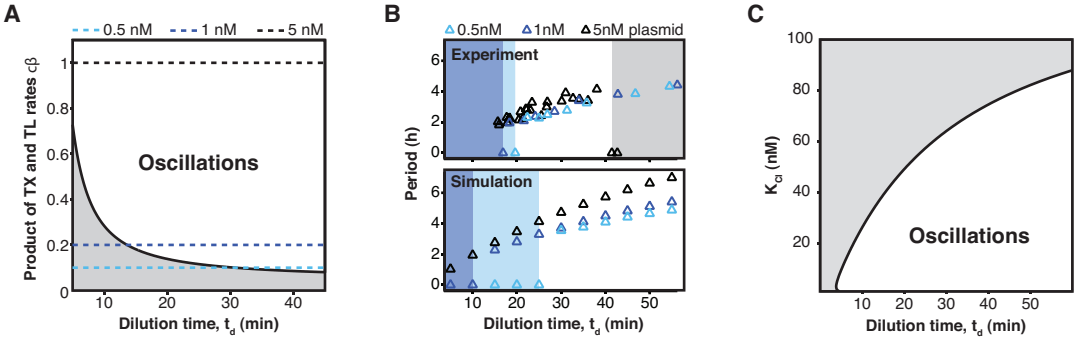

Fig. S1. Oscillation parameter regime for a 3-node repressilator network in terms of dilution time. (A) Transcription (TX) and translation (TL) rates supporting oscillations at different dilution times for a 3-node repressilator network. **(B)** We experimentally studied the effect of varying transcription rates on the WT repressilator by measuring the range of dilution times that supported sustained oscillations. Transcription rates could be rapidly adjusted by varying DNA template concentrations of the repressilator plasmid. For different DNA template concentrations, oscillations occurred in different ranges of dilution times. Markers at a period of 0 h indicate a stable steady state, and shaded regions highlight dilution times that did not support oscillations for a specific DNA template concentration. A simulation of the repressilator network produced similar results but did not capture loading effects on the biosynthetic machinery for high DNA template concentrations. **(C)** Increasing the K_M value of one repressor, as for CI repressor in the O_R2* repressilator version, reduces the range of dilution rates that support oscillations as indicated by our experimental results (**Fig. 2C**).

Figure S2

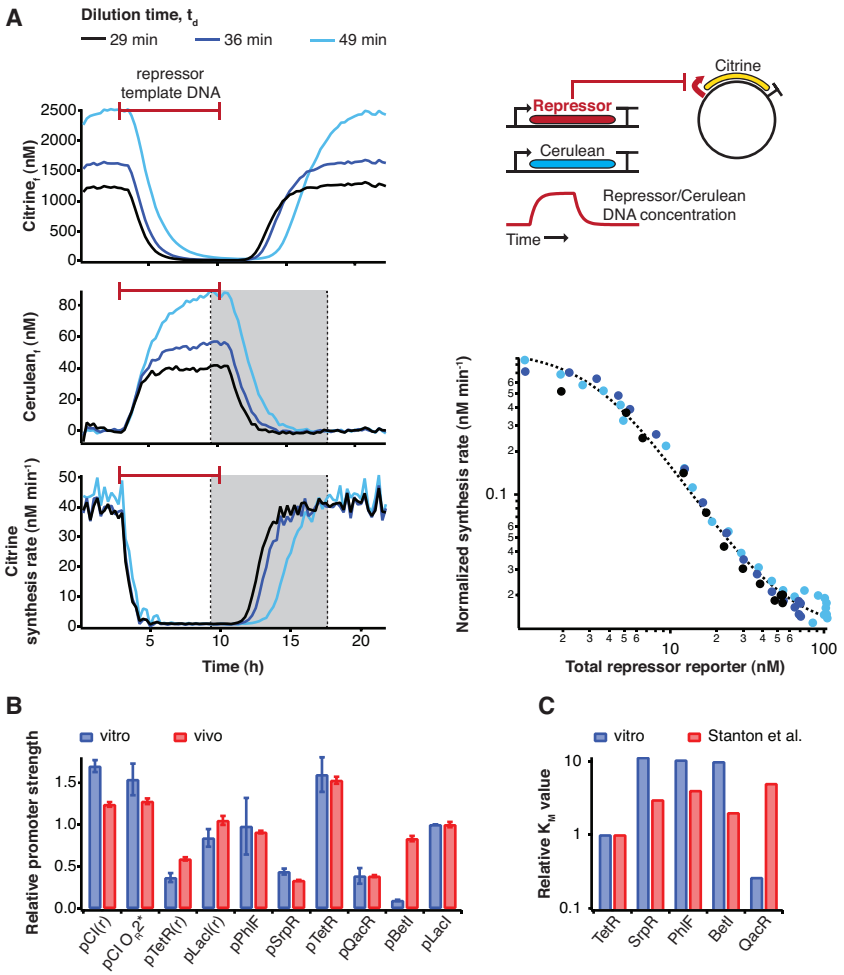

Fig. S2. Repressor characterization. (A) Transfer functions of the repressor – promoter pairs were determined using the cell-free framework as described in the Methods. Shown are experimental results and analysis using LacI - pLacI(r) as an example. Synthesis rates from the promoter of interest could be followed by Citrine fluorescence. Varying repressor template DNA concentration over time allowed us to determine synthesis rates at different repressor concentrations. Cerulean was co-expressed with the repressor and served as reporter for repressor concentration. Transfer functions were obtained by plotting Citrine synthesis rates from highest to lowest repressor concentration (grey shaded area) against total Cerulean concentration and were identical for different dilution times set in the nano-reactor device. **(B)** Comparison of relative promoter strengths (v_{max}), determined *in vitro* and *in vivo*. pCI(r), pTetR(r), and pLacI(r) are from (*8*); pTetR is from (*10*) and pLacI from (*28*). Error bars indicate standard deviations of three replicates. **(C)** Comparison of K_M values measured *in vitro* in this study with K_M values determined *in vivo* by Stanton et al. (*10*). K_M values were normalized to the K_M of TetR.

Figure S3

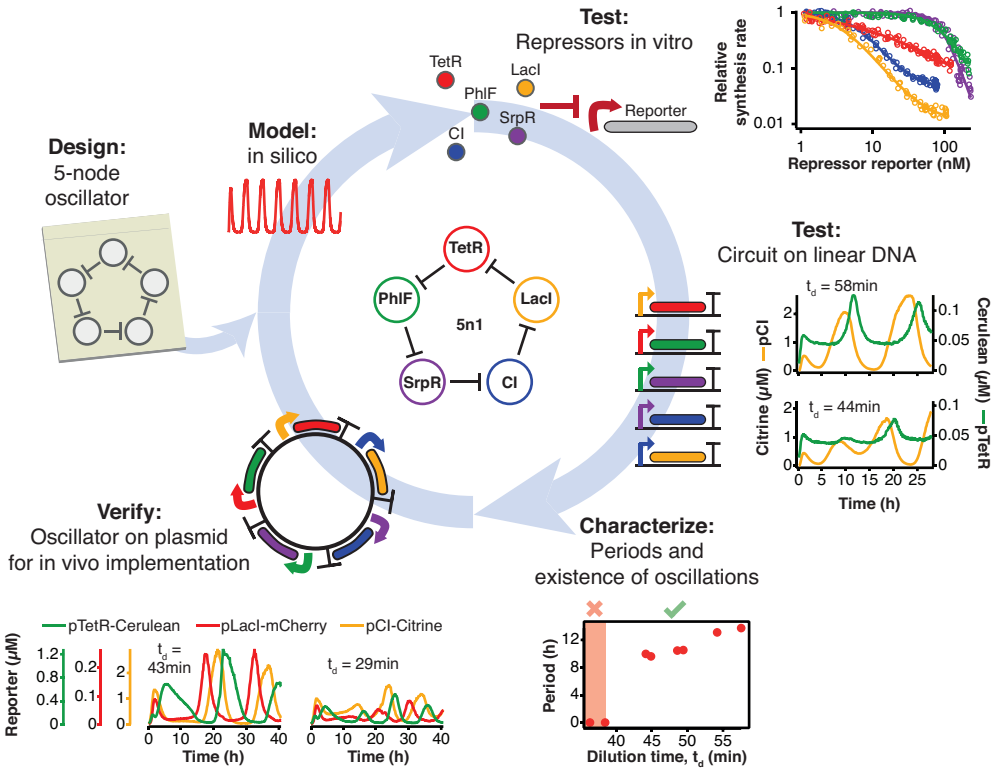

Fig. S3. Engineering a 5-node negative feedback oscillator using the cell-free framework. A novel network architecture, which shows the intended behavior *in silico* is first assembled on linear DNA using *in vitro* characterized parts. Initial circuit testing on linear DNA is advantageous because: i) linear DNA can be synthesized in a few hours, ii) it allows rapid testing of multiple circuit variants, iii) and allows expression strengths of network components to be easily tuned by varying their relative concentrations. A functional circuit can then be further characterized to identify parameter ranges that support the desired behavior and to experimentally test hypotheses. If an *in vivo* implementation is intended, the cloned plasmids are verified for correct function *in vitro* before *in vivo* implementation.

Figure S4

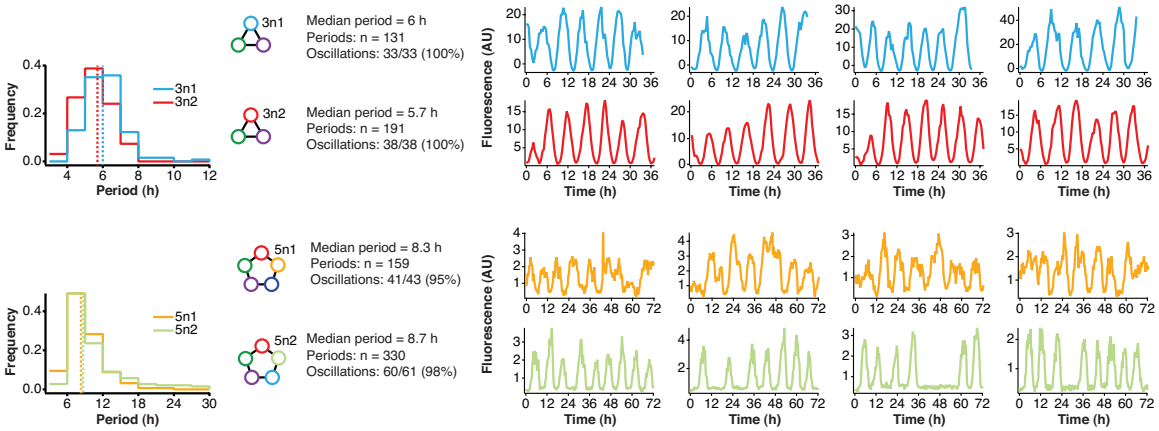

Fig. S4. Robust oscillations of 3-node and 5-node oscillators *in vivo*. 3-node (top) and 5-node networks (bottom) oscillate with periods that depend on the network size *in vivo*. Shown are the distributions of observed period lengths with medians indicated by dashed lines. Both 3-node and 5-node networks exhibited robust oscillation with all growing cells oscillating for the 3-node networks and more than 95% of growing cells oscillating for the 5-node networks (defined as at least two distinct oscillation peaks per trace). Shown are four example traces for all oscillators in addition to the ones shown in **Fig. 4A-B**. Both 3-node networks were analyzed using a strong pPhlF sfGFP-ssrA reporter and the two 5-node networks were analyzed using a weak pPhlF sfGFP-ssrA reporter.

Figure S5

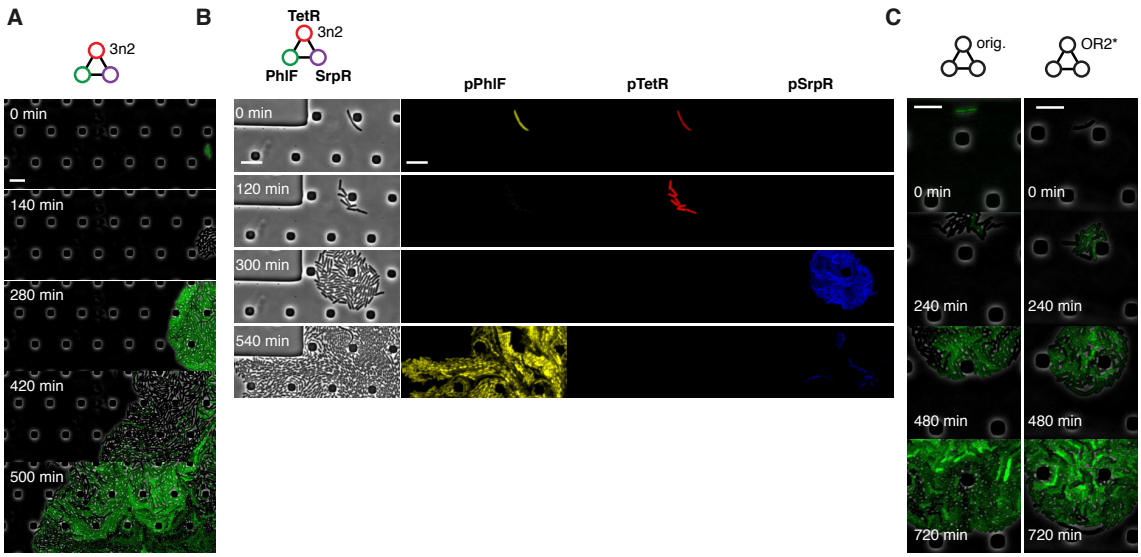

Fig. S5. Population level synchronization of 3-node oscillators *in vivo*. (A) 3n2 oscillator displays phase synchrony *in vivo*. 3n2 is run under a strong pPhlF sfGFP-ssrA reporter in the CellASIC microfluidic device. **(B)** 3n2 displays phase synchrony observing 3 reporters simultaneously. Reporters are a strong pPhlF Citrine-ssrA, pTetR mCherry-ssrA, and pSrpR Cerulean-ssrA. Shown is one oscillation cycle. **(C)** Original repressilator and O_R2* repressilator do not show phase synchrony. These are run under pTetR(r)-eGFP(ASV) in M9 minimal media; oscillations were not supported in LB. All scale bars: 10 μm.

Table S1

Transfer function parameters. Parameter values of repressor – promoter pairs were determined by fitting to the Hill equation as described in the Methods.

Name	**K_M**	**n**	**y_{min}**
CI – pCI (*8*)	5.9	1.9	0.04
CI – pCI(O_R2*) (*9*)	103	1.2	0
LacI – pLacI(r) (*8*)	4.1	1.9	0.01
TetR – pTetR(r) (*8*)	2.3	1.2	0.02
LacI – pLacI (*28*)	3.6	1.7	0.01
SrpR – pSrpR (*10*)	86	3.6	0
PhlF – pPhlF (*10*)	79	2	0
TetR – pTetR (*10*)	7.6	0.8	0
BetI – pBetI (*10*)	75.4	1.7	0
QacR – pQacR (*10*)	2.0	1.6	0.02

Table S2
Linear DNAs used in this study.

Name	Description	Notes
pJ23119-tetO-BCD2-phlF-ssrA(LAA)	# 3n2, 5n1, 4n	
pLacI-BCD2-tetR-ssrA(LAA)	& 5n1, 4n	
pLambdaCI-BCD2-lacI-ssrA(LAA)	% 5n1	
pPhlF-BCD2-srpR-ssrA(LAA)	# 3n2, 5n1, 4n	
pSprR-BCD2-lambdaCI-ssrA(LAA)	# 5n1	
pSrpR-BCD2-tetR-ssrA(LAA)	# 3n2	
pPhlF-BCD2-srpR	# 3n2/no-ssrA	
pSrpR-BCD2-tetR	# 3n2/no-ssrA	
pTetR-BCD2-phlF	# 3n2/no-ssrA	
pSrpR-BCD2-lacI-ssrA(LAA)	# 4n	
pBetI-BCD7-QacR-ssrA(LAA)	# 5n2	
pPhlF-BCD7-srpR-ssrA(LAA)	# 5n2	
pQacR-BCD7-tetR-ssrA(LAA)	# 5n2	
PSrpR-BCD7-BetI-ssrA(LAA)	# 5n2	
pTetR-BCD7-phlF-ssrA(LAA)	# 5n2	
pJ23151-BCD7-betI	$ transfer fxns	
pJ23151-BCD7-lacI	$ transfer fxns	
pJ23151-BCD7-lambdaCI	$ transfer fxns	
pJ23151-BCD7-phlF	$ transfer fxns	
pJ23151-BCD7-qacR	$ transfer fxns	
pJ23151-BCD7-srpR	$ transfer fxns	
pJ23151-BCD7-tetR	$ transfer fxns	
pLacI-BCD2-sfGFP-ssrA(LAA)	& test reporter	
pLambdaCI-BCD2-sfGFP-ssrA(LAA)	% test reporter	
pPhlF-BCD2-sfGFP-	# test reporter	

ssrA(LAA)		
pSrpR-BCD2-sfGFP-ssrA(LAA)	# test reporter	
pTetR-BCD2-sfGFP-ssrA(LAA)	# test reporter	

Promoter from Stanton et al. (2014)(*10*)
$ Promoter from Anderson promoter panel
% Promoter from Elowitz and Leibler (2000)(*8*)
& Promoter from Lutz and Bujard (1997)(*28*)

Table S3
Plasmids used in this study.

Name	Description	Resistance	Copy number	Notes
pZS1	% Original repressilator plasmid	ampR	pSC101	
pZS1 w/ OR2* mutation	%	ampR	pSC101	minimize passages
pZE21-GFP(AAV)	% Original repressilator reporter (pTetO1)	kanR	colE1	
pZE21-eGFP(ASV)	% pZE21-GFPAAV with eGFP replacement	kanR	colE1	
pET21a(+)-Histag-Cerulean	Expression vector for Cerulean purification	ampR	colE1	c. Transcriptic Inc.
pET21a(+)-Histag-Citrine	Expression vector for Citrine purification	ampR	colE1	c. Transcriptic Inc.
pET21a(+)-Histag-mCherry	Expression vector for mCherry purification	ampR	colE1	c. Transcriptic Inc.
pTetR(r)-BCD7-Citrine	% transfer fxns	kanR	pSC101*	
pTetR-BCD7-Citrine	# transfer fxns	kanR	pSC101*	c. Transcriptic Inc.
pSrpR-BCD7-Citrine	# transfer fxns	kanR	pSC101*	c. Transcriptic Inc.
pQacR-BCD7-Citrine	# transfer fxns, in vitro reporter	kanR	pSC101*	c. Transcriptic Inc.
pPhlF-BCD7-Citrine	# transfer fxns, in vitro reporter	kanR	pSC101*	c. Transcriptic Inc.
pLacI-BCD7-Citrine	& transfer fxns	kanR	pSC101*	c. Transcriptic Inc.
pLacI(r)-BCD7-Citrine	% transfer fxns	kanR	pSC101*	
pCI(OR2*)-BCD7-Citrine	* transfer fxns	kanR	pSC101*	
pCI-BCD7-Citrine	% transfer fxns	kanR	pSC101*	
pBetI-BCD7-Citrine	# transfer fxns	kanR	pSC101*	c. Transcriptic Inc.
3n1	oscillator plasmid	kanR	pSC101	minimize

			*	passages
3n2	oscillator plasmid	kanR	pSC101 *	minimize passages
5n1	oscillator plasmid	kanR	pSC101 *	minimize passages
5n2	oscillator plasmid	kanR	pSC101 *	minimize passages
pBetI-BCD7-phlF-ssrA(LAA)	# for building 3n1	ampR	pSC101 *	
pBetI-BCD7-qacR-ssrA(LAA)	# for building 5n2	ampR	pSC101 *	
pLacO1-BCD7-tetR-ssrA(LAA)	& for building 5n1	ampR	colE1	amplify in lacI repressor strain
pLambdaCI-BCD7-lacI-ssrA(LAA)	% for building 5n1	ampR	colE1	amplify in lambdaCI repressor strain
pPhlF-BCD7-srpR-ssrA(LAA)	# for building 3n1, 3n2, 5n1, 5n2	ampR	pSC101 *	
pQacR-BCD7-tetR-ssrA(LAA)	# for building 5n2	ampR	pSC101 *	
pSrpR-BCD7-betI-ssrA(LAA)	# for building 3n1, 5n2	ampR	pSC101 *	
pSrpR-BCD7-lambdaCI-ssrA(LAA)	# for building 5n1	ampR	pSC101 *	
pSrpR-BCD7-tetR-ssrA(LAA)	# for building 3n2	ampR	pSC101 *	
pTetR-BCD7-phlF-ssrA(LAA)	# for building 3n2, 5n1, 5n2	ampR	colE1	amplify in tetR repressor strain
pPhlF-BCD20-sfGFP-ssrA(LAA)	# 1 color strong reporter used in study	ampR	colE1	
pPhlF-BCD22-sfGFP-ssrA(LAA)	# 1 color weak reporter used in study	ampR	colE1	
pPhlF-BCD20-Citrine-ssrA(LAA)	# for building 3-color reporter plasmid	ampR	colE1	
pSrpR-BCD20-Cerulean-ssrA(LAA)	# for building 3-color reporter plasmid	ampR	colE1	
pTetR-BCD20-mCherry-ssrA(LAA)	# for building 3-color reporter plasmid	ampR	colE1	
3-color BCD20 reporter, pPhlF/pSrpR/pJ23119-tetO	3 color reporter plasmid	cmR	colE1	minimize passages

pTetR(r)-Citrine(ASV)	% in vitro reporter	kanR	colE1	
pTetR(r)-Cerulean(ASV)	% in vitro reporter	kanR	colE1	
pLacI(r)-mCherry(ASV)	% in vitro reporter	kanR	colE1	
pLacI(r)-Cerulean(ASV)	% in vitro reporter	kanR	colE1	
pCI-Citrine-(ASV)	% in vitro reporter	kanR	colE1	
pLacI(r)TetR(ASV)	% for initial conditions experiment	kanR	colE1	
pTetR(r)-CI(ASV)	% for initial conditions experiment	kanR	colE1	

Promoter from Stanton et al. (2014)(*10*)
$ Promoter from Anderson promoter panel
% Promoter from Elowitz and Leibler (2000)(*8*)
& Promoter from Lutz and Bujard (1997)(*28*)
* Promoter from Rosenfeld et al. (2005)(*9*)

Table S4
Strains used in this study.

Name	*E. coli* type	Resistance	Notes
Rosetta2	JS006	cmR	
pZS1 + pZE21-GFP(AAV)	JS006	kanR ampR	
pET21a(+)-Histag-Citrine	BL21-DE3	ampR	
pET21a(+)-Histag-Cerulean	BL21-DE3	ampR	
pET21a(+)-Histag-mCherry	BL21-DE3	ampR	
3n1 + pPhlF-BCD20-sfGFP-ssrA(LAA)	JS006	kanR ampR	minimize passages
3n1 + pPhlF-BCD22-sfGFP-ssrA(LAA)	JS006	kanR ampR	minimize passages
3n2 + pPhlF-BCD20-sfGFP-ssrA(LAA)	JS006	kanR ampR	minimize passages
3n2 + pPhlF-BCD22-sfGFP-ssrA(LAA)	JS006	kanR ampR	minimize passages
5n1 + pPhlF-BCD20-sfGFP-ssrA(LAA)	JS006	kanR ampR	cells unhealthy, minimize passages
5n1 + pPhlF-BCD22-sfGFP-ssrA(LAA)	JS006	kanR ampR	minimize passages
5n2 + pPhlF-BCD20-sfGFP-ssrA(LAA)	JS006	kanR ampR	minimize passages
5n2 + pPhlF-BCD22-sfGFP-ssrA(LAA)	JS006	kanR ampR	minimize passages
3n2 + 3-color BCD20 reporter, pPhlF/pSrpR/pJ23119-tetO	JS006	kanR cmR	minimize passages
pZS1 + pZE21-eGFP(ASV)	JS006	kanR ampR	
pZS1 w/ OR2* mutation + pZS21-eGFP(ASV)	JS006	kanR ampR	

Table S5
DNA concentrations used in experiments.

Experiment	DNA and concentration	Type of DNA
Repressilator orig./O_R2*, 3color	Repressilator pZS1 or pZS1 w/ O_R2* mutation, 0.5 nM (if not otherwise indicated)	Plasmid
	pTetR(r)-Cerulean(ASV), 5 nM	Plasmid
	pLacI(r)-mCherry(ASV), 5 nM	Plasmid
	pCI-Citrine(ASV), 5 nM	Plasmid
Repressilator, initial conditions	**Reaction in nano-reactor:**	
	Repressilator pZS1, 5 nM	Plasmid
	pLacI(r)-Cerulean(ASV), 5 nM	Plasmid
	pTetR(r)-Citrine-(ASV), 5 nM	Plasmid
	Pre-synthesis reaction (CI):	
	pTetR(r)-Citrine(ASV), 5 nM	Plasmid
	pTetR(r)-CI(ASV), 5 nM	Plasmid
	Pre-synthesis reaction (TetR):	
	pLacI(r)-Cerulean(ASV), 5 nM	Plasmid
	pLacI(r)TetR(ASV), 5 nM	Plasmid
Response curve measurements	Promoter plasmid: pXXX-BCD7-Citrine, 1 nM	Plasmid
	Repressor template: pJ23151-BCD7-XXX, 0-2.5 nM	Linear
	Repressor reporter: pJ23151-BCD7-Cerulean, 0-2.5 nM	Linear
3n1	3n1 oscillator plasmid, 5 nM	Plasmid
	pPhlF-BCD7-Citrine, 2.5 nM	Plasmid
3n2	pJ23119-tetO-BCD2-phlF-ssrA(LAA), 1.5 nM	Linear
	pPhlF-BCD2-srpR-ssrA(LAA), 12 nM	Linear
	pSrpR-BCD2-tetR-ssrA(LAA), 24 nM	Linear
	pTetR(r)-Cerulean(ASV), 5 nM	Plasmid
3n2/no-ssrA	pJ23119-tetO-BCD2-phlF, 1.5 nM	Linear
	pPhlF-BCD2-srpR, 12 nM	Linear
	pSrpR-BCD2-tetR, 24 nM	Linear

	pTetR(r)-Cerulean(ASV), 5 nM	Plasmid
4n	pJ23119-tetO-BCD2-phlF-ssrA(LAA), 0.75 nM	Linear
	pLacI-BCD2-tetR-ssrA(LAA), 6 nM	Linear
	pPhlF-BCD2-srpR-ssrA(LAA), 6 nM	Linear
	pSrpR-BCD2-lacI-ssrA(LAA), 12 nM	Linear
	pTetR(r)-Cerulean(ASV), 2.5 nM	Plasmid
	pLacI(r)-mCherry(ASV), 2.5 nM	Plasmid
	pPhlF-BCD7-Citrine, 2.5 nM	Plasmid
5n1	pJ23119-tetO-BCD2-phlF-ssrA(LAA), 1.1 nM	Linear
	pLacI-BCD2-tetR-ssrA(LAA), 16.8 nM	Linear
	pLambdaCI-BCD2-lacI-ssrA(LAA), 1.4 nM	Linear
	pPhlF-BCD2-srpR-ssrA(LAA), 5.6 nM	Linear
	pSprR-BCD2-lambdaCI-ssrA(LAA), 11.2 nM	Linear
	pCI-Citrine(ASV), 3 nM	Plasmid
	pTetR(r)-Cerulean(ASV), 2.5 nM	Plasmid
5n1, plasmid DNA	5n1 oscillator plasmid, 5 nM	Plasmid
	pTetR(r)-Cerulean(ASV), 5 nM	Plasmid
	pLacI(r)-mCherry(ASV), 5 nM	Plasmid
	pCI-Citrine(ASV), 5 nM	Plasmid
5n2	pBetI-BCD7-QacR-ssrA(LAA), 1 nM	Linear
	pPhlF-BCD7-srpR-ssrA(LAA), 12 nM	Linear
	pQacR-BCD7-tetR-ssrA(LAA), 4 nM	Linear
	pSrpR-BCD7-BetI-ssrA(LAA), 24 nM	Linear
	pTetR-BCD7-phlF-ssrA(LAA), 4 nM	Linear
	pTetR(r)-Cerulean(ASV), 2.5 nM	Plasmid
	pQacR-BCD7-Citrine, 2.5 nM	Plasmid

Movies

Note: All movies can be found on www.biorxiv.com under listed doi.

Movie S1: 3-color *in vitro* run of repressilator at t_d = 47 min. Shown on the right are individual channels of pCI-Citrine-ssrA, pTetR-Cerulean-ssrA, and pLacI-mCherry-ssrA. These are combined in the composite at the left.

Movie S2: 3n1 in mother machine, single trap. 3n1 using a pPhlF-BCD20-sfGFP-ssrA (strong) reporter is run in the mother machine at 29ºC in LB.

Movie S3: 3n2 in mother machine, single trap. 3n2 using a pPhlF-BCD20-sfGFP-ssrA (strong) reporter is run in the mother machine at 29ºC in LB.

Movie S4: Run of a panel of 3n2 oscillators in mother machine, using pPhlF-BCD20-sfGFP-ssrA (strong) reporter.

Movie S5: 5n1 in mother machine. 5n1 using a pPhlF-BCD22-sfGFP-ssrA (weak) reporter is run in the mother machine at 29ºC in LB.

Movie S6: 5n2 in mother machine. 5n2 using a pPhlF-BCD22-sfGFP-ssrA (weak) reporter is run in the mother machine at 29ºC in LB.

Movie S7: Run of a panel of 5n2 oscillators in mother machine, using pPhlF-BCD22-sfGFP-ssrA (weak) reporter.

Movie S8: 3n1 in CellASIC. 3n1 using a pPhlF-BCD20-sfGFP-ssrA (strong) reporter is run in CellASIC. This video corresponds to Fig. 4C. Conditions: 29ºC, LB media, 12.5% lamp intensity, 200 ms exposure, 2 psi flow rate.

Movie S9: 3n2 in CellASIC. 3n2 using a pPhlF-BCD20-sfGFP-ssrA (strong) reporter is run in CellASIC. This video corresponds to Fig. S5A. Conditions: 29ºC, LB media, 12.5% lamp intensity, 200 ms exposure, 2 psi flow rate.

Movie S10: 3n2 with 3-color output run in CellASIC. 3n2 using a pPhlF-BCD20-Citrine-ssrA, pTetR-BCD20-mCherry-ssrA, pSrpR-Cerulean-ssrA (strong) reporter is run in CellASIC. This video corresponds to Fig. S5B. Conditions: 29 C, LB media, 12.5% lamp intensity, 200 ms exposure for Citrine and Cerulean (500 ms for mCherry), 2 psi flow rate.

Chapter 6: Conclusion and Future Directions

In this thesis, we demonstrate that a biomolecular breadboard composed of an *in-vitro* lysate, TX-TL, can be used to prototype synthetic circuits cheaply and easily (Chapter 2). We furthermore show that circuits can be prototyped in under a business day by using linear DNA and modular assembly methods (Chapter 3), and that protein dynamics can be implemented in the breadboard through characterization of the AAA+ protease ClpXP (Chapter 4). Finally, we demonstrate that the biomolecular breadboard combined with a microfluidic device (Niederholtmeyer et al. 2015) can prototype novel biomolecular circuits *in vitro*, and that these circuits can be migrated to the *in vivo* environment (Chapter 5). Therefore, we believe that our biomolecular breadboard can serve as an intermediary from design to *in vivo* implementation.

An active area of future work is exhaustively determining the *in vitro* to *in vivo* connection for cell-free lysates, and implementing predictive *in silico* modeling to further speed up the design-build-test cycle. Basic transcriptional and translational items have been tested *in vitro* and *in vivo* (Chappell et al. 2013; Sun et al. 2014), transfer functions have been shown to be equivalent (Chappell et al. 2013; Sun et al. 2014; Niederholtmeyer et al. 2015), and circuits have been migrated from one environment to another (Niederholtmeyer et al. 2015; Takahashi et al. 2014). However, the limitations of *in vitro* prototyping to the *in vivo* environment are unknown. This can be addressed by high-throughput exploration of circuit variants *in vitro*, *in vivo*, and *in silico* to determine a percent association.

While technology development is an interesting scientific endeavor, its real value depends on its widespread adoption. Preliminary results have been promising; from the

completion of Chapter 2 to the publication of this thesis, more than fifteen universities and commercial organizations have adopted TX-TL use. Additionally, more than 30,000 reactions have been made using the protocol at Caltech. This has resulted in multiple projects which have either been published or have been written up using TX-TL technology developed in this thesis, exploring RNA cascades (Takahashi et al. 2014), prototyping methodology (Takahashi et al. 2015), novel sensors (de los Santos et al. 2015), high throughput droplet microfluidics (Ochs & Abate 2015), metabolic engineering (Wu et al. 2015), RNA thermometers (Satija et al. 2015), compositional context (Yeung et al. 2014), RNA aptamers logic circuits (J. Kim et al. 2014), resource limitations (Siegal-Gaskins et al. 2014; Siegal-Gaskins et al. 2013), and temperature robustness of circuit architectures (Sen et al. 2013). In one of these projects, a group of undergraduate students with limited biological experience were able to go from design to completion of a project within two weeks of full-time work and a publication within a year (Takahashi et al. 2014). The fast time-frame of these projects indicate a real time-savings in using the biomolecular breadboard.

While the breadboard developed in this thesis has found use in the biological research community, two communities that can most benefit are those with limited biological experience whom see biology as a tool for exploring fundamentally non-biological questions, and those who are just starting to learn biological procedures. While the breadboard is easy to use when reagents in Chapter 2 are pre-made, the protocol requires a well-equipped laboratory to execute and requires significant skilled labor and initial startup cost. The groups whom most benefit have the least access to this upfront capital. In addition, research into improving the breadboard relative to expression

strength and ability to match *in vivo* metrics is mostly based on process improvement, which is difficult to pose in an academic fashion. To remove these barriers, one area of future work is the commercialization of the biomolecular breadboard technology to allow for wider adoption. This commercialization effort would also encourage work into using TX-TL and the biomolecular breadboard for high value applications described in Chapter 1 in metabolic engineering.

References

Atsumi, S. et al., 2008. Metabolic engineering of Escherichia coli for 1-butanol production. *Metab Eng*, 10(6), pp.305–311.

Baneyx, F., 1999. Recombinant protein expression in Escherichia coli. *Curr Opin Biotechnol*, 10(5), pp.411–421.

Caschera, F. & Noireaux, V., 2013. Synthesis of 2.3 mg/ml of protein with an all Escherichia coli cell-free transcription-translation system. *Biochimie*, pp.1–7.

Casini, A. et al., 2014. R2oDNA Designer: Computational Design of Biologically Neutral Synthetic DNA Sequences. *ACS Synth Biol*, 3(8), pp.525–528.

Ceroni, F. et al., 2015. Quantifying cellular capacity identifies gene expression designs with reduced burden. *Nat Methods*.

Chappell, J., Jensen, K. & Freemont, P.S., 2013. Validation of an entirely in vitro approach for rapid prototyping of DNA regulatory elements for synthetic biology. *Nucleic Acids Res*, 41(5), pp.3471–3481.

Cheah, U.E., Weigand, W.A. & Stark, B.C., 1987. Effects of recombinant plasmid size on cellular processes in Escherichia coli. *Plasmid*, 18(2), pp.127–134.

Chen, C.-H. et al., 2007. A Synthetic Maternal-Effect Selfish Genetic Element Drives Population Replacement in Drosophila. *Science*, 316(5824), pp.597–600.

Chen, Y.-J. et al., 2013. Characterization of 582 natural and synthetic terminators and quantification of their design constraints. *Nat Methods*, 10(7), pp.659–664.

Couturier, M. et al., 1988. Identification and classification of bacterial plasmids. *Microbiological Reviews*, 52(3), pp.375–330.

de Kok, S. et al., 2014. Rapid and Reliable DNA Assembly via Ligase Cycling Reaction. *ACS synthetic …*, 3(2), pp.97–106.

de los Santos, E., Meyerowitz, J.T. & Mayo, S.L., 2015. Engineering Transcriptional Regulator Effector Specificity using Computational Design and In Vitro Rapid Prototyping: Developing a Vanillin Sensor. *bioRxiv*.

Diaz, R., Nordström, K. & Staudenbauer, W.L., 1981. Plasmid R1 DNA replication dependent on protein synthesis in cell-free extracts of E. coli. *, Published online: 22 January 1981; | doi:10.1038/289326a0*, 289(5795), pp.326–328.

Eid, J. et al., 2009. Real-Time DNA Sequencing from Single Polymerase Molecules. *Science*, 323(5910), pp.133–138.

Ellis, T., Wang, X. & Collins, J.J., 2009. Diversity-based, model-guided construction of

synthetic gene networks with predicted functions. *Nature Biotechnology*, 27(5), pp.465–471.

Endy, D., 2005. Foundations for engineering biology. *Nature*, 438(7067), pp.449–453.

Engler, C. et al., 2009. Golden Gate Shuffling: A One-Pot DNA Shuffling Method Based on Type IIs Restriction Enzymes J. Peccoud, ed. *PLoS One*, 4(5), p.e5553.

Fujii, Y. et al., 2004. Isolation and characterization of the bacteriophage WO from Wolbachia, an arthropod endosymbiont. *Biochemical and Biophysical Research Communications*, 317(4), pp.1183–1188.

Gibson, D.G. et al., 2009. Enzymatic assembly of DNA molecules up to several hundred kilobases. *Nat Methods*, 6(5), pp.343–345.

Hale, V. et al., 2007. Microbially Derived Artemisinin: A Biotechnology Solution to the Global Problem of Access to Affordable Antimalarial Drugs. *The American Journal of Tropical Medicine and Hygiene*, 77(6 Suppl), pp.198–202.

Heinemann, M. & Panke, S., 2006. Synthetic biology--putting engineering into biology. *Bioinformatics*, 22(22), pp.2790–2799.

Hoagland, M.B. et al., 1958. A soluble ribonucleic acid intermediate in protein synthesis. *J Biol ….*

Holland, T.M. & Bundy, B.C., 2012. Streamlined extract preparation for Escherichia coli-based cell-free protein synthesis by sonication or bead vortex mixing. *Biotechniques*.

J Heinrich Matthaei, M.W.N., 1961. CHARACTERISTICS AND STABILIZATION OF DNAASE-SENSITIVE PROTEIN SYNTHESIS IN E. COLI EXTRACTS. *Proc Natl Acad Sci U S A*, 47(10), p.1580.

Jewett, M.C. & Swartz, J.R., 2004. Substrate replenishment extends protein synthesis with an in vitro translation system designed to mimic the cytoplasm. *Biotechnol Bioeng*, 87(4), pp.465–471.

Karzbrun, E. et al., 2014. Synthetic biology. Programmable on-chip DNA compartments as artificial cells. *Science*, 345(6198), pp.829–832.

Keasling, J.D., 2014. *TestimonyBefore theSubcommittee on Research and Technology Committee on Science, Space, and Technology United States House of Representatives*,

Kelly, J.R. et al., 2009. Measuring the activity of BioBrick promoters using an in vivo reference standard. *J Biol Eng*, 3, p.4.

Kigawa, T. et al., 2004. Preparation of Escherichia coli cell extract for highly productive

cell-free protein expression. *J Struct Funct Genomics*, 5(1-2), pp.63–68.

Kim, D.-M. & Swartz, J.R., 2001. Regeneration of adenosine triphosphate from glycolytic intermediates for cell-free protein synthesis. *Biotechnol Bioeng*, 74(4), pp.309–316.

Kim, J. & Winfree, E., 2011. Synthetic in vitro transcriptional oscillators. *Mol Syst Biol*, 7, p.465.

Kim, J. et al., 2014. Synthetic logic circuits using RNA aptamer against T7 RNA polymerase. *bioRxiv*.

Kim, J., White, K.S. & Winfree, E., 2006. Construction of an in vitro bistable circuit from synthetic transcriptional switches. *Mol Syst Biol*, 2, p.68.

Kim, T.-W. et al., 2008. A highly efficient and economical cell-free protein synthesis system using the S12 extract of Escherichia coli. *Biotechnology and Bioprocess Engineering*, 13(4), pp.464–469.

Kim, T.-W. et al., 2007. Prolonged cell-free protein synthesis using dual energy sources: Combined use of creatine phosphate and glucose for the efficient supply of ATP and retarded accumulation of phosphate. *Biotechnol Bioeng*, 97(6), pp.1510–1515.

Kim, T.W. et al., 2006. Simple procedures for the construction of a robust and cost-effective cell-free protein synthesis system. *J Biotechnol*, 126(4), pp.554–561.

Kosuri, S. et al., 2010. A Scalable Gene Synthesis Platform Using High-Fidelity DNA Microchips. *Nature Biotechnology*, 28(12), p.1295.

Kotula, J.W. et al., 2014. Programmable bacteria detect and record an environmental signal in the mammalian gut. *Proceedings of the National Academy of Sciences of the United States of America*, 111(13), pp.4838–4843.

Kwon, Y.-C. & Jewett, M.C., 2015. High-throughput preparation methods of crude extract for robust cell-free protein synthesis. *Scientific reports*, 5, p.8663.

Lathe, R. et al., 1980. Cell-free synthesis of enterotoxin of E. coli from a cloned gene. *, Published online: 03 April 1980; | doi:10.1038/284473a0*, 284(5755), pp.473–474.

Le Cong et al., 2013. Multiplex Genome Engineering Using CRISPR/Cas Systems. *Science*, 339(6121), pp.819–823.

Lee, T.S. et al., 2011. BglBrick vectors and datasheets: A synthetic biology platform for gene expression. *J Biol Eng*, 5(1), pp.1–14.

Lilley, D.M.J., 1981. In vivo consequences of plasmid topology. *, Published online: 23 July 1981; | doi:10.1038/292380a0*, 292(5821), pp.380–382.

Liu, D.V., Zawada, J.F. & Swartz, J.R., 2005. Streamlining Escherichia Coli S30 Extract Preparation for Economical Cell-Free Protein Synthesis. *Biotechnol Prog*, 21(2), pp.460–465.

Mandel, M. & Higa, A., 1970. Calcium-dependent bacteriophage DNA infection. *J Mol Biol*, 53(1), pp.159–162.

Martin, V.J.J. et al., 2003. Engineering a mevalonate pathway in Escherichia coli for production of terpenoids. *Nature Biotechnology*, 21(7), pp.796–802.

Miroux, B. & Walker, J.E., 1996. Over-production of Proteins inEscherichia coli: Mutant Hosts that Allow Synthesis of some Membrane Proteins and Globular Proteins at High Levels. *J Mol Biol*, 260(3), pp.289–298.

Moon, T.S. et al., 2012. Genetic programs constructed from layered logic gates in single cells. *Nature*, 491(7423), pp.249–253.

Murphy, A.C., 2011. Metabolic engineering is key to a sustainable chemical industry. *Nat. Prod. Rep.*, 28(8), pp.1406–1425.

Mutalik, V.K. et al., 2013. Precise and reliable gene expression via standard transcription and translation initiation elements. *Nat Methods*, pp.1–15.

Nakamura, C.E. & Whited, G.M., 2003. Metabolic engineering for the microbial production of 1,3-propanediol. *Curr Opin Biotechnol*, 14(5), pp.454–459.

Niederholtmeyer, H. et al., 2015. *A cell-free framework for biological systems engineering*,

Nirenberg, M.W. & Matthaei, J.H., 1961. The dependence of cell-free protein synthesis in E. coli upon naturally occurring or synthetic polyribonucleotides. *Proceedings of the National Academy of Sciences of the United States of America*, 47(10), pp.1588–1602.

Noireaux, V. et al., 2005. Toward an artificial cell based on gene expression in vesicles. *Physical Biology*, 2(3), pp.P1–P8.

Noireaux, V., Bar-Ziv, R. & Libchaber, A., 2003. Principles of cell-free genetic circuit assembly. *Proceedings of the National Academy of Sciences of the United States of America*, 100(22), pp.12672–12677.

Ochs, C.J. & Abate, A.R., 2015. Rapid modulation of droplet composition with pincer microvalves. *Lab Chip*, 15(1), pp.52–56.

Paddon, C.J. et al., 2013. High-level semi-synthetic production of the potent antimalarial artemisinin. *Nature*, 496(7446), pp.528–532.

Pardee, K. et al., 2014. Paper-Based Synthetic Gene Networks. *Cell*, 159(4), pp.940–954.

Ro, D.K. et al., 2006. Production of the antimalarial drug precursor artemisinic acid in engineered yeast. *Nature*, 440(7086), pp.940–943.

Saeidi, N. et al., 2011. Engineering microbes to sense and eradicate Pseudomonas aeruginosa, a human pathogen. *Mol Syst Biol*, 7, p.521.

Sarrion-Perdigones, A. et al., 2011. GoldenBraid: An Iterative Cloning System for Standardized Assembly of Reusable Genetic Modules J. Peccoud, ed. *PLoS One*, 6(7), p.e21622.

Satija, R. et al., 2015. Design of a Toolbox of RNA Thermometers. *bioRxiv*.

Sawasaki, T. et al., 2002. A cell-free protein synthesis system for high-throughput proteomics. *Proceedings of the National Academy of Sciences of the United States of America*, 99(23), pp.14652–14657.

Sen, S., Kim, J. & Murray, R.M., 2013. Designing Robustness to Temperature in a Feedforward Loop Circuit. *bioRxiv*.

Shen, C.R. & Liao, J.C., 2008. Metabolic engineering of Escherichia coli for 1-butanol and 1-propanol production via the keto-acid pathways. *Metab Eng*, 10(6), pp.312–320.

Shimizu, Y. et al., 2001. Cell-free translation reconstituted with purified components. *Nature Biotechnology*, 19(8), pp.751–755.

Shin, J. & Noireaux, V., 2012. An E. coliCell-Free Expression Toolbox: Application to Synthetic Gene Circuits and Artificial Cells. *ACS Synth Biol*, 1(1), pp.29–41.

Shin, J. & Noireaux, V., 2010a. Efficient cell-free expression with the endogenous E. Coli RNA polymerase and sigma factor 70. *J Biol Eng*, 4(1), pp.8–9.

Shin, J. & Noireaux, V., 2010b. Study of messenger RNA inactivation and protein degradation in an Escherichia coli cell-free expression system. *J Biol Eng*, 4(1), pp.9–9.

Shin, J., Jardine, P. & Noireaux, V., 2012. Genome Replication, Synthesis, and Assembly of the Bacteriophage T7 in a Single Cell-Free Reaction. *ACS Synth Biol*, 1(9), pp.408–413.

Siegal-Gaskins, D. et al., 2014. Gene circuit performance characterization and resource usage in a cell-free "breadboard." *ACS Synth Biol*, 3(6), pp.416–425.

Siegal-Gaskins, D., Noireaux, V. & Murray, R.M., 2013. Biomolecular resource utilization in elementary cell-free gene circuits. *2013 American Control Conference (ACC)*, pp.1531–1536.

Smanski, M.J. et al., 2014. Functional optimization of gene clusters by combinatorial

design and assembly. *Nature Biotechnology*, 32(12), pp.1241–U104.

Spirin, A.S. et al., 1988. A continuous cell-free translation system capable of producing polypeptides in high yield. *Science*, 242(4882), pp.1162–1164.

Sprinzak, D. et al., 2010. Cis-interactions between Notch and Delta generate mutually exclusive signalling states. *Nature*, 465(7294), pp.86–90.

Stanton, B.C. et al., 2014. Genomic mining of prokaryotic repressors for orthogonal logic gates. *Nat Chem Biol*, 10(2), pp.99–105.

Sun, Z.Z. et al., 2014. Linear DNA for Rapid Prototyping of Synthetic Biological Circuits in an Escherichia coliBased TX-TL Cell-Free System. *ACS Synth Biol*, 3(6), pp.387–397.

Takahashi, M.K. et al., 2015. Characterizing and prototyping genetic networks with cell-free transcription–translation reactions. *Methods*.

Takahashi, M.K. et al., 2014. Rapidly Characterizing the Fast Dynamics of RNA Genetic Circuitry with Cell-Free Transcription-Translation (TX-TL) Systems. *ACS Synth Biol*.

Temme, K., Zhao, D. & Voigt, C.A., 2012. Refactoring the nitrogen fixation gene cluster from Klebsiella oxytoca. *Proceedings of the National Academy of Sciences of the United States of America*, 109(18), pp.7085–7090.

Tsuruta, H. et al., 2009. High-Level Production of Amorpha-4,11-Diene, a Precursor of the Antimalarial Agent Artemisinin, in Escherichia coli A. Gregson, ed. *PLoS One*, 4(2), pp.e4489–12.

Walker, T. et al., 2011. The wMel Wolbachia strain blocks dengue and invades caged Aedes aegypti populations. *Nature*, 476(7361), pp.450–453.

Wang, H.H. et al., 2009. Programming cells by multiplex genome engineering and accelerated evolution. *Nature*, 460(7257), pp.894–898.

Watson, J.D. & Crick, F., 1953. Molecular structure of nucleic acids. *Nature*.

Wiechert, W., 2001. 13C Metabolic Flux Analysis. *Metab Eng*, 3(3), pp.195–206.

Wood, W.B. & Berg, P., 1962. Effect of Enzymatically Synthesized Ribonucleic Acid on Amino Acid Incorporation by a Soluble Protein-Ribosome System from Escherichia Coli. *Proceedings of the National Academy of Sciences of the United States of America*, 48(1), pp.94–&.

Wu, Y.Y. et al., 2015. *Prototyping 1,4-butanediol (BDO) biosynthesis pathway in a cell-free transcription-translation (TX-TL) system*,

Yang, W.C. et al., 2012. Simplifying and streamlining Escherichia coli-based cell-free protein synthesis. *Biotechnol Prog*, 28(2), pp.413–420.

Yeung, E. et al., 2014. Modeling the effects of compositional context on promoter activity in an E. coli extract based transcription-translation system. *53rd IEEE Conference on ….*

Yim, H. et al., 2011. Metabolic engineering of Escherichia coli for direct production of 1,4-butanediol. *Nat Chem Biol*, 7(7), pp.445–452.

Zubay, G., 1973. In-Vitro Synthesis of Protein in Microbial Systems. *Annual Review of Genetics*, 7, pp.267–287.